

**UNIVERSITÀ DEGLI  
STUDI DI PADOVA**  
Facoltà di Scienze MM.FF.NN.  
Facoltà di Ingegneria

**ISTITUTO NAZIONALE  
DI FISICA NUCLEARE**  
Laboratori Nazionali di Legnaro

*in collaborazione con Confindustria Veneto*

**TESI DI MASTER**  
in  
“Surface Treatments for Industrial Applications”

# **Study of Thin Film Solar Cell based on Copper Oxide Substrate by DC Reactive Magnetron Sputtering**

*Relatore: Prof. Vincenzo Palmieri  
Dott. Cristian Pira*

*Candidato: Dott. Lytovchenko Oleksiyi*

Anno accademico 2008-09



## INDEX

1 Introduction	4
1.1 Solar Energy Conversion	11
1.2 History of photovoltaic's	12
1.3 Basic principles of photovoltaic.	19
1.3.1 P- or n-type contact metal/semiconductor Schottky	30
1.3.2 Homojunction Device	30
1.3.3 Heterojunction solar cell	32
1.3.4 P-i-n and n-i-p devices.	32
1.4 Advantages and disadvantages of photovoltaics.	32
1.5 Thin film photovoltaic and materials	34
1.5.1 Thin film	34
1.5.2 Thin film absorber materials	34
1.5.3 Different thin film solar cell technologies	38
1.5.3.1 Crystalline silicon thin film solar cells	38
1.5.3.2 Amorphous and microcrystalline silicon thin film solar cells	39
1.5.3.3 Copper indium gallium selenide and cadmium telluride solar cell structures	41
1.5.3.4 Basic structure of thin film organic solar cells	42
2 Materials, experimental setup and methods.	49
2.1 Copper (I) oxide	49
2.2 Copper (II) oxide	52
2.3 Titanium Oxide:	54
2.3.1 The main structure and crystallographic properties of Rutile	54
2.3.2 Anatase	55
2.3.3 Brookite	56
2.3.4 Titanium oxide thin film application, doping and deposition methods	57

2.4 Copper oxide and titanium oxide combination properties and application	59
2.5 Methods end setups description	62
2.5.1 The reactive DC-Magnetron Sputtering Process	62
2.5.1.1 The Principle of sputtering	62
2.5.1.2 The Sputter Parameters	65
2.5.1.3 The Sputter System	66
2.5.2 Thin films cartelization	68
2.5.2.1 Thickness measurements	68
2.5.2.2 X-ray diffraction microstructure analysis.	69
2.5.2.3 Four-Point Probe method	71
2.5.2.4 The hot point probe method	74
3. Experimental results	75
Introduction	75
3.1 Cu <sub>2</sub> O thin film deposition by reactive dirrect current (DC) magnetron sputtering.	75
3.1.1 Influence of oxygen/argon flux ratio on Cu <sub>x</sub> O sputtered films.	76
3.1.1.1 Sputtering at room temperature.	77
3.1.1.2 Sputtering depositions Cu <sub>2</sub> O at 200°C.	80
3.1.2 Influence of temperature on cuprum oxide thin film properties deposited by DC magnetron reactive sputtering	85
3.2 Reactive DC sputtering of TiO <sub>x</sub> thin film	87
3.3 Copper oxide photovoltaic cell development	91
3.3.1 Cu <sub>2</sub> O photovoltaic “wet” solar cell	91
3.3.2 Cu/Cu <sub>2</sub> O/Cu (metal/semiconductor)	

thin film structure created by reactive DC sputtering at various temperatures	97
3.3.3 Photovoltaic effect in Cu/Cu <sub>2</sub> O/TiO <sub>2</sub> /Au (heterojunction) thin film structure created by reactive DC sputtering	99
3.3.4 Performance comparison of different photovoltaic cell build	103
<i>CONCLUSIONS</i>	106

## **1 Introduction**

### **1.1 Solar energy conversion**

Availability of affordable energy has enabled spectacular growth of industrialization and human development in all parts of the world. With growth (low accelerating In developing countries. demands on energy sources and infrastructure are being stretched to new limits. Additional energy issues include the push for renewable resources with reduced greenhouse gas emissions and energy security affected by the uneven distribution of energy resources around the globe. Together, these issues present a field of opportunity for innovations to address energy challenges throughout the world and all along the energy flow. These energy challenges form the backdrop for this special expanded in [1]. There is introduced the global landscape of materials issues associated with energy. It examines the complex web of energy availability, production. Storage, transmission, distribution, use, and efficiency. It focuses on the materials challenges that lie at the core of these areas and discusses how revolutionary concepts can address them. At the Figure 1.1 presented the world total energy primary energy supply [1].

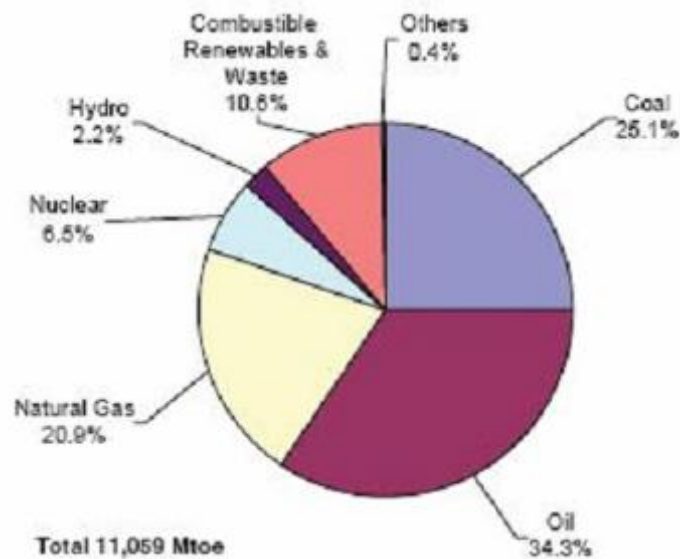


*Figure 1.1 World total primary energy supply (2004) by source. Mtoe is million tons of oil equivalent*

Photovoltaics (PV) are an important energy technology for many reasons. As a solar energy technology, it has numerous environmental benefits. As a domestic source of electricity, it contributes to the nation's energy security. As a relatively young, high-tech industry, it helps to create jobs and strengthen the economy. As it costs increasingly less to produce and use, it becomes more affordable and available.

Few power-generation technologies have as little impact on the environment as photovoltaics. As it quietly generates electricity from light, PV produces no air pollution or hazardous waste. It does not require liquid or gaseous fuels to be transported or combusted. In addition, because its energy source - sunlight - is free and abundant, PV systems can guarantee access to electric power.

PV frees us from the cost and uncertainties surrounding energy supplies from politically volatile regions. In addition to reducing our trade deficit, a robust domestic PV industry creates new jobs and strengthens the world economy. Photovoltaics is about to celebrate 50 years of its modern era.

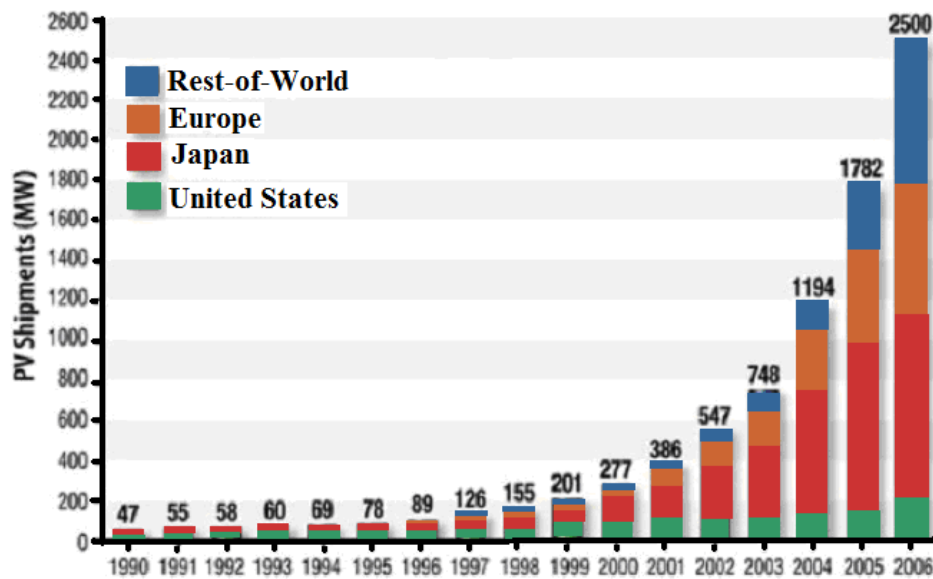


*Figure 1.2 World photovoltaic module production (in megawatts), total consumer, and commercial per country [1]). Most of this production is from crystalline or multicrystalline Si solar cells at present.*

During this time, the industry has grown from small satellite power supplies to utility-scale systems that are now produced and routinely installed in many countries of the world (figure 1.2, 1.3). Solar cells capable of producing power in excess of 500 MW were manufactured in 2002, providing electricity to a variety of applications ranging from small consumer products, power systems for isolated dwellings and remote industrial equipment to building-integrated solar arrays and megawatt-size power stations.



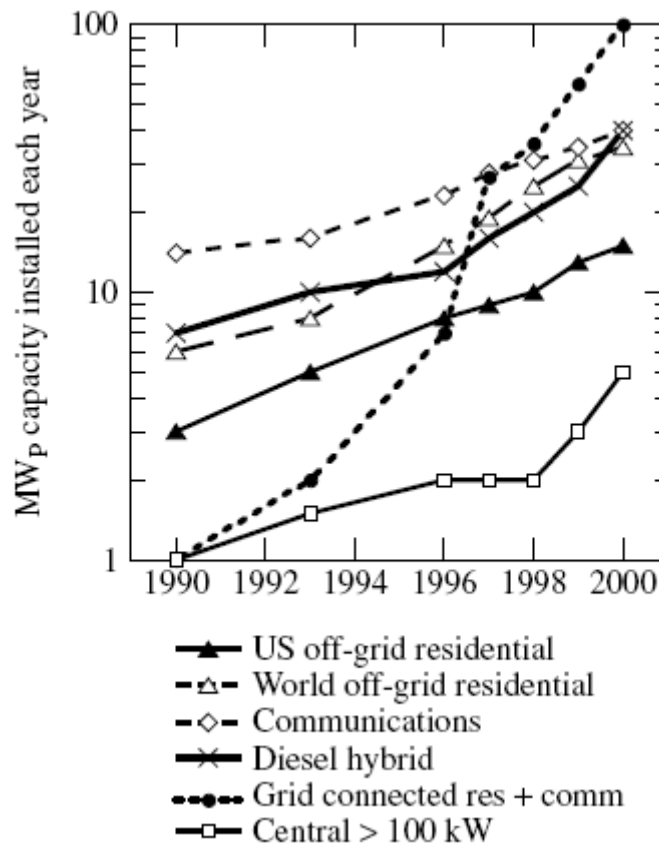


Figure 1.3 Trend in worldwide PV applications (From Reference [5] Maycock P, *Renewable Energy World* 3, 59–74 (2000)).

Solar electricity, also known as photovoltaics (PV), has shown since the 1970s that the human race can get a substantial portion of its electrical power without burning fossil fuels (coal, oil or natural gas) or creating nuclear fission reactions. Photovoltaics helps us avoid most of the threats associated with our present techniques of electricity production and also has many other benefits. Photovoltaics has shown that it can generate electricity for the human race for a wide range of applications, scales, climates, and geographic locations. Photovoltaics can bring electricity to a rural homemaker who lives 100 kilometers and 100 years away from the nearest electric grid connection in her country, thus allowing her family to have clean, electric lights instead of kerosene lamps, to listen to a radio, and to run a sewing machine for additional income. Or, photovoltaics can provide electricity to remote transmitter stations in the mountains allowing better communication without building a road to deliver

diesel fuel for its generator. It can help a major electric utility in Los Angeles, Tokyo, or Madrid to meet its peak load on hot summer afternoons when air conditioners are working full time. It allows homes and businesses a new level of guaranteed energy availability and security, and photovoltaics has been powering satellites orbiting the Earth or flying to Mars for over 30 years. The examples of possible application are presented at figure 1.4.

Photovoltaics is an empowering technology that allows us to do totally new things, as well as, do old things better. It allows us to look at whole new modes of supplying electricity to different markets around the world and out of the world (in outer space). It also allows us to do what we already do (generate electricity, which is distributed over the transmission grid) but to do it in a sustainable, pollution-free, equitable fashion. Why is photovoltaics equitable? Because nearly every one has access to sunlight.



*Figure 1.4 Solar roof and Solar Car Auburn University.*

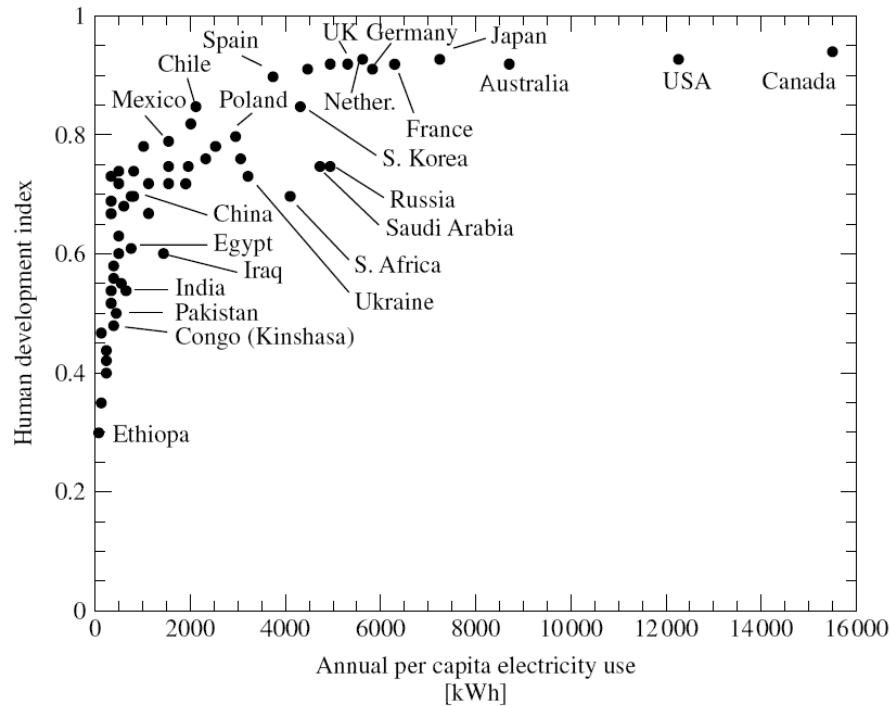


*Figure.1.5 Human development index (HDI) vs. per capita kW usage [3]*

Electricity is the most versatile form of energy we have. It is what allows citizens of the developed countries to have nearly universal lighting on demand, refrigeration, hygiene, interior climate control in their homes, businesses and schools, and widespread access to various electronic and electromagnetic media. Access to and consumption of electricity is closely correlated with quality of life. Figure 5 shows the Human Development Index (HDI) for over 60 countries, which includes over 90% of the Earth's population, versus the annual per capita electricity use [3]. The HDI is compiled by the UN and calculated on the basis of life expectancy, educational achievement, and per capita Gross Domestic Product. To improve the quality of life in many countries, as measured by their HDI, will require increasing their electricity consumption by factors of 10 or more, from a few hundred to a few thousand kilowatt-hrs (kWh) per year. How will we do it? Our choices are to continue applying the answers of the last century such as burning more fossil fuels (and releasing megatons of CO<sub>2</sub>, SO<sub>2</sub>, and NO<sub>2</sub>) or building more nuclear plants (despite having no method of safely disposing of the high-level radioactive waste) or to apply the new millennium's answer of

renewable, sustainable, nonpolluting, widely available clean energy like photovoltaics (figure 6) and wind. (Wind presently generates over a thousand times more electricity than photovoltaics but it is very site-specific, whereas photovoltaics is generally applicable to most locations.) The largest solar-power plant is located in Spain, Murcia (26 MW). Among top 50 solar-power plants, 31 plants are in Spain. (cf. Germany: 14, U.S.A : 2, Korea: 1, Japan: 1, and Portugal: 1) Korea's solar plant is the 7th in the world (see figure 1.7)



*Figure 1.6 Solar Arrays*



Germany, Brandis (24 MW)  
(40 MW is planned.)



Spain, Calaveron (21.2 MW)



Spain, Beneixama (20 MW)



Korea, Sinan (19.6 MW)

*Figure 1.7 Solar Cell Plants*

### 1.1 Solar Energy Conversion.

On Figure 1.8. Solar photons convert naturally into three forms of energy: electricity, chemical fuel, and heat that link seamlessly with existing energy chains.

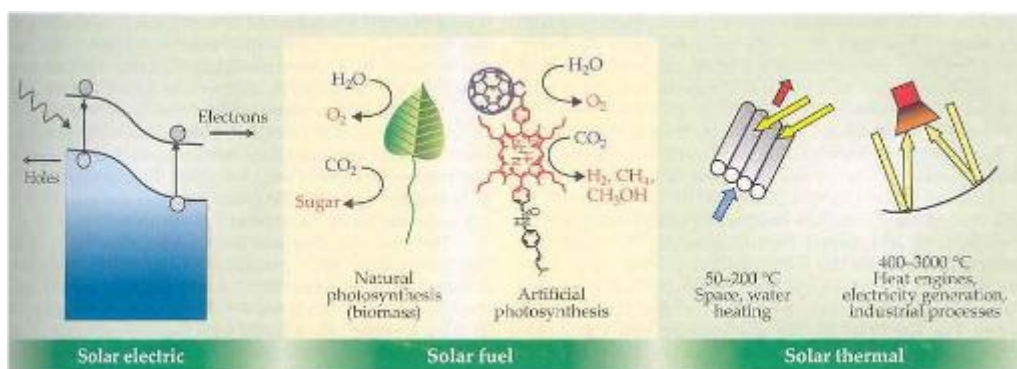


*Figure 1.8 Solar photons conversion*

Despite the enormous energy flux supplied by the Sun, the three conversion routes supply only a tiny fraction of our current and future energy needs. Solar electricity, at between 5 and 10 times the cost of electricity from fossil fuels, supplies just 0.015% of the world's electricity demand. Solar fuel, in the form of



biomass, accounts for approximately 11 % of world fuel use, but the majority of that is harvested unjustifiably. Solar heat provides 0.3% of the energy used for heating space and water. It is anticipated that by the year 2030 the world demand for electricity will double and the demands for fuel and heat will increase by 60%, The utilization gap between solar energy's potential and our use of it can be overcome by raising the efficiency of the conversion processes, which are all well below their theoretical limits[4].

Photovoltaic conversion efficiencies		
	Laboratory best*	Thermodynamic limit
Single junction		31%
Silicon (crystalline)	25%	
Silicon (nanocrystalline)	10%	
Gallium arsenide	25%	
Dye sensitized	10%	
Organic	3%	
Multijunction	32%	66%
Concentrated sunlight (single junction)	28%	41%
Carrier multiplication		42%
*As verified by the National Renewable Energy Laboratory. Organic cell efficiencies of up to 5% have been reported in the literature.		

## 1.2 History of photovoltaic's

The history of photovoltaics goes back to the nineteenth century, as shown in Table 1.1. The first functional, intentionally made PV device was by Fritts [5] in 1883. He melted Se into a thin sheet on a metal substrate and pressed a Au-leaf film as the top contact. It was nearly 30 cm<sup>2</sup> in area. He noted, “the current, if not wanted immediately, can be either stored where produced, in storage batteries, . . . or transmitted a distance and there used.” This man foresaw today’s PV technology and applications over a hundred years ago. The modern era of photovoltaics started in 1954 when researchers at Bell Labs in the USA

accidentally discovered that  $pn$  junction diodes generated a voltage when the room lights were on. Within a year, they had produced a 6% efficient Si  $pn$  junction solar cell [6]. In the same year, the group at Wright Patterson Air Force Base in the US published results of a thin-film heterojunction solar cell based on Cu<sub>2</sub>S/CdS also having 6% efficiency [7]. A year later, a 6% GaAs  $pn$  junction solar cell was reported by RCA Lab in the US [8]. By 1960, several key papers by Prince [9], Loferski [10], Rappaport and Wysoski [11], Shockley (a Nobel laureate) and Queisser [12], developed the fundamentals of  $pn$  junction solar cell operation including the theoretical relation between band gap, incident spectrum, temperature, thermodynamics, and efficiency. Thin films of CdTe were also producing cells with 6% efficiency [13]. By thistime, the US space program was utilizing Si PV cells for powering satellites. Since space was still the primary application for photovoltaics, studies of radiation effects and more radiation-tolerant devices were made using Li-doped Si [14]. In 1970, a group at the Ioffe Institute led by Alferov (a Nobel laureate), in the USSR, developed a heteroface GaAlAs/GaAs [15] solar cell which solved one of the main problems that affected GaAs devices and pointed the way to new device structures. GaAs cells were of interest due to their high efficiency and their resistance to the ionizing radiation in outer space. The year 1973 was pivotal for photovoltaics, in both technical and nontechnical areas. A significant improvement in performance occurring in 1973 was the “violet cell” having an improved short wavelength response leading to a 30% relative increase in efficiency over state-of-the-art Si cells [16]. GaAs heterostructure cells were also developed at IBM in the USA having 13% efficiency [17]. Also in 1973, a crucial nontechnical event occurred called the *Cherry Hill Conference*, named after the town in New Jersey, USA, where a group of PV researchers and heads of US government scientific organizations met to evaluate the scientific merit and potential of photovoltaics. The outcome was the decision that photovoltaics was worthy of government support, resulting in the formation of the US Energy Research and Development Agency, the world’s first government group whose mission included fostering research on renewable energy, which ultimately became the US Dept. of Energy. Finally, in October 1973, the first World Oil Embargo was instituted by the Persian Gulf oil

producers. This sent shock waves through the industrialized world, and most governments began programs to encourage renewable energy especially solar energy. Some would say this ushered in the modern age of photovoltaics and gave a new sense of urgency to research and application of photovoltaics in terrestrial applications. In the 1980s, the industry began to mature, as emphasis on manufacturing and costs grew. Manufacturing facilities for producing PV modules from Si wafer *pn* junction solar cells were built in the USA, Japan, and Europe. New technologies began to move out of the government, university and industrial laboratories, and into precommercialization or “pilot” line production. Companies attempted to scale up the thin-film PV technologies like a-Si and CuInSe<sub>2</sub>, which had achieved >10% efficiency for small area (1 cm<sup>2</sup>) devices made with carefully controlled laboratory scale equipment. Much to their disappointment, they found that this was far more complicated than merely scaling the size of the equipment. Most large US semiconductor companies, gave up their R/D efforts (IBM, General Electric, Motorola) lacking large infusions of private or government support to continue. One common result was the purchase of American companies and their technologies by foreign companies. In 1990, the world’s largest solar manufacturer was Arco Solar (CA, USA), owned by oil company Atlantic Richfield, which had c-Si and thinfilm a-Si in production and thin-film CuInSe<sub>2</sub> in precommercialization. They were sold to the German firm Siemens and renamed Siemens Solar (in 2001, the Dutch company Shell Solar would buy Siemens, becoming another large internationally based company with multiple PV technologies in production). Also in 1990, Energy Conversion Devices (MI, USA) formed a joint venture called United Solar Systems Corp. with the Japanese manufacturer Canon to commercialize ECD’s roll-to-roll triple-junction a-Si technology. In 1994, Mobil Solar Energy (MA, USA), which had developed a process for growing solar cells on Si ribbon (called the Edge defined film growth or EFG process) instead of more costly wafers, was sold to the German company ASE and renamed ASE Americas. The British solar company BP Solar acquired patents to electrodeposition of thin-film CdTe solar cells in 1989, when it’s parent company purchased the American oil giant Standard Oil of Ohio. At the same time, it acquired the patents of the University of New South Wales (Australia) to



fabricate the Laser-Grooved Buried-Grid (LGBG) cells, which became the most efficient silicon cells in fabrication. In 1996, it signed a license agreement with the Polytechnic University of Madrid (Spain) to exploit the Euclides concentration technology that used their LGBG cells as concentrator cells. In 1999, BP Solar acquired Solarex from Enron (another huge fossil-fuel energy company) that had crystalline and amorphous Si solar cell technology. Thus, BP Solar established themselves with manufacturing interests in all three technology options (standard Si wafers, thin films and concentrators).<sup>1</sup> Meanwhile, the Japanese PV industry began to take off. Production of c-Si modules and intensive research on thin-film technology in Japan led to many innovative device designs, improved materials processing, and growing dominance in the world PV market. Along with the maturing of the solar cell technology, the BOS needed to grow. Many products like inverters, which convert the DC power into AC power, and sun trackers had only limited application outside of a PV power system, so once again there was only limited technical and financial resources for development. In many system evaluations, the inverter was repeatedly identified as the weak link in terms of reliability and AC power quality [24]. Their costs have not fallen nearly as fast as those for the PV modules. While much effort and resources had been focused on the solar cell cost and performance, little attention had been paid to installation and maintenance costs. It was quickly discovered that there was room for much improvement. An early development that helped many companies was to sell PV cells for consumer-sized, small-scale power applications. The solar-powered calculator, pioneered by Japanese electronics companies as a replacement for battery-powered calculators in the early 1980s, is the best-known example. This led to the early use of thin-film a-Si PV cells for various applications. Another example was solar-powered outdoor lighting. These novel consumer applications, where portability and convenience were more valued than low price, allowed the PV companies to maintain some small income while continuing to develop power modules. Another application was the rural electrification of remote villages in an attempt to help roughly one-third of the world's citizens to gain access to a modest amount of modern communication and lighting. Most of these PV installations were very small, on the order of 10 to 40 W per household (100 times smaller

than the “needs” of a modern home in the developed world.) Most of these installations were funded by some international aid agency. Reviews and follow-up studies of these programs have indicated very large failure rates, primarily due to lack of technical infrastructure [25], training, cultural misunderstandings, design of the payment structure, and other nontechnical reasons [26]. Rarely have the PV modules failed. Even with subsidies from the international agencies, the high initial cost of ownership (\$100–1000) was still a major barrier in much of the world where this represents a year’s income for a family [27].

On the opposite end of the size scale were the MW-size PV plants installed by utilities in developed countries in the 1980s to evaluate their potential in two applications: as a peak-load-reduction technology, where the photovoltaics provides additional power primarily to meet the peak demand during the afternoon [28]; or as distributed generators, to reduce transmission and distribution losses [29]. Several American utilities investigated these applications, to assess the technical as well as financial benefits for photovoltaics in utility scale applications. Other novel configurations of grid-tied PV systems were evaluated as so-called “demand side management” options where the onsite distributed photovoltaics is used to reduce demand rather than increase supply [30].

Although American utilities lost interest in PV in the late 90s due to deregulation, gridconnected applications in Europe and Japan began to grow rapidly, primarily owing to strong government support. Both small- and large-scale grid connected PV installations are blossoming in these countries [31, 32].

Yet another important development in the application of PV in the late 1990s, was building integrated PV (BIPV [33]), where PV cells are incorporated into a standard building product, such as a window or a roof shingle, or into an architectural feature like an exterior sun awning or semitransparent skylight. In this way, the cost of the PV is partially offset by the cost of the building materials, which would have been required anyway, so the incremental cost of the photovoltaics is much lower. The success of grid-connected residential or BIPV commercial applications has been possible because several countries led by Germany have established high rates to pay for the PV electricity produced by

solar installations in private houses. In this scheme, the installation owner receives \$0.5/kWh for the electricity they feed into the public electric grid (as of 2001). But the owner buys the electricity consumed in their own house at the normal cost of  $\sim$  \$0.1/kWh from the grid. Additionally, German banks provided generous loans for purchasing the installation. Similar concepts are used in Spain, the Netherlands, and other countries in Europe. But, the success has been still bigger in Japan where homebuilders receive a rebate from the government for about 30% of the PV system cost. Then, their electric bill is determined by the utility using the “net metering” where the customer pays only the net difference between what they used and what they generated. Rebates and net metering are available in some, but not all, states in the USA as of 2002. Interestingly, government support of photovoltaics in Japan has been decreasing while the market for PV homes has continued showing an impressive growth rate.

*Table 1.1 Notable events in the history of photovoltaics*

- 1839 Becquerel (FR) discovered photogalvanic effect in liquid electrolytes
- 1873 Smith (UK) discovered photoconductivity of solid Se
- 1877 Adams and Day (UK) discover photogeneration of current in Se tubes;  
the first observation of PV effect in solids
- 1883 Fritts (US) makes first large area solar cell using Se film
- 1954 First 6% efficient solar cells reported: Si (Bell Lab, USA) and  
Cu<sub>2</sub>S/CdS (Air Force, USA)
- 1955 Hoffman Electronics (USA) offers 2% efficient Si PV cells at \$1500/W
- 1958 NASA Vanguard satellite with Si backup solar array
- 1959 Hoffman Electronics (USA) offers 10% efficient Si PV cells
- 1963 Sharp Corp (JP) produces first commercial Si modules
- 1966 NASA Orbiting Astronomical Observatory launched with 1 kW array
- 1970 First GaAs heterostructure solar cells by Alferov, Andreev et al. in the  
USSR
- 1972 First PV conference to include a session on terrestrial applications  
(IEEE)
- 1973 A big year in photovoltaics: Worldwide oil crisis spurs many nations to

consider renewable energy including photovoltaics; Cherry Hill Conference in USA (established photovoltaics' potential and legitimacy for government research funding); World's first solar powered residence (University of Delaware, USA) built with  $\text{Cu}_2\text{S}$  (not c-Si!) solar modules

- 1974 Project Sunshine initiated in Japan to foster growth of PV industry and applications; Tyco (USA) grows 2.5 cm wide Si ribbon for photovoltaics, first alternative to Si wafers

- 1975 First book dedicated to PV science and technology by Hovel (USA)

- 1980 First thin-film solar cell >10% using  $\text{Cu}_2\text{S}/\text{CdS}$  (USA)

- 1981 350 kW Concentrator array installed in Saudi Arabia

- 1982 First 1 MW utility scale PV power plant (CA, USA) with Arco Si modules on 2-axis trackers

- 1984 6 MW array installed in Carrisa Plains CA, USA [18]

- 1985 A big year for high-efficiency Si solar cells: Si solar cell >20% under standard sunlight (UNSW, Australia) [19] and >25% under 200X concentration (Stanford Univ. USA) [20]

- 1986 First commercial thin-film power module, the a-Si G4000 from Arco Solar (USA)

- 1987 Fourteen solar powered cars complete the 3200 km World Solar Challenge race (Australia) with the winner averaging 70 kph

- 1994 GaInP/GaAs 2-terminal concentrator multijunction >30% (NREL, USA) [21]

- 1995 “1000 roofs” German demonstration project to install photovoltaics on houses, which triggered the present favorable PV legislation in Germany, Japan and other countries

- 1996 Photoelectrochemical “dye-sensitized” solid/liquid cell achieves 11% (EPFL, Switzerland) [22]

- 1997 Worldwide PV production reaches 100 MW per year

- 1998  $\text{Cu}(\text{InGa})\text{Se}_2$  thin-film solar cell reaches 19% efficiency (NREL, US) [23] comparable with multicrystalline Si. First concentrating array for space launched on Deep Space 1 by US (5 kW using high efficiency GaInP/GaAs/Ge triple junction cells)



contacts with one becoming the *n*-side (lots of negative charge), the other the *p*-side (lots of positive charge).

Silicon (Si), one of the most abundant materials in the Earth's crust, is the semiconductor used in crystalline form (c-Si) for 90% of the PV applications today. Surprisingly, other semiconductors are better suited to absorb the solar energy spectrum. These other materials are in development or initial commercialization today. Some are called thin-film semiconductors, of which amorphous silicon (a-Si), copper indium gallium diselenide (Cu(InGa)Se<sub>2</sub> or CIGS), and cadmium telluride (CdTe). Solar cells may operate under concentrated sunlight using lenses or mirrors as concentrators allowing a small solar cell area to be illuminated with the light from larger area. This saves the expensive semiconductor but adds complexity to the system, since it requires tracking mechanisms to keep the light focused on the solar cells when the sun moves in the sky. Silicon and III-V semiconductors, made from compounds such as gallium arsenide (GaAs) and gallium indium phosphide (GaInP) are the materials used in concentrator technology that is still in its demonstration stage. For practical applications, a large number of solar cells are interconnected and encapsulated into units called PV modules, which is the product usually sold to the customer. They produce DC current that is typically transformed into the more useful AC current by an electronic device called an inverter. The inverter, the rechargeable batteries (when storage is needed), the mechanical structure to mount and aim (when aiming is necessary) the modules, and any other elements necessary to build a PV system are called the balance of the system (BOS).

As mentioned before, solar cells are made of materials called semiconductors, which have weakly bonded electrons occupying a band of energy called the *valence band*. When energy exceeding a certain threshold, called the *band gap energy*, is applied to a valence electron, the bonds are broken and the electron is somewhat "free" to move around in a new energy band called the *conduction band* where it can "conduct" electricity through the material. Thus, the free electrons in the conduction band are separated from the valence band by the band gap (measured in units of electron volts or eV). This energy needed to free the electron can be supplied by photons, which are particles of light. Photon is

absorbed and energy is given to an electron in the crystal lattice. Usually this electron is in valence band, tightly bound in covalent bonds. Energy given by the photon “excites” it into the conduction band. Covalent bond now has one fewer electron (hole). Bonded electrons of neighboring atoms can move into the ‘hole’, leaving another hole behind – hole can propagate through lattice. Free electrons flow through the material to produce electricity. Positive charges (holes) flow in opposite direction. Different PV materials have different band gap energies. Photons with energy equal to the band gap energy are absorbed to create free electrons. Photons with less energy than the band gap energy pass through the material. Photons absorption creates mobile electron-hole pairs (see figure 1.9).

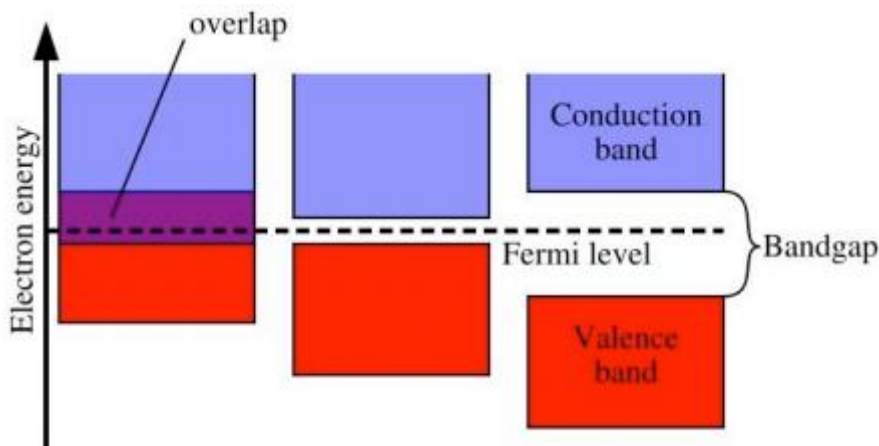


*Figure 1.9 Photons absorption in different materials*

Figure 1.10 shows the idealized relation between energy (vertical axis) and the spatial boundaries (horizontal axis). When the solar cell is exposed to sunlight, photons hit valence electrons, breaking the bonds and pumping them to the conduction band. There, a specially made selective contact that collects conduction-band electrons drives such electrons to the external circuit. The electrons lose their energy by doing work in the external circuit such as pumping water, spinning a fan, powering a sewing machine motor, a light bulb, or a computer. They are restored to the solar cell by the return loop of the circuit via a second selective contact, which returns them to the valence band with the same energy that they started with. The movement of these electrons in the external

circuit and contacts is called the *electric current*.

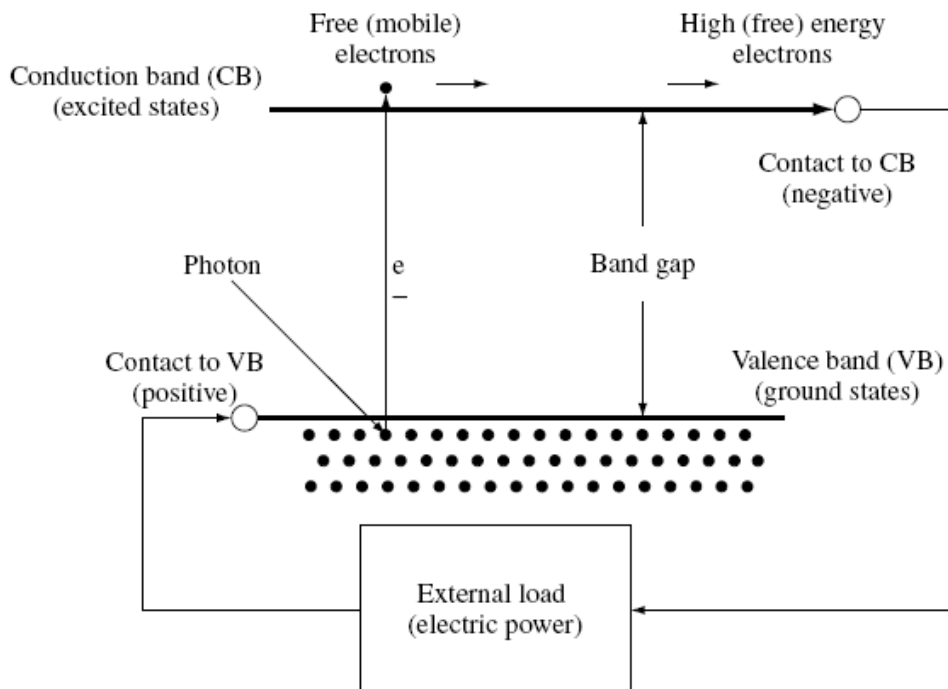


Figure 1.10 Schematic of a solar cell. Electrons are pumped by photons from the valence band to the conduction band. There they are extracted by a contact selective to the conduction band (an *n*-doped semiconductor) at a higher (free) energy and delivered to the outside world via wires, where they do some useful work, then are returned to the valence band at a lower (free) energy by a contact selective to the valence band (a *p*-type semiconductor)

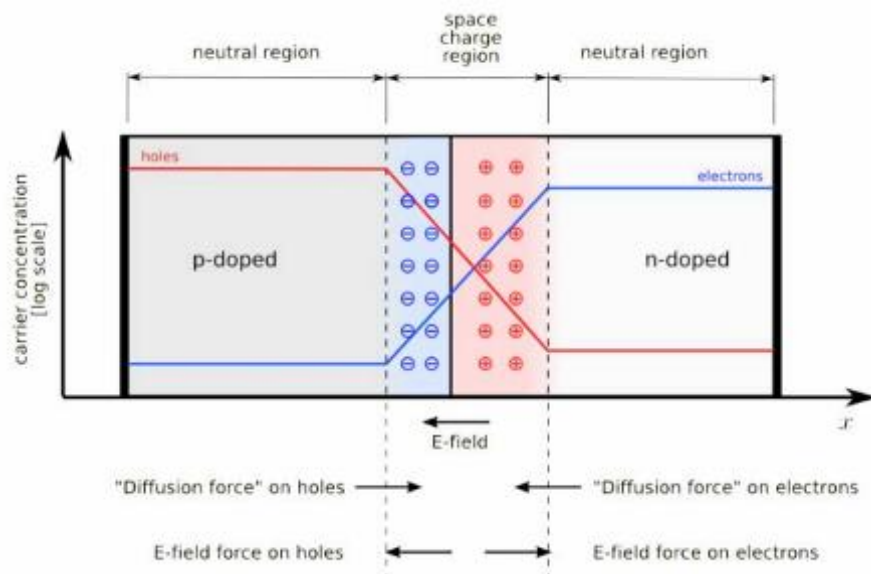


Figure 1.11 The *p-n* junction in thermal equilibrium.



The potential at which the electrons are delivered to the external world is slightly less than the threshold energy that excited the electrons; that is, the band gap. Thus, in a material with a 1 eV band gap, electrons excited by a 2 eV photon or by a 3 eV photon will both still have a potential of slightly less than 1 V (i.e. the electrons are delivered with an energy of 1 eV). The electric power produced is the product of the current times the voltage; that is, power is the number of free electrons times their potential.

Sunlight is a spectrum of photons distributed over a range of energy. Photons whose energy is greater than the band gap energy (the threshold energy) can excite electrons from the valence to conduction band where they can exit the device and generate electrical power. Photons with energy less than the energy gap fail to excite free electrons. Instead, that energy travels through the solar cell and is absorbed at the rear as heat. Solar cells in direct sunlight can be somewhat (20–30°C) warmer than the ambient air temperature. Thus, PV cells can produce electricity without operating at high temperature and without mobile parts. These are the salient characteristics of photovoltaics that explain safe, simple, and reliable operation.

The p-n junction in thermal equilibrium w/ zero bias voltage applied. Electrons and holes concentration are reported respectively with blue and red lines. Gray regions are charge neutral. Light red zone is positively charged; light blue zone is negatively charged. Electric field shown on the bottom, the electrostatic force on electrons and holes and the direction in which the diffusion tends to move electrons and holes.

At the Figure 1.11 is presented p-n junction in thermal equilibrium w/ zero bias voltage applied. Electrons and holes concentration are reported respectively with blue and red lines. Gray regions are charge neutral. Light red zone is positively charged; light blue zone is negatively charged. Electric field shown on the bottom, the electrostatic force on electrons and holes and the direction in which the diffusion tends to move electrons and holes.

There is much more to sunlight than the portion of the spectrum that can see. Sunlight incident on the earth's surface can deliver up to 1000 W of power to a 1

m<sup>2</sup> area. If the solar energy incident on 1 m<sup>2</sup> could be converted into electricity with 100% efficiency, the resulting electrical power could operate ten 100 W light bulbs, a toaster, or a computer with monitor and printer. Unfortunately, the conversion efficiency from solar energy to electrical energy is nowhere near 100%. Direct conversion efficiencies from 5% to 20% are typical.

Photovoltaic cells convert sunlight directly to electricity. Their principle of operation is the same as that for photodiode light detectors. As mentioned before these devices are fabricated from semiconductor materials, such as silicon (Si), gallium arsenide (GaAs), and copper sulfide (Cu<sub>2</sub>S) and other materials. In a photovoltaic cell, incident sunlight photons remove electrons in the semiconductor from their bonds so that they are free to move around inside the semiconductor material. The empty electron bond states that are left behind act like positive charges, are also mobile, and are called “holes.”

Photovoltaic cells generally consist of at least two thin layers, one atop the other, and each having different, intentionally added impurities called dopants (see Figure 1.12). The result is that one layer is “n-type,” having an excess of (negative) electrons, while the other layer is “p-type,” having an excess of positive holes. This two-layer structure, called a p-n junction, results in a “built-in” electric field. When photons create free electrons and holes near the p-n junction, the built-in electric field makes them move in opposite directions; the electrons move to the n side and the holes move to the p side. Thus, an electromotive force (emf) is generated between the p and n layers, with the p side positive and the n side negative. If wires connect the p and n sides to a “load,” for example a light bulb or a calculator, a voltage exists across that load and an electric current flows through the load. The power delivered to the load is simply:

$$P = V \times I$$

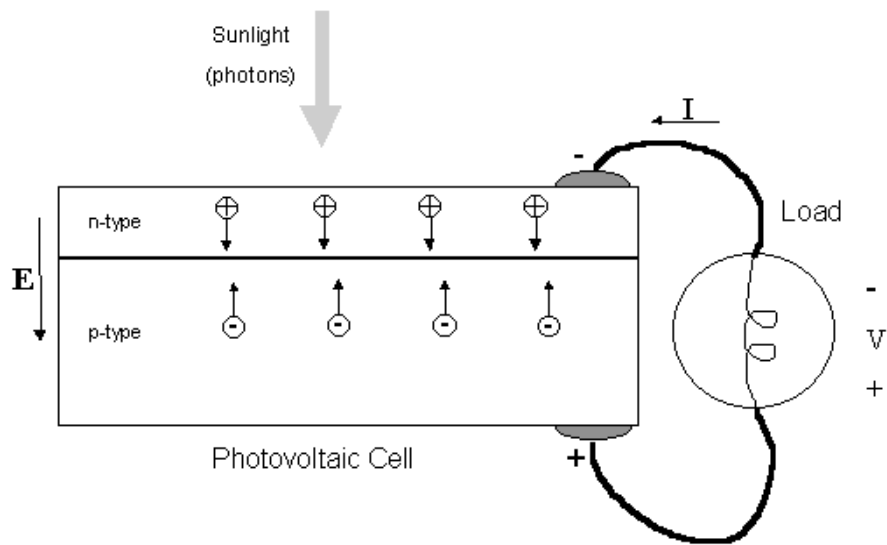


*Figure 1.12 Photovoltaic cell connected to a load (an incandescent*

Thus, a photovoltaic cell converts optical energy directly to electrical energy.

Specific data about a photovoltaic cell is often presented in the form of a characteristic curve, as shown in Figure 1.13. The curve gives the current supplied by the cell as a function of the voltage supplied by the cell, for a known value of photovoltaic irradiance. Two quantities identified on this current-voltage (or I-V) characteristic curve are frequently used when describing the performance of a photovoltaic cell. These quantities are  $V_{oc}$  and  $I_{sc}$ .

When no load is connected to a photovoltaic cell, the device is said to be in an “open circuit” condition, meaning that no current can flow. A good voltmeter acts like an open circuit, and if it is connected to the cell terminals, the voltage measured is called the open circuit voltage, denoted  $V_{oc}$  in Figure 1.14. When the photovoltaic cell terminals are connected with a wire, the device is said to be in a “short circuit” condition, meaning that the voltage between the terminals is zero. The current that flows through the wire is called the short circuit current, denoted  $I_{sc}$  in Figure 1.14. A good ammeter acts nearly like a short circuit (that is, it has a very low resistance), so if the photovoltaic cell terminals are connected to an ammeter, the measured current is nearly  $I_{sc}$ . (See figure 1.14)

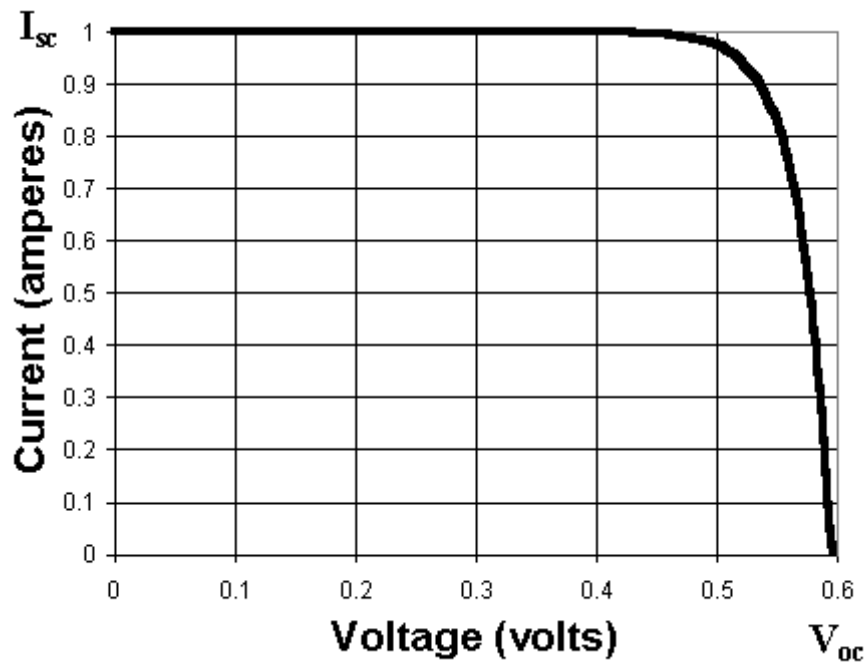


Figure 1.13. Current vs. voltage characteristics for an “ideal” silicon photovoltaic cell. Notice that the short circuit current and the open circuit voltage are identified on the axes. The actual quantitative data depends on the irradiance and the cell area.

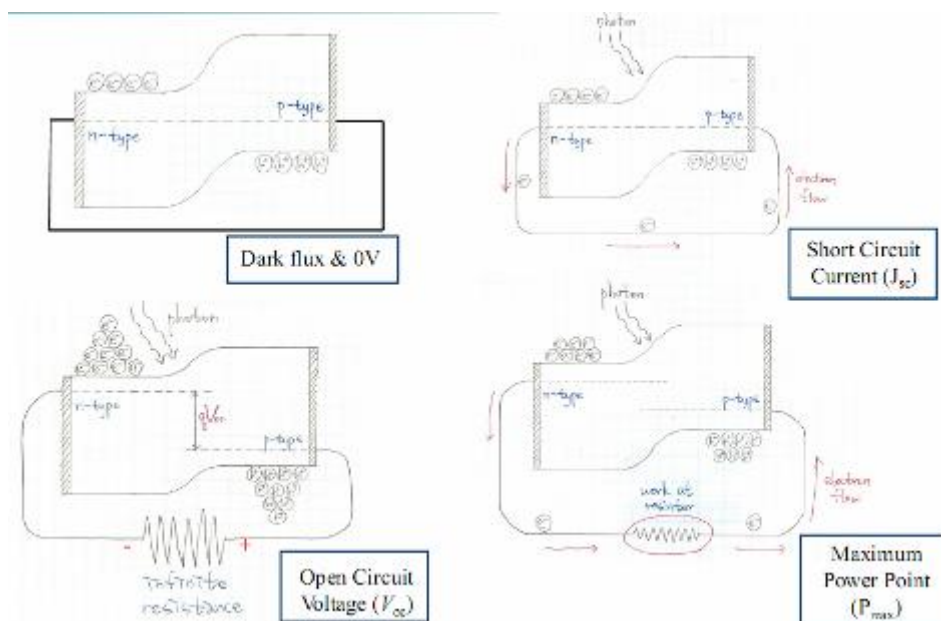


Figure 1.14 Energy Band of p-n Junction Solar Cell, Short circuit current  $I_{sc}$  open circuit voltage  $V_{oc}$ .

The available solar radiation is frequently described by giving an air mass value, such as “air mass zero” (AM0), “air mass one” (AM1), “air mass 1.5” (AM1.5), etc. AM0 refers to the solar radiation available just outside the earth’s atmosphere. The corresponding total solar irradiance is  $1353 \text{ W/m}^2$ , and this value is called the “solar constant.” AM1 refers to the solar radiation available at the earth’s surface when the sun is at the zenith (total solar irradiance  $\sim 925 \text{ W/m}^2$ ). In general, when  $x > 1$ , AMx is defined to be the solar radiation available at the earth’s surface when the sun is at angle

$$\theta = \cos^{-1} \frac{1}{x}$$

from the zenith. Rewriting this equation, you can say that the air mass value is

$$x = \frac{1}{\cos \theta}$$

If you sketch this situation (as you will be asked to do later), you will see that  $x$  is the ratio of the length of the path that sunlight takes through the atmosphere to the vertical thickness straight up through the atmosphere from sea level. The value of  $x$  obviously depends on the latitude, the season (solar declination), and the hour of the day. The *effective* value of  $x$  also depends on the altitude, the weather, and the air quality.

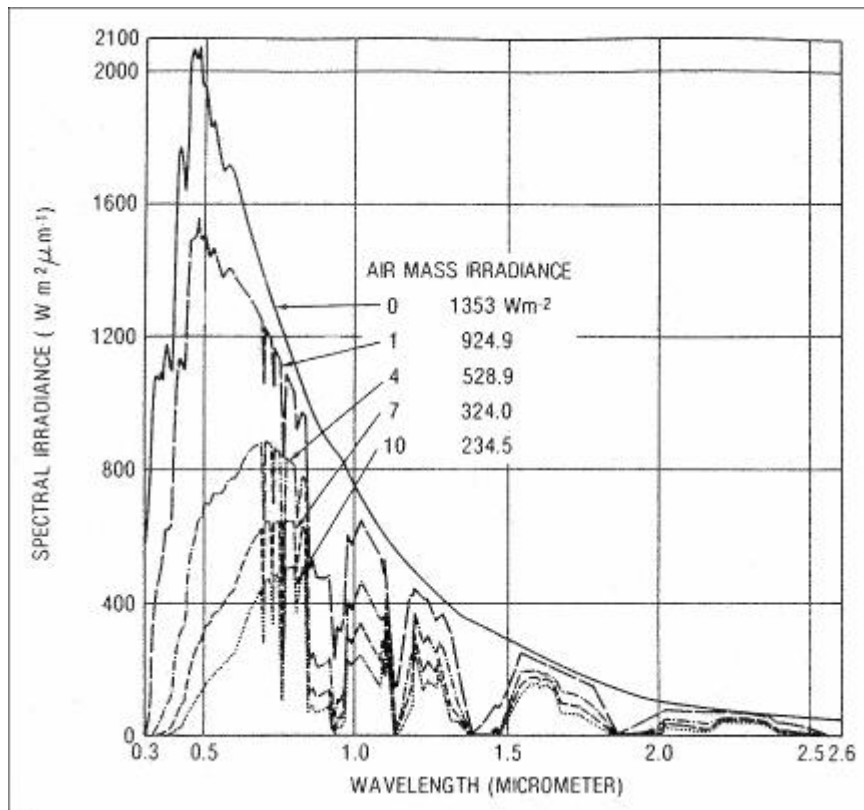


*Figure 1.15. Solar spectral irradiance curves for several air mass values and very clear air. Each total irradiance value listed in the table in the center of the graph is equal to the total area under the corresponding curve.*

Sunlight consists of a broad spectrum of wavelengths, not all of them visible, with substantial power density from 300 nm (ultraviolet) to 2000 nm (infrared), as shown in Figure 1.15. Not all of the light that hits a photovoltaic cell is absorbed in a useful manner. Some is reflected and some of the photons do not have sufficient energy to remove electrons from their bonds. A significant fraction of the energy in sunlight is in the form of photons having energies less than 1 eV (or wavelengths greater than 1240 nm), as shown in Figure 1.18. However, in silicon, photons having energy less than 1.12 eV (or wavelengths greater than 1110 nm) cannot create free electrons and holes. Consequently, these photons are “wasted.” The highest energy photons in sunlight are also wasted or underutilized for reasons that are beyond the scope of this experiment. There are also other energy loss mechanisms in photovoltaic cells. For example, the quality of the p-n junction is an important factor. The net result is that the efficiency of most silicon

photovoltaic cells is less than 20%, meaning that less than 20% of the incident optical power can be converted to electrical power.

An important feature of any power source is that to extract the maximum power from it, the load must be “matched” to the source. In the case of a photovoltaic cell that is used to power some device, such as a DC motor, a light bulb, or a calculator, the “effective resistance” of the load must be properly chosen to get the maximum power (and highest efficiency) from the cell.

Main types of solid state cell structures are following.

### 1.3.1 P- or n-type contact metal/semiconductor Schottky [34-38]

On figure Figure 1.16 are presented energy band structures of metal-semiconductor photovoltaic.

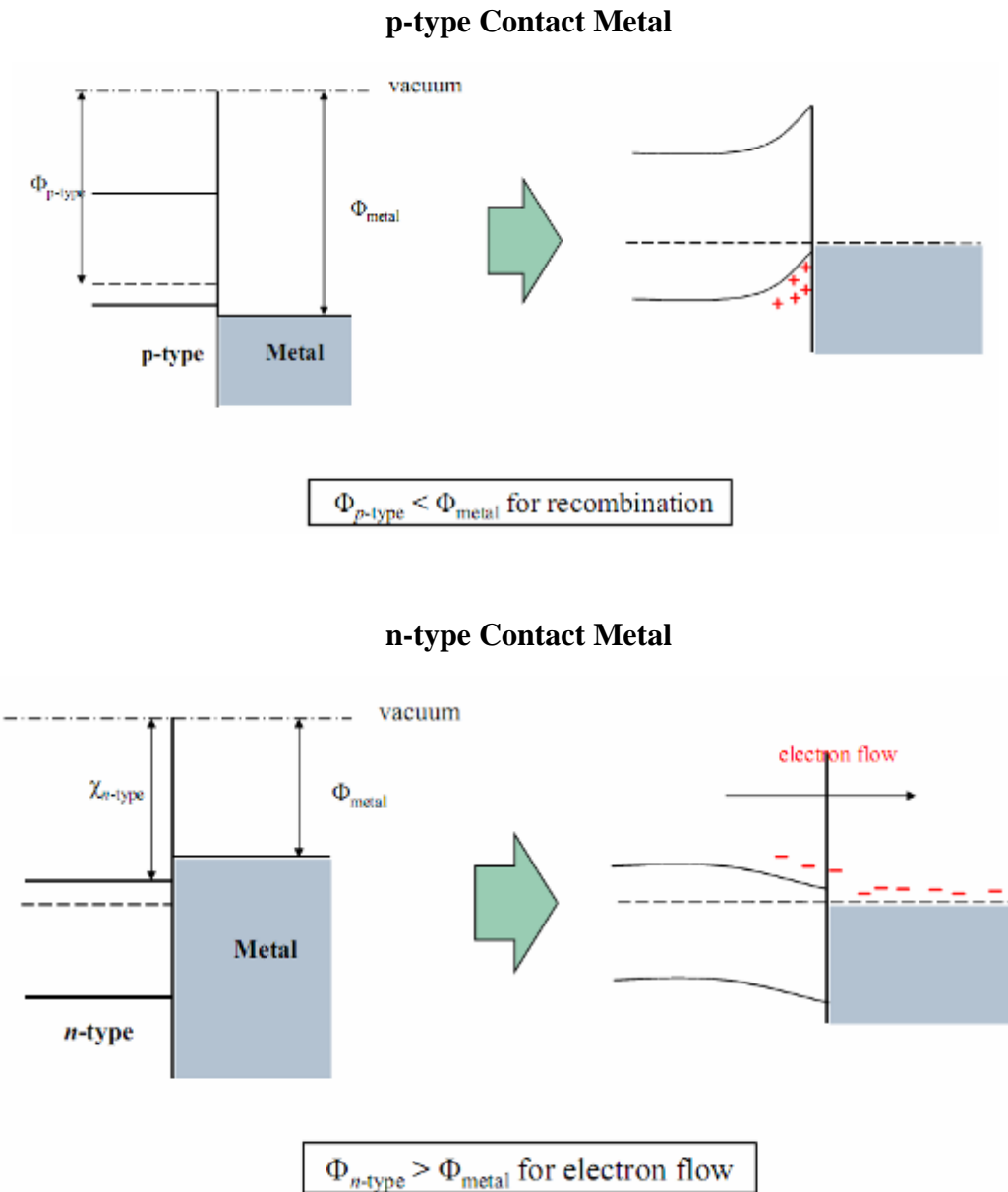


Figure 1.16 Metal n- p- semiconductor contact Schottky solar cell

### 1.3.2 Homojunction Device.

-Single material altered so that one side is p-type and the other side is n-type (see Figure 1.17):



-p-n junction is located so that the maximum amount of light is absorbed near it.

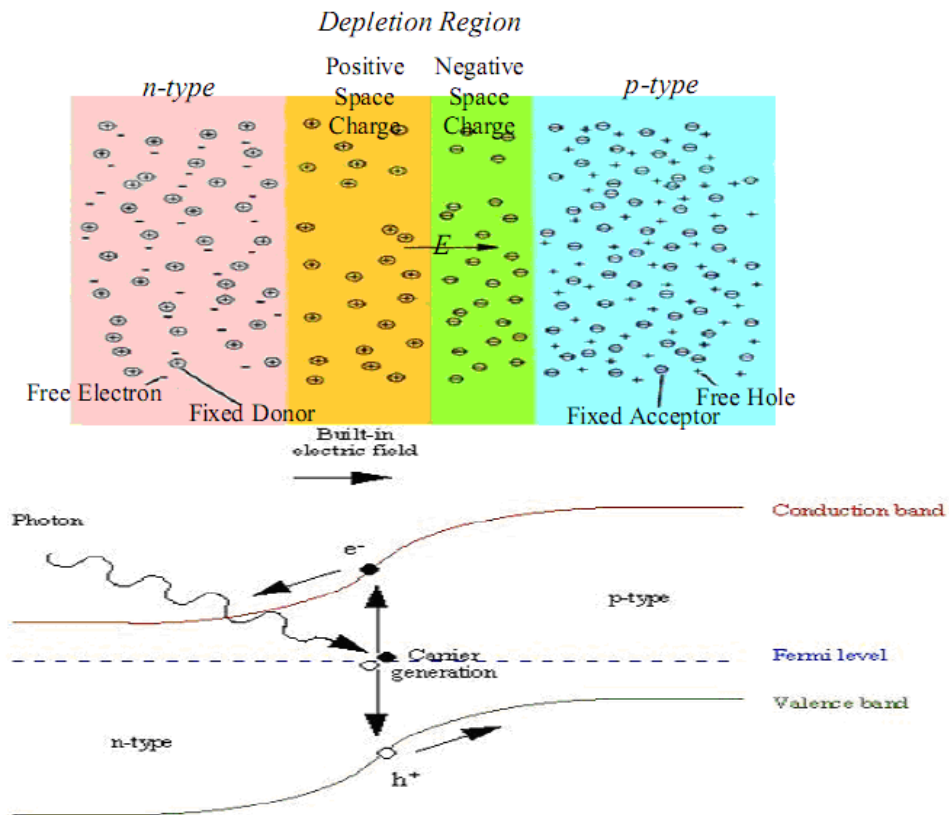


Figure 1.17 P-n Junctions: Essential for Solar Cell

### 1.3.3 Heterojunction solar cell

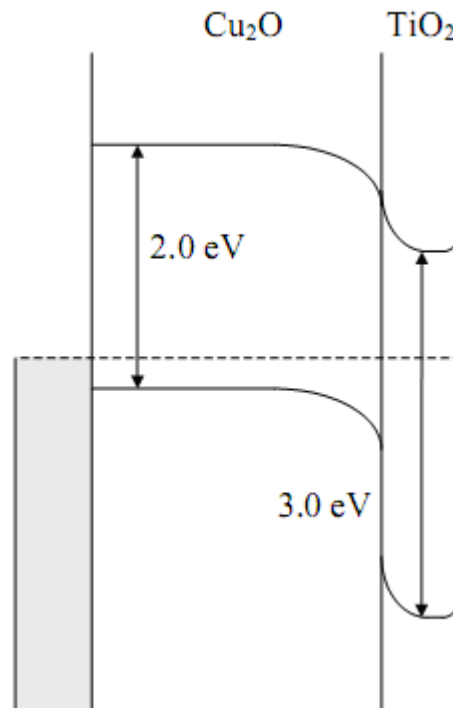


Figure 1.18 Energy band diagram for the  $\text{Cu}_2\text{O}/\text{TiO}_2$  heterostructure. [39]

- Junction is formed by contacting two different semiconductors.
- Top layer - high bandgap selected for its transparency to light.
- Bottom layer - low bandgap that readily absorbs light.

### 1.3.4 P-i-n and n-i-p devices.

- A three-layer sandwich is created,
- Contains a middle intrinsic layer between n-type layer and p-type layer.
- Light generates free electrons and holes in the intrinsic region.

### 1.4 Advantages and disadvantages of photovoltaics.

Photovoltaics is the technology that generates direct current (DC) electrical power measured in Watts (W) or kiloWatts (kW) from semiconductors when they are illuminated by photons. As long as light is shining on the solar cell (the name for the individual PV element), it generates electrical power. When the light stops,

the electricity stops. Solar cells never need recharging like a battery. Some have been in continuous outdoor operation on Earth or in space for over 30 years.

*Table 1.2 lists some of the advantages and disadvantages of photovoltaics.*

*Note, that they include both technical and nontechnical issues.*

Advantages of photovoltaics	Disadvantages of photovoltaics
Fuel source is vast and essentially infinite	Fuel source is diffuse (sunlight is a relatively low-density energy)
No emissions, no combustion or radioactive fuel for disposal (does not contribute perceptibly to global climate change or pollution)	
Low operating costs (no fuel)	High installation costs
No moving parts (no wear)	
Ambient temperature operation (no high temperature corrosion or safety issues)	
High reliability in modules (>20 years)	Poorer reliability of auxiliary (balance of system) elements including storage
Modular (small or large increments)	
Quick installation	
Can be integrated into new or existing building structures	
Can be installed at nearly any point-of-use	Lack of widespread commercially available system integration and installation so far
Daily output peak may match local demand	Lack of economical efficient energy storage
High public acceptance	
Excellent safety record	

Often, the advantages and disadvantages (Table 1.2) of photovoltaics are almost completely opposite of conventional fossil-fuel power plants. For example, fossil-fuel plants have disadvantages of: a wide range of environmentally hazardous emissions, parts which wear out, steadily increasing fuel costs, they are not modular (deployable in small increments), and they suffer low public opinion (no one wants a coal burning power plant in their neighborhood). Photovoltaics suffers none of these problems. The two common traits are that both PV and fossil fueled power plants are very reliable but lack the advantage of storage.

Notice that several of the disadvantages are nontechnical but relate to economics and infrastructure. They are partially compensated for by a very high public acceptance and awareness of the environmental benefits. During the late 1990s, the average growth rate of PV production was over 33% per annum.

## **1.5 Thin film photovoltaic and materials**

### **1.5.1 Thin film**

The definition of thin film solar cell technology given by Chopra *et al.* [40] provides a good starting point and also yields a criterion to discriminate the term ‘thin film’ from ‘thick film’. They define a thin film as a material ‘created *ab initio* by the random nucleation and growth processes of individually condensing/reacting atomic/ionic/molecular species on a substrate. The structural, chemical, metallurgical and physical properties of such a material are strongly dependent on a large number of deposition parameters and may also be thickness dependent. Thin films may encompass a considerable thickness range, varying from a few nanometers to tens of micrometers and thus are best defined in terms of the production processes rather than by thickness. One may obtain a thin material (not a thin film) by a number of other methods (normally called thick-film techniques) such as by thinning bulk material, or by depositing clusters of microscopic species in such processes as screen-printing, electrophoresis, slurry spray, plasma gun, ablation, etc.’ The given definition still leaves room for a broad field of technologies to deposit the thin film (plasma, sputtering, evaporation, deposition from the liquid phase, etc.) and to tailor its electrical and morphological properties (crystalline, amorphous and intermediary forms). For the inorganic non-crystalline Si materials and technologies is presented in [40].

### **1.5.2 Thin film photovoltaic materials**

Conventionally, photovoltaic materials use inorganic semiconductors. The semiconductors of interest allow the formation of charge-carrier separating junctions. The junction can be either a homojunction (like in Si) or a heterojunction with other materials to collect the excess carriers when exposed to light. In principle, a large number of semiconductor materials are eligible, but only a few of them are of sufficient interest. Ideally, the absorber material of an efficient terrestrial solar cell should be a semiconductor with a bandgap of 1–1.5 eV with a high solar optical absorption ( $10^4 - 10^5 \text{ cm}^{-1}$ ) in the wavelength region of 350–1000 nm, a high quantum yield for the excited carriers, a long diffusion length low recombination velocity. If all these constraints are satisfied and the

basic material is widely available, the material allows in principle the manufacturing of a thin-film solar cell device. From the point of view of processing, manufacturing and reproducibility, *elemental* semiconductors provide a simple and straightforward approach to manufacture thin-film solar cells. The first material at hand is the material which dominates the PV market nowadays: silicon.

Crystalline silicon is a semiconductor material with a bandgap of 1.1 eV. Because of the indirect bandgap character of silicon for photons with energy lower than 3.4 eV, it is clearly not an ideal material for thin-film solar cells. Nevertheless, there is a substantial R&D effort being put into developing thin-film solar cells based on crystalline Si. The thin film of crystalline Si can be grown either by low-temperature deposition techniques which yield microcrystalline Si or by high-temperature techniques. In the latter case the material properties of the grown crystalline Si film are similar to the properties of bulk crystalline Si solar material. Because of its relatively low absorption coefficient, crystalline Si layers have to be at least 30  $\mu\text{m}$  thick to absorb sufficient light unless optical enhancement techniques are used to improve the effective absorption. As a result of its high refractive index (4) crystalline Si allows efficient optical confinement with optical pathlength enhancements up to a factor 50. It will come as no surprise to the reader that optical enhancement is therefore a substantial part of the research in the field of thin-film crystalline Si.

Si can also be deposited in its amorphous form. Amorphous Si as such is a material of little use for photovoltaics because of the extremely high dangling bond density and intragap state density in the material ( $>10^{19} \text{ cm}^{-3}$ ), resulting in immediate recombination of photoexcited excess carriers and pins the Fermi level, excluding controllable doing. The properties of amorphous Si are drastically improved by alloying it with H, which passivates most of the dangling bonds and reduces the intragap state density to  $10^{16} \text{ cm}^{-3}$  or less. The alloying with H takes place in a natural way during the deposition of the film which is deposited by cracking a Si precursor (most often  $\text{SiH}_4$ ) by means of a plasma and the material formed is denoted as a-Si:H. In comparison with crystalline Si, a-Si:H has a number of properties which make it attractive as an absorber layer for thin-film

solar cells. The bandgap of a-Si:H, is to some extent tailorable by the method and conditions of deposition. In addition, the material is relatively easy to dope, which allows the manufacturing of homojunction devices and, last but not least, it has a high optical absorption coefficient over the wavelength range of interest. Under suitable deposition conditions and strong hydrogen dilution, nanocrystalline and microcrystalline materials are obtained. While the crystallite size and volume fraction are very small, these crystallites catalyze the crystallization of the remainder of the amorphous matrix upon annealing. Microcrystalline materials deposited by this method are found to have less defect density and are more stable against light degradation compared with a-Si. Recently developed improved efficiency materials consist of this heterogeneous mixture of the amorphous and an intermediate range order microcrystalline material. a-Si:H has emerged as an attractive material which, for some time, was challenging the supremacy of crystalline Si cells in the Eighties. Because of stability problems and the lower efficiencies as compared with crystalline Si, the market share of a-Si:H based thin-film solar cells remained limited. Nevertheless, the present shortage of crystalline Si and the developments around multijunction structures and micro/nanocrystalline Si extensions provide a new opportunity for this technology to make it to the marketplace. Recently also carbon came into the picture as a candidate material for thin-film solar cells, with first results being reported for boron-doped diamond-like carbon [41] and fullerene films [42].

III–V compound materials like GaAs, InP and their derived alloys and compounds, which most often have a direct bandgap character, are ideal for photovoltaic applications, but are far too expensive for large-scale commercial applications, because of the high cost of the necessary precursors for the deposition and the deposition systems itself. The deposition systems for these materials are either based on molecular beam epitaxy or metalorganic chemical vapour deposition.

More appealing from the point of view of ease of processability and cost of material and deposition are the “II–VI compound materials” like CdTe or variations on this like CuInSe<sub>2</sub>.

The interest in these materials for thin-film solar cell manufacturing is essentially based on two elements. Because of the chemical structure of these materials the internal (grain boundaries, interfaces) and external surfaces are intrinsically well passivated and characterized by a low recombination velocity for excess carriers. The low recombination activity at the grain boundaries allows high solar cell efficiencies even when the material is polycrystalline with grain sizes in the order of only a few  $\mu\text{m}$ . This is to be contrasted with crystalline Si where grain boundaries are normally characterized by a high recombination velocity. Moreover, the polycrystallinity allows a large number of substrates (glass, steel foil, . . . ) and is compatible with low-cost temperature deposition techniques, as there is no need for epitaxial growth or high temperatures to obtain large grain sizes. A second important property is the possibility to tailor the bandgap e.g. replacing Se by S in  $\text{CuInSe}_2$  results in a material with a higher bandgap. This property allows one to build in bandgap gradients aiding the collection of excess carriers and, ultimately, could even be used to develop multijunction solar cells. With the increasing number of components in ternaries and even quaternaries, the number of possible material combinations increases. An interesting alternative to inorganic semiconductor absorbers are organic semiconductors, which combine interesting optoelectronic properties with the excellent mechanical and processing properties of polymeric/plastic materials. In organic semiconductors, absorption of photons leads to the creation of bound electron–hole pairs (excitons) with a binding energy of 0.5 eV rather than free charges. The excitons carry energy, but no net charge, and have to diffuse to dissociation sites where their charges can be separated and transported to the contacts. In most organic semiconductors, only a small portion (30 %) of the incident light is absorbed because the majority of semiconducting polymers have bandgaps higher than 2.0 eV.

The typically low charge-carrier and exciton mobility require the active absorber layer thickness to be less than 100 nm. This thickness is sufficient to absorb most of the incident solar photons if light trapping is used, although the lowrefractive index calls for adapted approaches.

More importantly, organic semiconductors can be processed from solutions at or near room temperature on flexible substrates using simple, cheap and low-energy deposition methods such as spinning or printing thereby yielding cheaper devices. Even though the efficiency of these devices is poor at present, they may find immediate applications for disposable solar cell based small power applications. Among the major issues to be addressed before reasonable market penetration of the organic devices takes place are the improvement of the stability of conjugate polymers, and the matching of the bandgap of the organic materials with the solar spectrum for higher conversion efficiency by using blended/composite polymers and suitable dyes.

### **1.5.3 Different thin film solar cell technologies**

Based on the available semiconductor absorber materials discussed above one can go systematically over the different related thin film solar cell technologies.

#### **1.5.3.1 Crystalline silicon thin film solar cells**

There are a large variety of crystalline Si thin film approaches. The one that is closest to the classical crystalline Si solar cell structure is the ‘epitaxial solar cell approach’. The basic idea behind this thin film approach, is the realization of a thin crystalline Si film of high electronic quality on a low cost Si carrier substrate by means of epitaxial growth as shown in Figure 1.19a. The depicted structure strongly resembles the structure of a classical, self supporting bulk crystalline Si solar cell and, as a result, the basic solar cell process to produce the solar cell is very similar to the practices used within the photovoltaics (PV) industry nowadays. Its structural similarity would result in a low acceptance threshold in the solar cell industry, which is presently still dominated by crystalline Si. A special case is the ‘lift-off approach’ where, by means of a crystalline Si template based on porous Si, a thin cell is realized which is lifted off before or after the cell process.

The epitaxial cell approach relies on the use of a Si substrate. There are also attempts to develop thin film crystalline Si solar cell structures on non-Si substrates. Because of the high temperatures ( $>600\text{ }^{\circ}\text{C}$ ) used for the film deposition, glass is not suitable as a substrate. Rather, low cost ceramic substrates



and graphite are the substrates of choice. In case the substrate is nonconductive, novel solar cell structures are needed to contact the solar cell as shown in Figure 1.19b. The Si layer, deposited on top of these substrates, will be micro or polycrystalline with a grain size determined by the growth temperature and supersaturation conditions during the silicon layer deposition. It turns out to be difficult to realize solar cells with proper energy conversion efficiencies in material with a grain size of 1–10  $\mu\text{m}$ , although substantial progress has been made recently in this field. On ceramic substrates which withstand high temperatures, liquid phase recrystallization is often applied to increase the final grain size, whereas laser recrystallization and rapid thermal annealing is being developed for substrates which can only withstand process temperatures  $>650\text{ }^{\circ}\text{C}$  for a limited time.

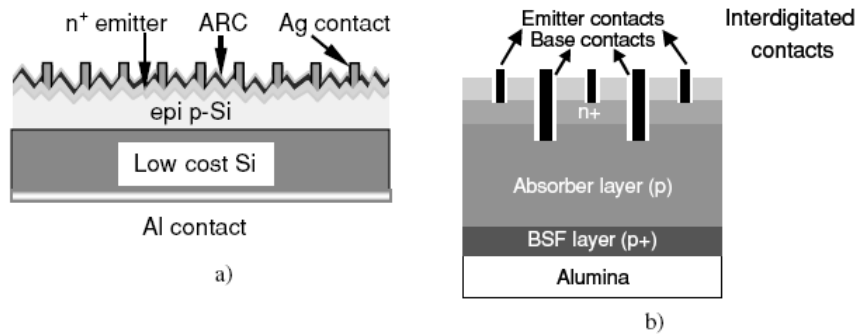


*Figure 1.19 a) Schematic of a epitaxial cell on a highly doped low cost Si substrate (ARC stands for anti-reflective coating; b) Novel solar cells with a nonconductive substrate.*

### 1.5.3.2 Amorphous and microcrystalline silicon thin film solar cells

Because a-Si:H can be doped efficiently p- and n-type, the cell structure is based on a homojunction. As a result of the short carrier lifetime and the low carrier mobility collection by pure diffusion of excess carriers is not very effective. Therefore a-Si:H solar cells also include a drift zone to improve the carrier collection. As a result the structure of the solar cell device is a p-i-n-structure where an intrinsic a-Si:H layer is sandwiched between a thin n+ and p+-type layer. Because of the low doping in the intrinsic part, the electrical field will extend all over the intrinsic layer. As mentioned before, the properties of the material and the junction device are severely affected by the light induced creation

of metastable defects, known as the Staebler–Wronski effect. Light induced degradation of a-Si:H devices and, as a consequence, a reduction of the electrical field in the intrinsic part of the cell is tackled by reducing the a-Si:H layer thickness so that the photogenerated carriers need to move only a short distance before they reach the electrode. However, thinning down also results in lower light absorption and thus optical confinement techniques employing diffusely reflecting front and back contacts are required to increase the effective layer thickness in order to absorb the photons. Over a period of time, extensive research and development work on deposition techniques and device structure have resulted in development of single junction and multijunction devices with high efficiency and moderately good stability. A typical a-Si:H based multijunction solar cell structure is shown in Figure 1.20 a.

As the cost of the Ge precursors is high and the electronic quality of the a-SiGe:H layers is lower than for a-Si:H layers, a lot of effort is being done in replacing the a-SiGe:H part of the cell by other solutions like microcrystalline Si. This leads to the ‘micromorph’ cell concept combining an a-Si:H topcell with a microcrystalline Si bottomcell as shown in Figure 1.20 b.

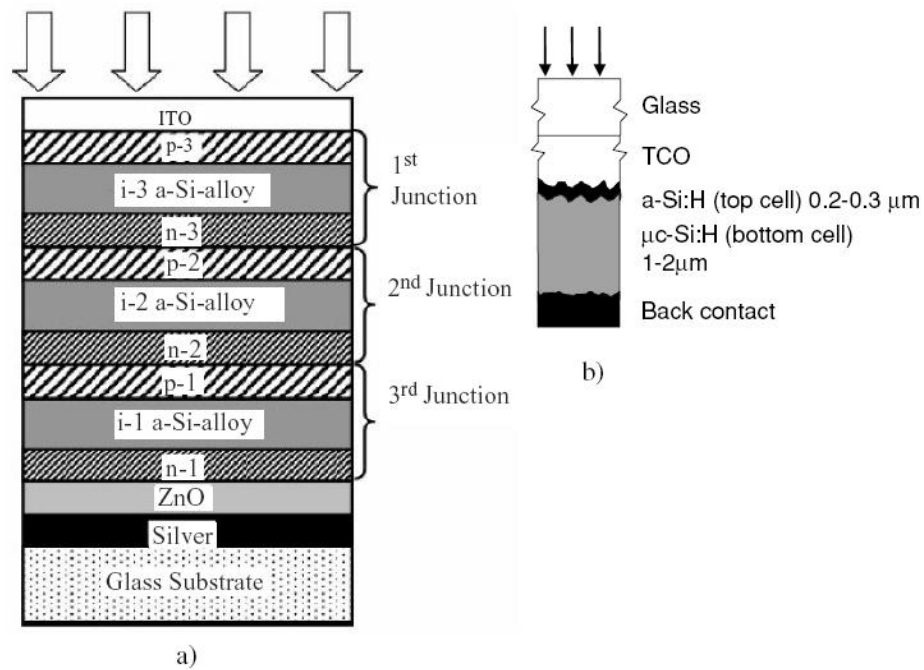
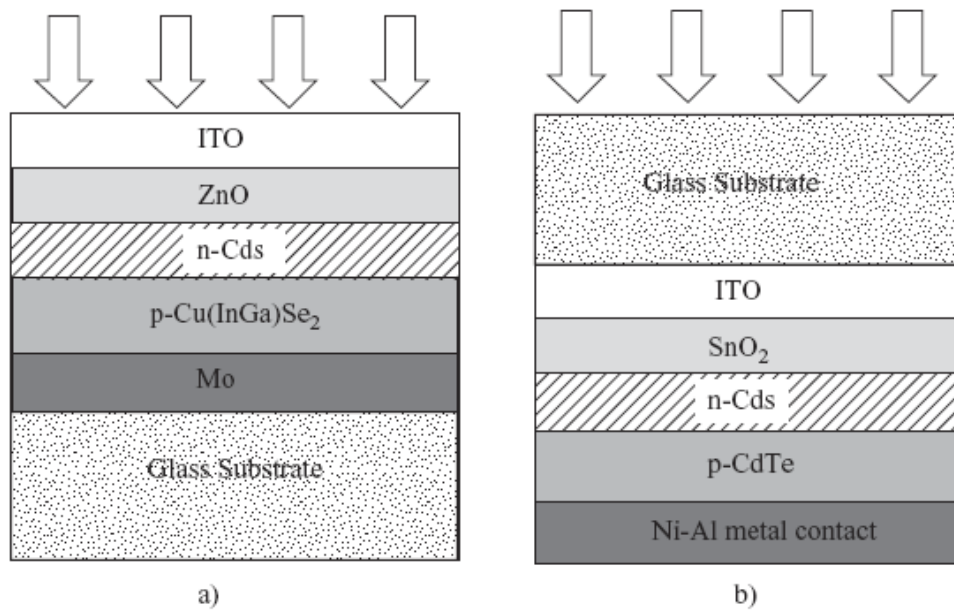


Figure 1.20 a) Cross section of typical multijunction solar cell based on a-Si:H. In order to improve the performance the lower a-Si:H subcells are sometimes replaced by a-SiGe:H alloys; b) In the second approach (the micromorph concept) improved stability is obtained by replacing the a-Si:H bottom cell by a microcrystalline Si solar cell (taken from [40]).

### 1.5.3.3 Copper indium gallium selenide and cadmium telluride solar cell structures

Both superstrate and substrate device structures are currently being pursued for copper indium gallium selenide ( $\text{CuIn}(\text{Ga})\text{Se}_2$ , CIGS) device fabrication. The film growth and interdiffusion and hence the device properties are dependent on the device structure. These CIGS solar cells, based on the superstrate structure, are inferior to the substrate structure, because of the interdiffusion of CdS during high temperature CIGS film growth. A best device efficiency of 10.2% was reported for the superstrate structure. On the other hand, a substrate configuration like the one shown in Figure 1.22 a with CdS buffer layer resulted in a 19.2% efficiency device. Cadmium telluride devices are fabricated preferably in the superstrate configuration because the CdTe surface is exposed for contacting. In

addition, the benign feature of CdS diffusion during the processing reduces the lattice mismatch between CdTe and CdS. Cadmium telluride solar cells use borosilicate glass for high temperature deposition (600°C) and soda lime glass for low temperature deposition (60–500°C). Cadmium telluride has also been deposited on thin metallic foils such as stainless steel, Mo, Ni and Cu. Molybdenum is best suited for CdTe deposition, owing to better thermal matching.



*Figure 1.22 a) Schematic view of the typical substrate structure of CIGS solar cells; b) Schematic view of the typical superstrate structure of CdTe solar cell[40].*

#### **1.5.3.4 Basic structure of thin film organic solar cells**

The term ‘organic solar cell’ has to be correctly defined. The term covers those photovoltaic devices where the organic layer is an essential part of the photovoltaic process. The basic steps in photovoltaic conversion are light absorbance, charge carrier generation, charge carrier transport and extraction/injection of charge carriers through externally accessible contacts. More specifically, the term ‘organic solar cell’ is applicable whenever at least the

two first steps are being realized by means of an organic layer. By this definition, full organic devices as well as hybrid devices are being covered.

Organic solar cells have already been the subject of R&D efforts for a long time because of the potentially very low cost of the active layer material. Originally, most of the attempts to realize organic solar cell devices were based on essentially the same concepts as thin film p-n or p-i-n devices. This resulted in energy conversion efficiencies of about 1% with the main limitation being the short exciton diffusion length and insufficient exciton dissociation. The breakthrough for solar cells incorporating an organic part came with the advent of concepts that radically deviated from the planar hetero- or homojunction solar cells. The generic idea behind these concepts is the existence of a bulk distributed interface to capture the excited carrier and to increase the exciton dissociation rate. The ‘Graetzel cell’ is a prominent example of this generic idea belonging to the class of hybrid cells. Within the pores of a porous  $\text{TiO}_2$  layer a monolayer of an organic sensitizer is adsorbed on the pore walls as shown in Figure 1.23 a. After absorption of a photon, the excited electron within the sensitizer molecule is immediately transferred to the conduction band of  $\text{TiO}_2$ , after which the electron diffuses through the porous network to the contact. The oxidized sensitizer molecule is reduced to the original state by supplying electrons through a liquid electrolyte within the pores. Cells based on this hybrid concept show confirmed energy conversion efficiencies up to 11% for small area cells, whereas upscaled modules exhibit efficiencies between 5 and 7%. Standing issues of this type of hybrid solar cells are the replacement of the sensitizer by a material with increased absorption in the red and infrared part of the spectrum, the replacement of the liquid electrolyte by a solid state hole conductor and the improvement of the cell stability.

The full organic counterpart of the hybrid cell is the bulk donor–acceptor heterojunction concept (see Figure 1.23 b), which is based on blends of two organic compounds, one with donor character, the other with acceptor properties. The excitons dissociate very efficiently at the interfaces between donor and acceptor phases and flow through the percolated donor and acceptor subnetworks to the contacts, which are carrier selective. Efficiencies up to 5% were reported

for this type of cell based on the P3HT/PCBM donor–acceptor couple. This acceptor (PCBM) is often used, because exciton dissociation turns out to be extremely efficient with transfer times in the 100 fs range. Alternatives in which PCBM is replaced by a polymer with acceptor characteristics were also reported (e.g. CN-PPV/MEH-PPV pair). For this type of organic cell, standing issues are the extension of the active layer absorbance towards the red and infrared range, the use of materials with higher mobilities (in this context also tests with liquid crystal materials should be mentioned) and the critical issue of stability. In the framework of improving the red and infrared sensitivity of the donors, the majority of the activities are directed towards thiophenes, which could also improve stability.

For the sake of completeness it should be mentioned that there is also a nonorganic counterpart of these three-dimensional junction devices. These are the ETA (extremely thin absorber) structures, shown in Figure 1.23c.

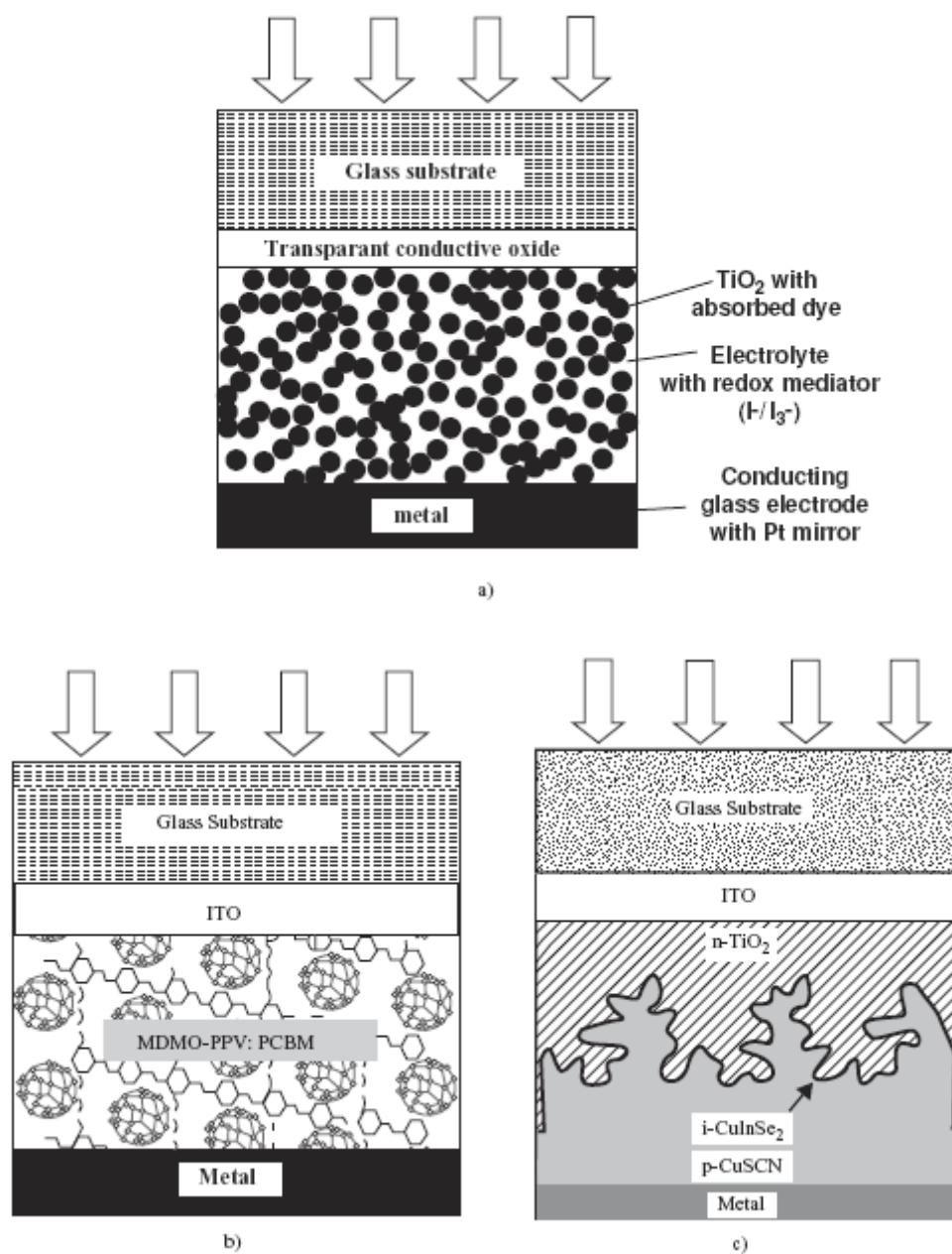


Figure 1.23 Structures of a) the Graetzel cell based on nanocrystalline porous  $\text{TiO}_2$ ; b) the bulk donor–acceptor heterojunction concept; c) the structure of ETA cells.

## **Conclusions**

Photovoltaics constitute a new form of producing electric energy that is environmentally clean and very modular. In stand-alone installations, it must use storage or another type of generator to provide electricity when the sun is not shining. In grid-connected installations storage is not necessary: in the absence of sunlight, electricity is provided from other (conventional) sources.

PV electricity is highly appreciated by the public. It is unique for many applications of high social value such as providing electricity to people who lack it in remote areas.

Often, international donor agencies are providing the funding, as many of the users are very poor. Photovoltaics is very suitable as the power supply for remote communication equipment. Its use is increasing rapidly to produce electricity in grid-connected houses and buildings in industrialized countries, despite a 5 to 10 times higher cost than conventional electricity. Often, publicly funded programs are required to enable photovoltaics to compete by partially offsetting its higher costs.

Largely, because of grid-connected PV applications such as homes and businesses, the expansion of the PV market has been very rapid in the last years of the twentieth century and it is expected to continue during the next few years of the twenty-first century. Then, the growth will probably continue at a slower pace unless new technological advances are developed and commercialized. In that case, growth could accelerate. Photovoltaics is poised to become a large global high-tech industry, manufacturing and selling modules in nearly every country. Governments and entrepreneurs should be aware of this. Public R&D support has always been generous. It must continue to be so for those countries that want to maintain leadership in this technology. Partial subsidization of PV installations is permitting an unprecedented development of the PV industry and will also help the industry of the countries involved in this endeavor to take the lead.

Crystalline Si technology, both monocrystalline and multicrystalline is today clearly dominant, with about 90% of the market. It will remain dominant at least for the next ten years. The trend is towards the multicrystalline option. Si is one of



the most abundant elements in the Earth's crust but the purified Si used in today's solar cells is obtained primarily as off-grade poly-Si and scrap wafers from the microelectronic industry. Soon it will not be enough for the growing PV industry. Thus, some concerns exist regarding a shortage of the purified silicon for the PV industry. However, it is doubtful that Si technology will be able to reach competition with conventional electricity. Consequently, low-cost alternatives and high-efficiency novel concepts, many already in development, are needed.

Thin-film technology is one of the candidates to take over from Si technology in the long-term. There are many technological options regarding thin-film materials and methods of deposition but their primary claim to the throne currently occupied by Si is that they can be ultimately produced at much lower cost.

Concentration of sunlight is another candidate for mass penetration of photovoltaics, although it will not be easily accepted for the grid-connected houses, one of the most promising applications today. Concentrators will probably find incipient niche markets in big stand-alone applications or as small, central-power plants during the present decade. Finally, new materials and device designs based on III-V semiconductor alloys, such as GaInP allowing more efficient use of the solar spectrum are now being developed for space applications. With the use of concentrators, they may be of interest for terrestrial applications, with the potential of reaching competitive costs with conventional electricity. Other options, such as quantum dots and dye-sensitized solar cells, are still in the initial research phase. They must compete not only with the ubiquitous Si but also with the other options, mentioned above for funding for further development.

Thus, photovoltaics possesses a panoply of novel technologies that almost ensures that alternatives will be available when the current Si wafer technology cannot reach prices low enough to compete with conventional electricity. If this happens, a strong industry and infrastructure – first developed for the Si technology – will be able to seamlessly take this new PV technology and apply it worldwide. In any case, the present “subsidies” to research or application must be considered as public investment in a policy with strong public support and long-term human benefits.

The widespread contribution of PV electricity in electric grids will require a new type of grid management that can accept small generators as well as small consumers. On the other hand, hybrid forms of electricity generation, including photovoltaics, will play an important role in the future development of stand-alone applications and minigrids. The general cost reduction will make photovoltaics available to more and more people in developing countries helping their development with little degradation of air quality associated with fossil-fuel generators.

In summary, it is very likely that photovoltaics will become in the next half century an important source of world electricity. Public support and global environmental concerns will keep photovoltaics viable, visible, and vigorous both in new technical developments and user applications. Nations which encourage photovoltaics will be leaders in this shining new technology, leading the way to a cleaner, more equitable twenty-first century, while those that ignore or suppress photovoltaics will be left behind in the green, economic energy revolution.

## 2 Materials, experimental setup and methods.

### 2.1 Copper (I) oxide (Cu<sub>2</sub>O):

Copper oxide or cuprous oxide (Cu<sub>2</sub>O) or Cuprite:

It is an oxide of copper. It is insoluble in water and organic solvents. Copper oxide is found as the mineral cuprite in some red-colored rocks. When it is exposed to oxygen, copper will naturally oxidize to copper (I) oxide, albeit at a very slow rate. With further heating, copper (I) oxide will form copper (II) oxide.

Molar mass **143.09 g/mol**

Appearance **brownish-red solid**

Density **6.0 g/cm<sup>3</sup>**

Melting point **1235 °C, 1508 K**

Boiling point **1800 °C, 2073 K**

Solubility in water: **Insoluble in water and soluble in acid**

The cuprous oxide (Cu<sub>2</sub>O) electronic and transport properties presented in [43,44].

Cu<sub>2</sub>O is usually p-type. As grown material has high resistivity ( $\rho > 10^6 \Omega\text{cm}$ ). Resistivity depends strongly on annealing or photoexcitation [43]. The resistivity (lowest bulk resistivity) are 42  $\Omega\text{ cm}$  at  $T = 300\text{ K}$  for sputtered film [45], 35  $\Omega\text{ cm}$  at  $T = 300\text{ K}$  undoped [46] and 9  $\Omega\text{ cm}$   $T = 300\text{ K}$  Cd-doped.

Thermal activation energy of the conductivity  $E_a$  0.20-0.38 eV at  $T = 298\text{ K}$  for oxygen saturated sample [47], 0.48-0.70 eV at  $T = 298\text{ K}$  sample annealed at 1050°C [47] and 0.49-0.70 eV at  $T = 298\text{ K}$  sample annealed at 1050°C and 750°C [47], 0.01 eV at  $T < 200\text{ K}$  sputtered film [45], 0.18 eV at  $T > 200\text{ K}$  sputtered film [45].

Minority carrier lifetime  $\tau$  is  $10^{-8}$ - $10^{-9}\text{ s}$  at  $T = 300\text{ K}$  [48].

Photoexcited carrier lifetime is  $10^{-8}\text{ s}$  at  $T = 4\text{ K}$  for cyclotron resonance [49].

Activation energies of electronic conductivity in Cu<sub>2</sub>O have been ascribed to numerous deep levels (reviews in [43,44]). Optical absorption [50] or emission in the near infrared [51,52,53] shows the existence of three maxima of the density of states, the first near 1.7 eV, at 1.4 eV and 0.8 eV; sometimes a weaker peak at 1.5 eV. The highest energy corresponds well to the deep acceptor level near 0.4 eV.

Photoconductivity [54,55]. Photovoltaic effect [46]. Photoelectric effect [56], "Photomemory" (persistent photoconductivity) has been explained using two levels at  $E_c = -1.1$  eV (A trap) and  $E_c = -1.0$  eV (B trap) [57,58]. Temperature dependence of the electrical conductivity and switching phenomena in  $\text{Cu}_2\text{O}$  single crystal are reported from the ambient to 200 °C [47].

Mobility is  $\mu = 70 \text{ cm}^2 \text{ V}^{-1} \text{ s}^{-1}$  at  $T = 298 \text{ K}$  in oxygen saturated sample [47].

The structure and crystallographic properties are following [59,60]:

#### **Name and formula**

Mineral name: Cuprite, syn

Empirical formula:  $\text{Cu}_2\text{O}$

#### **Crystallographic parameters**

Crystal system: Cubic

a (Å): 4.2696

b (Å): 4.2696

c (Å): 4.2696

Most important Peak (see Figure 2.1)

No.	h	k	l	d [Å]	2Theta[deg]	I [%]
2	1	1	1	2.46500	36.419	100.0
3	2	0	0	2.13500	42.298	37.0

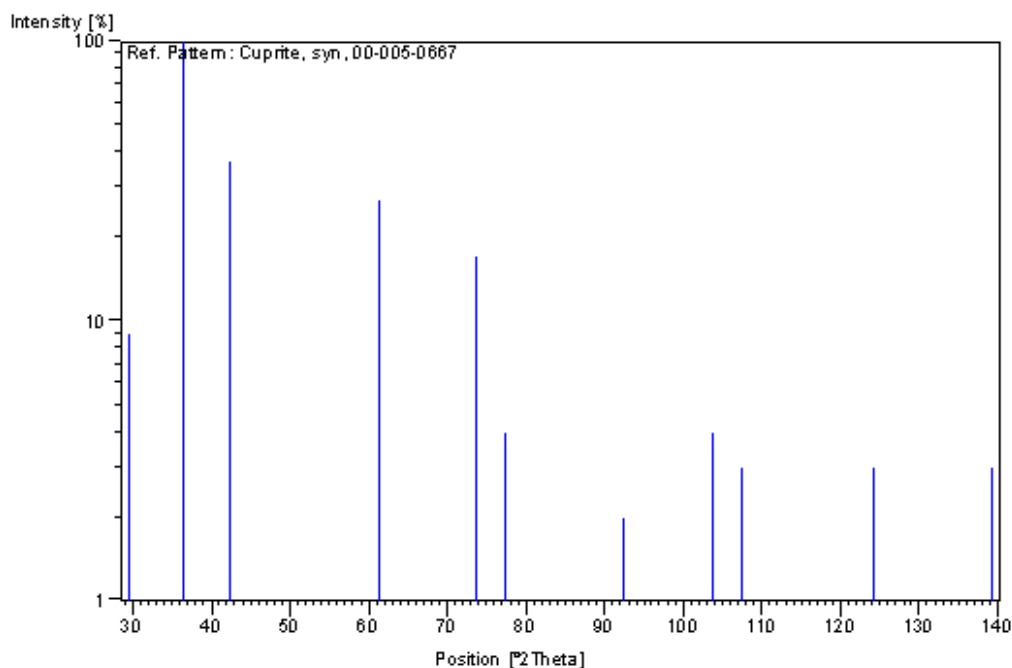


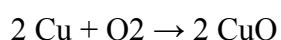
*Figure 2.1 Copper (I) oxide XRD Stick Pattern*

Cuprous oxide ( $\text{Cu}_2\text{O}$ ) is a well-known p-type semiconductor with a direct band gap of 2.0 eV.  $\text{Cu}_2\text{O}$  thin films have high optical transmittance at wavelengths above 600 nm with a slightly yellowish appearance and a high optical absorption coefficient at the wavelengths below.  $\text{Cu}_2\text{O}$  in thin-film form is an attractive material for many device applications because of its p-type semi-conductivity, high absorption coefficient, abundant availability, non-toxic nature, and low production cost.  $\text{Cu}_2\text{O}$  thin films find diverse applications in oxygen and humidity sensors, electro chromic devices [61], and photovoltaic devices such as thin-film hetero-junction solar cells [62–66].  $\text{Cu}_2\text{O}$  thin films can be prepared by various techniques such as activated reactive evaporation [67], thermal oxidation [68], vacuum evaporation [69], chemical vapour deposition [70], sol–gel process [71,72], electro-deposition [73], and sputtering [74–79]. Among these deposition techniques, direct-current (dc) reactive magnetron sputtering is one of the best techniques for preparation of  $\text{Cu}_2\text{O}$  thin films due to the advantages of high deposition rates, excellent uniformity over large area substrates, and good controllability on the chemical composition and the physical properties of sputter-

deposited thin films. The physical properties of the sputter deposited thin films are highly influenced by the deposition parameters such as oxygen partial pressure, oxygen flow rate, substrate temperature, substrate bias voltage, sputtering pressure, and sputtering power[80-83].

## 2.2 Copper (II) oxide (CuO)

Copper (II) oxide or cupric oxide (CuO) is the higher oxide of copper. As a mineral, it is known as tenorite. It is a black solid with an ionic structure, which melts above 1200 °C with some loss of oxygen. It can be formed by heating copper in air:



Empirical formula is CuO and chemical formula is CuO.

### Crystallographic parameters

Crystal system: Monoclinic

a (Å): 4.6691

b (Å): 3.4805

c (Å): 5.1183

### Most important XRD Peak (Figure 2.2)

No.	h	k	l	d [Å]	2Theta[deg]	I [%]
2	-1	1	1	2.53415	35.392	100.0
3	1	1	1	2.34848	38.295	80.7

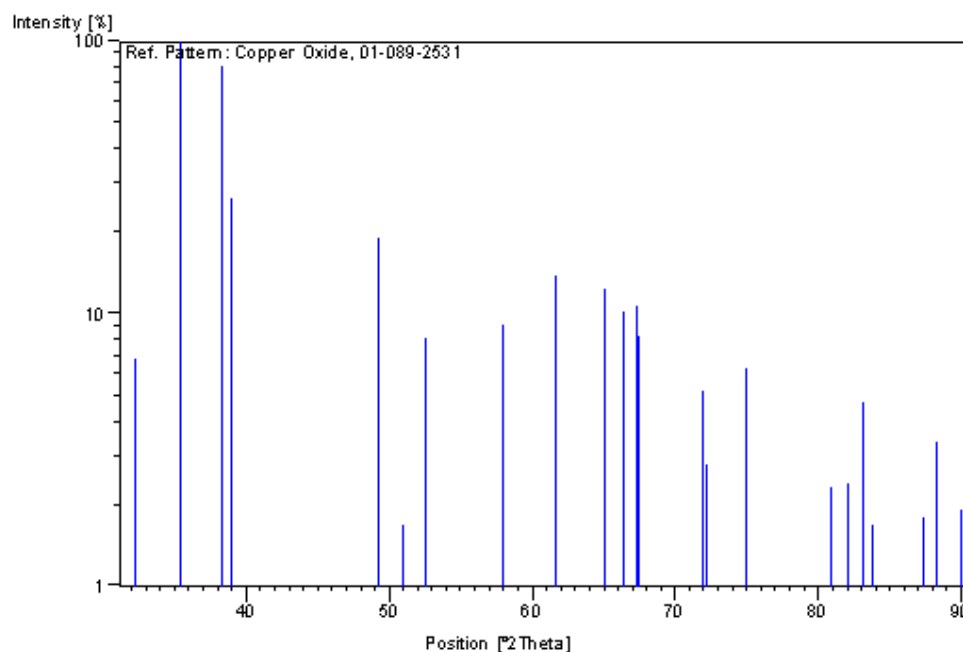


*Figure 2.2 CuO XRD Stick Pattern*

Copper (II) oxide has application as a p-and n-type semiconductor, because it has a narrow band gap of 1.2 eV. It is an abrasive used to polish optical equipment. Cupric oxide can be used to produce dry cell batteries. It has also been used in wet cell batteries as the cathode, with lithium as an anode, and dioxalane mixed with lithium perchlorate as the electrolyte. The film of cupric oxide can be obtained and deposited by reactive sputtering deposition. Properties of the film strongly depend on sputtering condition.[69,80,81,85]

## 2.3 Titanium Oxide

Titanium dioxide occurs in nature as well-known minerals rutile, anatase and brookite. Rutile and anatase have tetragonal Crystal system and brookite orthorhombic. The main properties is presented in *Table 2.1*

Molecular formula $\text{TiO}_2$	Molar mass 79.866 g/mol
Appearance White solid	Density 4.23 g/cm <sup>3</sup>
Melting point	1843 °C
Boiling point	2972 °C
Solubility in water	7.4x10 <sup>-5</sup> M
Refractive index ( $n_D$ )	2.488 (anatase) 2.609 (rutile) 2.583 (brookite)
Molecular formula $\text{TiO}_2$	Molar mass 79.866 g/mol
Appearance White solid	Density 4.23 g/cm <sup>3</sup>

### 2.3.1 The main structure and crystallographic properties of Rutile [86]:

#### Crystallographic parameters

Crystal system: Tetragonal

a (Å): 4.6570

b (Å): 4.6570

c (Å): 3.0093

#### Most important XRD Peak (see Figure 2.3)

No.	h	k	l	d [Å]	2Theta[deg]	I [%]
1	1	1	0	3.29300	27.056	100.0



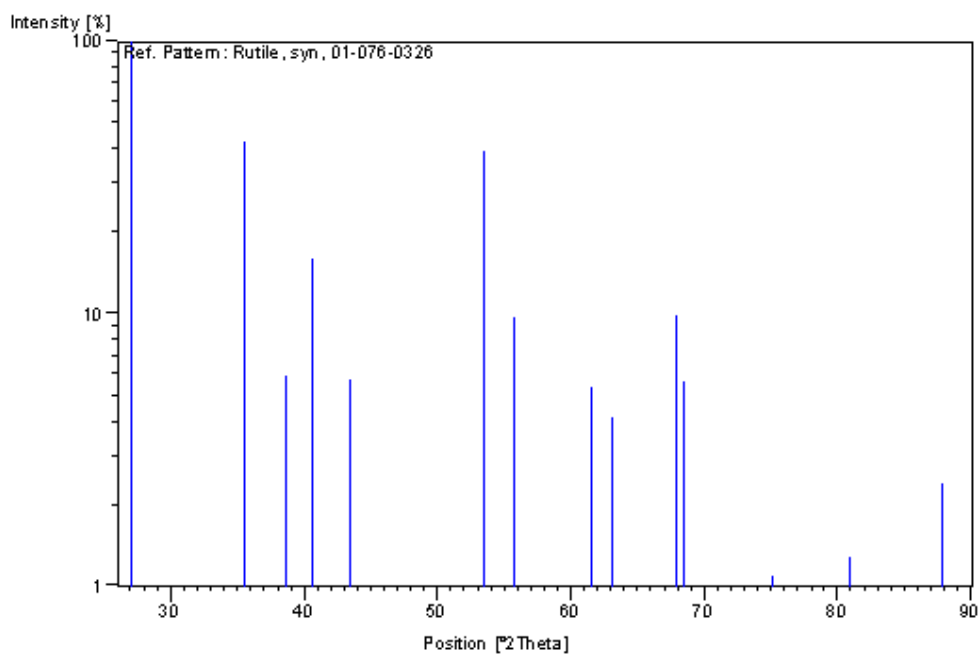


*Figure 2.3 Rutile XRD Stick Pattern*

### 2.3.2 Anatase [87]

#### Name and formula:

Empirical formula:  $\text{O}_2\text{Ti}_{0.72}$

Chemical formula:  $\text{Ti}_{0.72}\text{O}_2$

#### Crystallographic parameters

Crystal system: Tetragonal

Space group:  $I4_1/amd$

Space group number: 141

a (Å): 3.7830

b (Å): 3.7830

c (Å): 9.4970

Most important XRD Peak (see Figure 2.4):

No.	h	k	l	d [Å]	2Theta[deg]	I [%]
1	1	0	1	3.51444	25.322	100.0

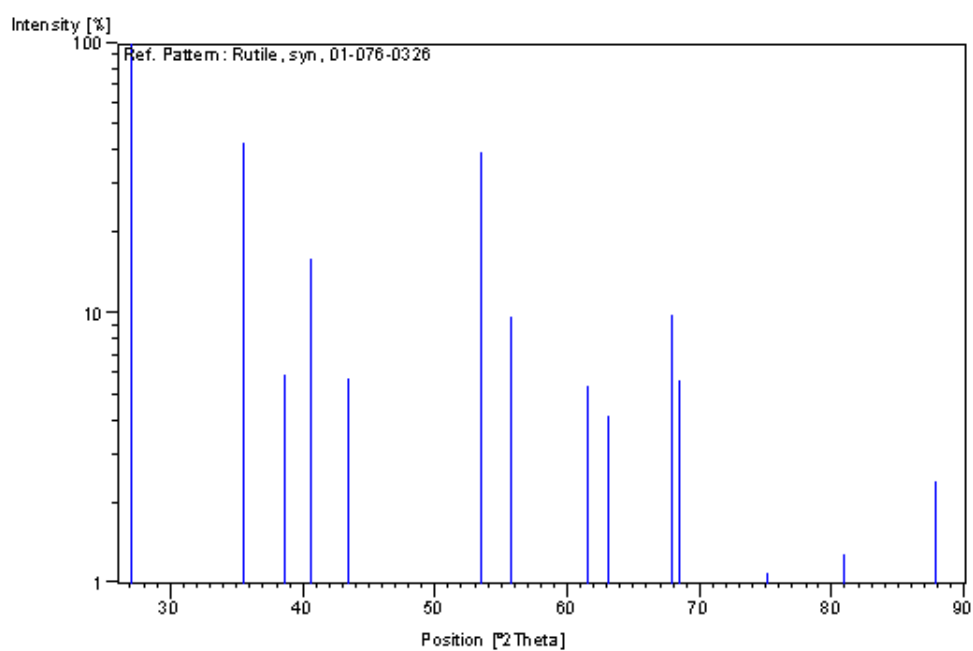


*Figure 2.4 Anatase XRD Stick Pattern*

### 2.3.3 Brookite [88,89]:

#### Crystallographic parameters

Crystal system: Orthorhombic

a (Å): 9.1660

b (Å): 5.4360

c (Å): 5.1350

Brookite XRD Peak list(see Figure 2.5):

No.	h	k	l	d [Å]	2Theta[deg]	I [%]
2	1	1	0	3.22000	27.681	100.0

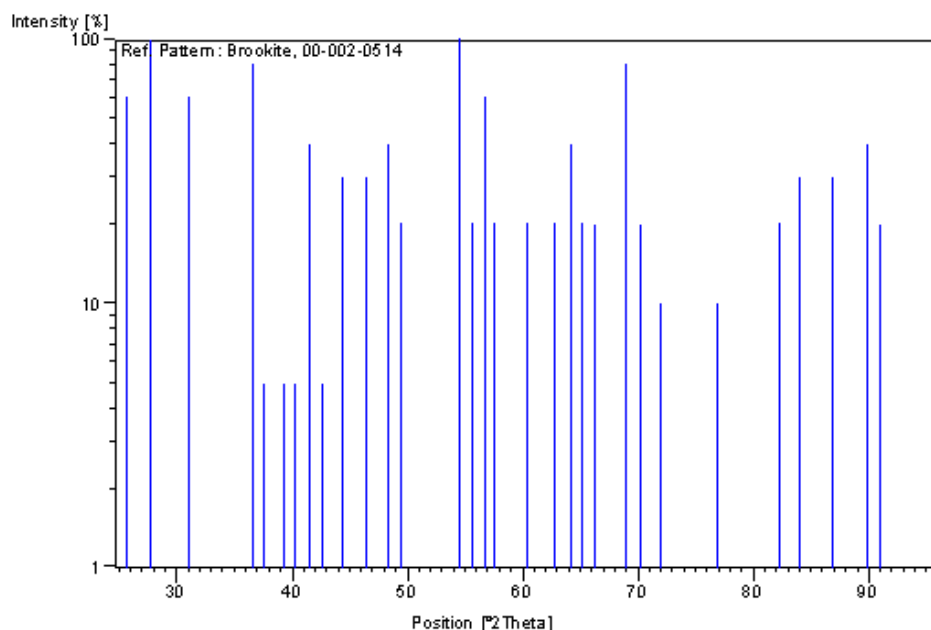


*Figure 2.5 Brookite XRD Stick Pattern*

#### **2.3.4 Titanium oxide thin film application, doping and deposition methods**

Titanium oxide  $\text{TiO}_2$  thin films are widely used in various fields such as optical and protective coatings and optical fibers because of their excellent chemical stability, mechanical hardness and optical transmittance with high refractive index. Recently,  $\text{TiO}_2$  thin films have become the most promising materials in environmental cleaning such as photocatalytic purifier [90,91] and photochemical solar cells [92,93].

$\text{TiO}_2$  is a large band gap semiconductor, which has gained a lot of importance as catalyst for breakdown of organic substances under UV illumination. It is a chemically and biologically inert material with good photostability [94,95]. As mentioned before the three main crystal phases of  $\text{TiO}_2$ , rutile is the thermodynamically stable phase, but anatase and brookite have a high kinetic

stability. In thin film processing usually, the anatase phase is formed at temperatures below ca. 873 K [94]. The anatase (bandgap=3.2 eV) is the more active phase in photocatalysis compared to rutile (bandgap=3.0 eV) [94]. On the other hand, it has been argued that a mixture of anatase and rutile may show the highest photocatalytic activity [96,97]. About the brookite phase very little is known. Therefore, most studies discuss pure anatase or rutile thin films.

Since the doping of nitrogen [100] into titanium dioxide was discovered to induce photocatalytic activity under visible light irradiation [98,99], the synthesis and characterization of nitrogen-doped titanium dioxide (N-dopedTiO<sub>2</sub>) have attracted extensive interest with a vision to efficiently utilize the solar energy.

A number of techniques, such as CVD [101], sol–gel [102,103], plasma source ion implantation [104], pulsed laser deposition [105], and magnetron sputtering [106-108] have been used to deposit TiO<sub>2</sub> thin films onto several kinds of supporters. Magnetron sputtering of TiO<sub>2</sub> films has aroused special interest, because it is an industrial process applicable to large-area deposition, and high quality TiO<sub>2</sub> films can be achieved even at low substrate temperatures. Only anatase and rutile have been observed in the thin films. In addition, amorphous TiO<sub>2</sub> films are often observed if the substrate temperature is low during deposition [109]. These three different phases as well as the grain size, crystalline structure, morphology and orientation of the TiO<sub>2</sub> layers can be controlled by the process parameters such as sputtering gases, O<sub>2</sub> partial pressure, substrate temperature, annealing process and some special sputtering techniques [110-112].

The properties of the titanium oxide film, prepared by reactive magnetron sputtering, depend not only on the preparation technique but also on the sputtering conditions, such as discharge pressure [113], reactive gas partial pressure [114] and DC discharge current [115].

## **2.4 Copper oxide and titanium oxide combination properties and application**

$\text{Cu}_2\text{O}$  is an attractive material for photovoltaic energy conversion. The band gap is 2.0 eV, which is in the acceptable range for photovoltaic materials. The theoretical efficiency of a  $\text{Cu}_2\text{O}$  solar cell is about 20% under AM 1 solar illumination. Furthermore,  $\text{Cu}_2\text{O}$  is a candidate material for low-cost solar cells, since copper is very abundant, and since large-grain  $\text{Cu}_2\text{O}$  can be grown by oxidizing copper. Although  $\text{Cu}_2\text{O}$  rectifiers were studied from 1920 to 1940, very little effort has been devoted to actual solar-cell development. The best cell efficiencies obtained have been on the order of 1 %.[116] The primary cause for this apparent "efficiency plateau" is that barrier heights of Schottky barrier solar cells are in the range 0.7-0.9 eV, regardless of the choice of metal. The most probable explanation of the barrier-height results is that most metals reduce  $\text{Cu}_2\text{O}$  to form a copper-rich region, or that a large density of states exists at the  $\text{Cu}_2\text{O}$  surface, which dictates the barrier-height magnitude.

Surface analyses combined with barrier-height studies indicate that  $\text{Cu}_2\text{O}$  Schottky barriers made with low-work- function metals are essentially Cu/ $\text{Cu}_2\text{O}$  cells due to reduction of the  $\text{Cu}_2\text{O}$  surface and subsequent interdiffusion phenomena. The copper-rich region essentially determines the barrier height. It is clear that to fabricate efficient  $\text{Cu}_2\text{O}$  solar cells; one must either utilize a MIS structure or a heterojunction [116]. The interfacial layer in a MIS structure could serve two purposes: it could inhibit reduction of the  $\text{Cu}_2\text{O}$  surface, and it would hopefully block out majority-carrier flow. The n-type partner in a heterojunction must not react with  $\text{Cu}_2\text{O}$ . If such a material is determined, then very efficient solar cells are possible.

Heterojunction solar cell with 2% efficiency based on a  $\text{Cu}_2\text{O}$  substrate was obtained in [117] made by deposition of transparent conducting oxide (TCO) films on  $\text{Cu}_2\text{O}$  substrates. TCO usually is based on ZnO,  $\text{In}_2\text{O}_3$ ,  $\text{SnO}_2$ , and CdO. On the other hand for the reasons mentioned before [116] is a  $\text{TiO}_2$  good candidate to n-type partner in heterojunction with  $\text{Cu}_2\text{O}$ .  $\text{Cu}_2\text{O}$  thin films

deposited on a  $\text{TiO}_2$  substrate typically form a p–n heterojunction. This system has been widely investigated for photocatalysis and solar cell applications [118–120]. The band gap energies of  $\text{Cu}_2\text{O}$  and  $\text{TiO}_2$  are 2.0 and 3.2 eV [121–123], respectively (see Figure 2.6). Both the conduction band minimum and the valence band maximum of  $\text{Cu}_2\text{O}$  lie above those of  $\text{TiO}_2$ ; therefore, the electrons excited to the conduction band of  $\text{Cu}_2\text{O}$  would transfer to  $\text{TiO}_2$ , whereas the holes generated in the valence band in  $\text{TiO}_2$  prefer opposite transfer to  $\text{Cu}_2\text{O}$ . Charge carriers separated in different semiconductors effectively reduce the chance of electron-hole pair recombination also prolong their lifetime, thus increasing the quantum efficiencies. In addition, working range of the wavelength is extended to a visible region due to absorption of visible light by  $\text{Cu}_2\text{O}$ , further enhancing the efficiency of the solar energy transition. Synergistic cooperation of these effects enables the  $\text{Cu}_2\text{O}/\text{TiO}_2$  system exhibit great potential for solar cell and photocatalysis applications [124–127]. Transport properties of the heterojunctions are, however, largely influenced by band discontinuities and interface states [128–129]. Band discontinuities at the interface are usually determined by the barrier heights for charge carriers to be overcome at the interface; therefore, their magnitudes dramatically influence the performance of the heterojunctions. Energy of the photogenerated electrons will be also lost during the transfer process if the band discontinuities are large. In addition, the interface states act as the recombination centers or carriers traps. The band structure at  $\text{Cu}_2\text{O}/\text{TiO}_2$  heterojunctions interface is strongly depending on condition of film deposition, in particular for the sputtering deposition [130].

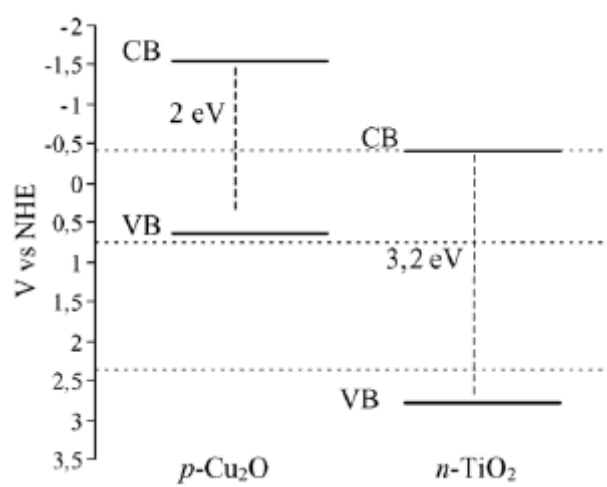


Figure 2.6 Energetic diagrams of  $\text{Cu}_2\text{O}/\text{TiO}_2$  [89]

## 2.5 Methods and setups description

### 2.5.1 The reactive DC-Magnetron Sputtering Process

In presented work thin film deposition have been performed by dc-magnetron sputter process. This process offers the advantage of a homogeneous area deposition. For the required properties of the film deposition parameters have been optimized. Their influence on the resulting layers is studied.

#### 2.5.1.1 The Principle of sputtering

Within the sputtering process, gas ions out of plasma are accelerated towards a target consisting of the material to be deposited. Material is detached ('sputtered') from the target and afterwards deposited on a substrate in the vicinity. The process is realized in a closed recipient, which is pumped down to a vacuum base pressure before deposition starts (see Figure 2.8). To enable the ignition of plasma usually argon is feed into the chamber up to a pressure between  $10^{-5}$ - $10^{-6}$  mbar. By natural cosmic radiation, there are always some ionized Ar<sup>+</sup>-ions available. In the dc-sputtering a negative potential U up to some hundred Volts is applied to the target. As a result, the Ar-ions are accelerated towards the target and set material free (see Figure 2.7), on the other hand they produce secondary electrons. These electrons cause a further ionization of the gas.

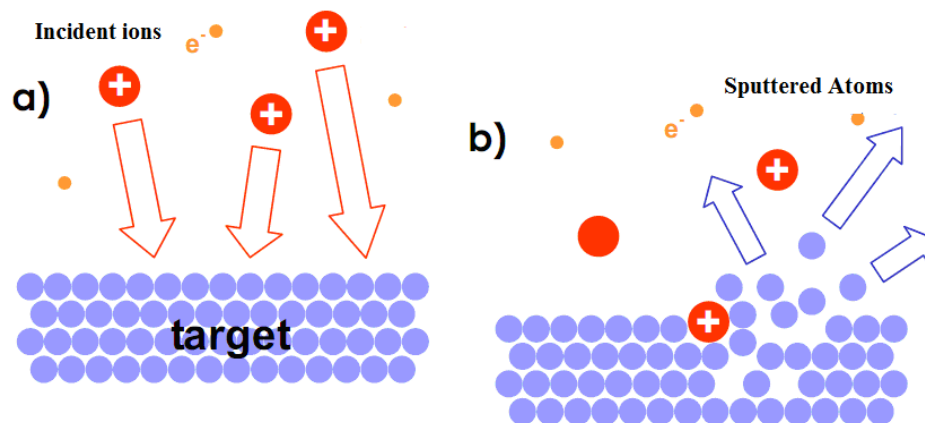


*Figure 2.7 Sputtering mechanism: a) incident ions; b) ions collide target and erode it[131]*



The gas pressure  $p$  and the electrode distance  $d$  determine a break-through voltage  $U_D$ —from which on a self sustaining glow discharge starts — following the equation  $U_D = A \cdot pd / (\ln(pd) + B)$  with materials constants  $A$  and  $B$ . Graphically spoken the ionization probability rises with an increase in pressure and hence the number of ions and the conductivity of the gas also increase. The break through voltage drops. For a sufficient ionization rate a stable burning plasma results, where from a sufficient amount of ions is available for sputtering of the material.

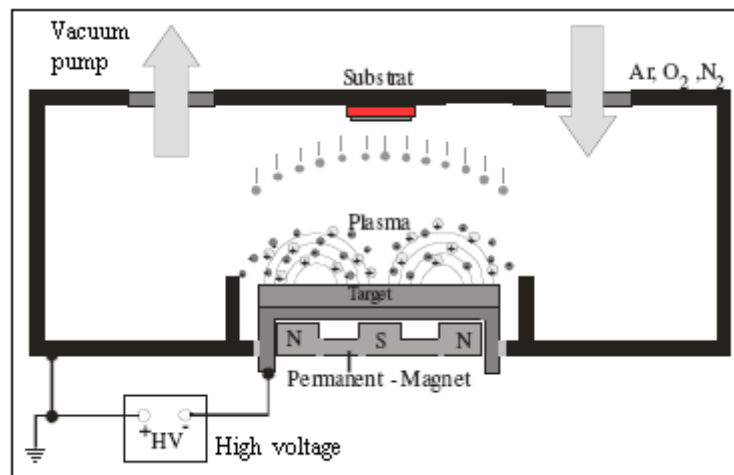


*Figure 2.8 The principle of the sputtering process*

To increase the ionization rate by emitted secondary electrons even further, a ring magnet below the target is used in the magnetron sputtering. The electrons in its field are trapped in cycloids and circulate over the targets surface (see Figure 2.9).

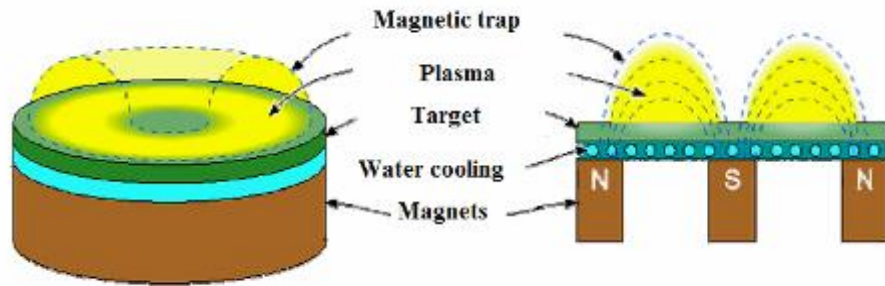


*Figure 2.9 Magnetron sputtering system [131]*

By the longer dwell time in the gas, they cause a higher ionization probability and hence form a plasma ignition at pressures, which can be up to one hundred times smaller than for conventional sputtering. On the one hand, higher deposition rates can be realized thereby. On the other hand less collisions occur for the sputtered material on the way to the substrate because of the lower pressure and hence the kinetic energy at the impact on the substrate is higher (see also below). The electron density and hence the number of generated ions is highest, where the **B**-field is parallel to the substrate surface. The highest sputter yield happens on the target area right below this region. An erosion zone is formed which follows the form of the magnetic field.

The bombardment of a non-conducting target with positive ions would lead to a charging of the surface and subsequently to a shielding of the electrical field. The ion current would die off. Therefore, the dc-sputtering is restricted to conducting materials like metals or doped semiconductors. In our setup were used Au, Cu and Ti target. The reactive sputtering in ambient of other gases like oxygen or nitrogen are fed into the sputter chamber additionally to the argon, to produce oxidic or nitridic films.

The reactive gas chemically reacts with deposited film on substrate creating desired material properties. However, reactive gas also reacts with target and erodes it. This phenomenon is called as “target poisoning” and decres sputtering rate, so is appear difficulties to control sputtering process. When

reactive gas is introduced, one part of the reactive gas is pumped other part react with sputtered material and create desired composition. For this reason, reactive sputtering rate is low than pure metal sputtering.

Description of reactive sputtering process in argon and oxygen gases mixing (see Figure 2.10):

- $q_t$ : reactive gas flux consummated on target surface
- $q_c$ : reactive gas flux consummated on surfaces where target's material is sputtered;
- $q_p$ : pumped reactive gas flux and used in any process.

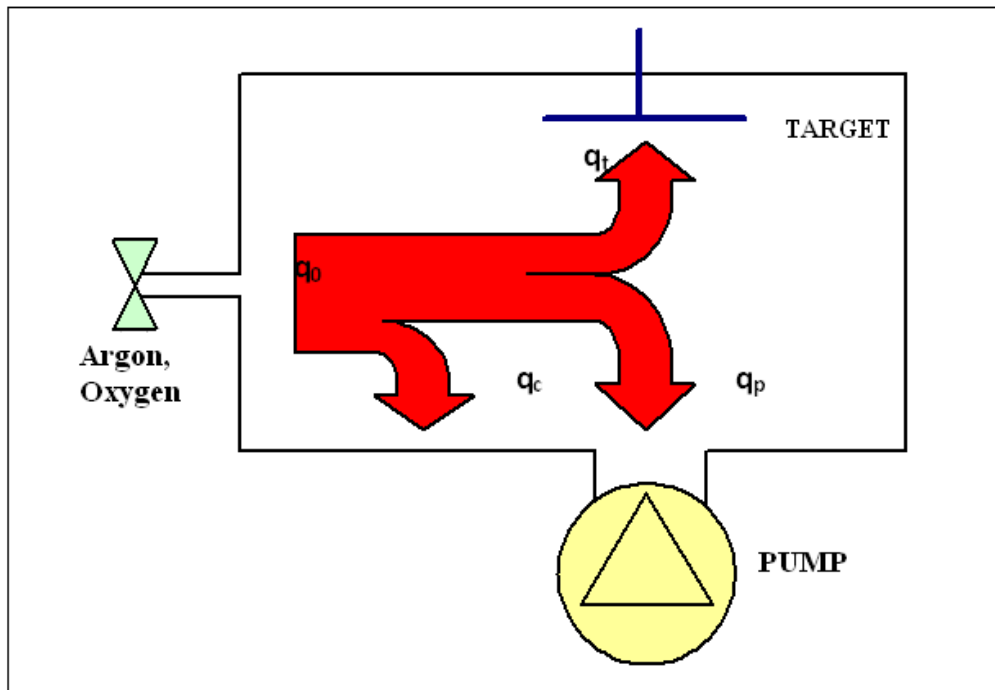


*Figure 2.10 Fluxes of gas during reactive sputtering*

### 2.5.1.2 The Sputter Parameters

The resulting film properties can be controlled by adjusting the following sputter parameters:

The sputter current  $I_{sp}$  determines mainly the rate of the deposition process and hence the time which remains for the arriving particles during the growth process for either surface diffusion and agglomeration on existing growth centers or nucleation with other adatoms. The applied voltage determines the maximum

energy, with which sputtered particles can escape from the target (reduced by the binding energy). Energies of the sputtered particles show a broad distribution with a maximum of the distribution between 1 eV and 10 eV. The applied voltage determines also the sputter yield, which is the number of sputtered particles per incoming ion. The pressure  $p$  in the sputter chamber determines the mean free path  $\lambda$  for the sputtered material, which is proportional to  $1/p$ . Together with the target substrate distance (TS) the pressure controls, how many collisions occur for the particles on their way from the target to the substrate. This can influence the porosity of the films. In addition, the crystallinity, adhesion and texture can be affected. Via the gas mixture one can control the stoichiometry of films, which are sputtered from a metallic target. The oxygen flow  $q(\text{O}_2)$  is the parameter varied, whereas the desired total pressure is kept constant by regulation of the Ar-flow  $q(\text{Ar})$ .

The substrate temperature can have a strong impact on the growth behaviour with respect to crystallinity or density of the samples. It can be adjusted between room temperature and 700°C. Nevertheless, even during sputtering without external heating the substrate temperature may rise considerably, especially during long sputtering times.

#### **2.5.1.3 The Sputter System**

Substrate and target surface are parallel to each other and have a distance 13 cm. Magnetron with the target of 2 inch diameter were used (see Figure 2.11).



*Figure 2.11 Photo of magnetron with Au target.*

It is bonded to a water cooling system. Electrical potential was applied on target and vacuum chamber (see Figure 2.12) was grounded.



*Figure 2.12 Photo of vacuum chamber.*

The sample holder was heated by electrical furnace. Temperature was controlled by thermo-couple. Vacuum chamber were pumped by rotary and turbo pump. The pressure was controlled by full-range and capacitive vacuum detectors. The gases (Ar, O<sub>2</sub> and N<sub>2</sub>) flows were controlled and operated by fluxmeter. Full setup photo is presented in Figure 2.13.



*Figure 2.13 Photo of sputtering system setup.*

## **2.5.2 Thin films characterization**

### **2.5.2.1 Thin film thickness measurements**

In order to verify the thickness of deposited films it has been used profilometer Veeco model Dektat 8 (see Figure 2.14). The instrument is constituted from a tip, which slides on a sample to measure pressing on it with a constant force. The roughness of the surface is reflected in a vertical movement of the tip and the cantilever in which it is fixed. The cantilever it is connected to a condenser, and the vertical movement of the tip is translate in a variation of the

ability to this condenser, than the system it converts in a profile visualized on the screen of the PC (to which the profilometer is connected).

The sample to measure must be flat and sufficiently hard. Moreover he must have a zone not deposited in such way from being able to measure the difference of height between this and the zone film covered. The scanning comes carried out from the deposited area to in order to prevent that an error in the selection of the length of scanning.

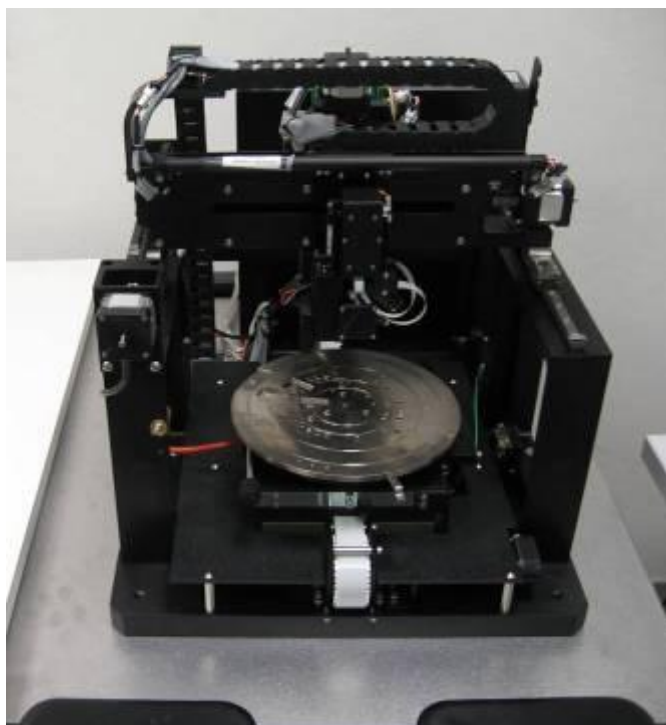


*Figure 2.14 Photos of Dektak 8 Veeco profilometer*

The measure on the samples carried out executing 6 various scanning of 2 millimetres length, on 3 various points of the film edge. For every scanning the thickness of the film was calculated medium value from measurements of deposited films. On the 6 values are averaged in order to obtain the medium thickness, of the film.

#### **2.5.2.2 X-ray diffraction microstructure analysis.**

One of the phenomena of interaction of X-rays with crystalline matter is its diffraction, produced by the reticular planes that form the atoms of the crystal. A crystal diffracts an X-ray beam passing through it to produce beams at specific

angles depending on the X-ray wavelength, the crystal orientation and the structure of the crystal.

In the macroscopic version of X-ray diffraction, a certain wavelength of radiation will constructively interfere when partially reflected between surfaces (i.e., the atomic planes) that produce a path difference equal to an integral number of wavelengths. This condition is described by the Bragg law:

$$2d_{(hkl)} \sin \theta = n\lambda$$

In addition, reticular parameter is defined as  $a = \sqrt{h^2 + k^2 + l^2} \cdot d_{hkl}$

where  $n$  is an integer,  $\lambda$  is the wavelength of the radiation,  $d$  is the spacing between surfaces and  $\theta$  is the angle between the radiation and the surfaces. This relation demonstrates that interference effects are observable only when radiation interacts with physical dimensions that are approximately the same size as the wavelength of the radiation. Since the distances between atoms or ions are about  $10^{-10}$  m (1Å), diffraction methods require radiation in the X-ray region of the electromagnetic spectrum, or beams of electrons or neutrons with similar wavelength. So, through X-ray spectra one can identify and analyse any crystalline matter. The degree of crystallinity or order will conditionate the quality of the obtained result. In this work Bragg Philips Xpert-Pro diffractometer is used (see Figure 2.15). As X-ray beam source Cu target X-ray tube used. To identify and analyse deposited film the  $2\theta$  XRD spectra were measured [132]. Diffractometer was set “thin film condition” measurement.





*Figure 2.15 Photo of Philips X'Pert Pro diffractometer used in experiment.*

Scherrer showed that the average dimension of the crystals that compose a crystalline powder is related with the profile of the peak by means of the equation:

$$D = \frac{K\lambda}{\beta \cos\Theta}$$

Where K is proportionality constant approximately similar to the unit,  $\beta$  the FWHM of the peak in radians (theoretically corrected from the instrumental broadening), D the size of the crystal in the direction perpendicular to the reflecting planes and  $\lambda$  the wavelength of the X-rays used. This is the most usual and simple equation that allows to evaluate grain size.

### **2.5.2.3 Four-Point Probe method [133]**

In this work four-point method were used. The purpose of the 4-point probe is to measure the resistivity of any semiconductor material. It can measure either bulk or thin film specimen, each of which consists of a different expression.

The 4-point probe setup used consists of four equally spaced tungsten metal tips with finite radius. Each tip is supported by springs on the other end to minimize sample damage during probing. The four metal tips are part of an auto-mechanical stage, which travels up and down during measurements. A high impedance current source is used to supply current through the outer two probes; a voltmeter measures the voltage across the inner two probes (see Figure 2.16) to determine the sample resistivity. Typical probe spacing is  $\sim 1$  mm.

In a sheet resistance measurement, several resistances need to be considered, as shown in Figure 1 (a). The probe has a probe resistance  $R_p$ . It can be determined by shorting two probes and measuring their resistances. At the interface between the probe tip and the semiconductor, there is a probe contact resistance,  $R_{cp}$ . When the current flows from the small tip into the semiconductor and spreads out in the semiconductor, there will be a spreading resistance,  $R_{sp}$ . Finally, the semiconductor itself has a sheet resistance  $R_s$ .

The equivalent circuit for the measurement of semiconductor sheet resistance by using the four-point probe is shown in Figure. 2.16(c). Two probes carry the current and the other two probes sense the voltage. Each probe has a probe resistance  $R_p$ , a probe contact resistance  $R_{cp}$  and a spreading resistance  $R_{sp}$  associated with it. However, these parasitic resistances can be neglected for the two voltage probes because the voltage is measured with a high impedance voltmeter, which draws very little current. Thus, the voltage drops across these parasitic resistances are insignificantly small. The voltage reading from the voltmeter is approximately equal to the voltage drop across the semiconductor sheet resistance.

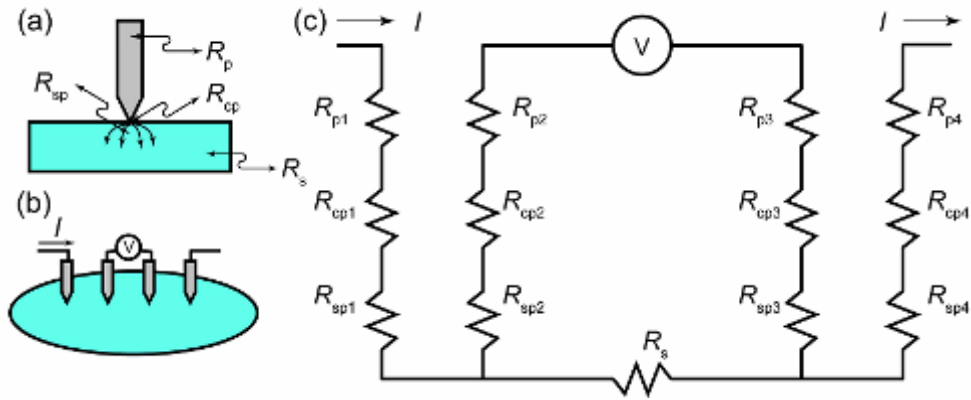


Figure 2.16: Four-point probe measurement of semiconductor sheet resistance

By using the four-point probe method, the semiconductor sheet resistance can be calculated:

$$R_s = F(V/I),$$

where  $V$  is the voltage reading from the voltmeter,  $I$  is the current carried by the two current-carrying probes, and  $F$  is a correction factor. For collinear or in-line probes with equal probe spacing, the correction factor  $F$  can be written as a product of three separate correction factors:

$$F = F_1 F_2 F_3$$

$F_1$  corrects for finite sample thickness,  $F_2$  corrects for finite lateral sample dimensions, and  $F_3$  corrects for placement of the probes with finite distances from the sample edges. For very thin samples with the probes being far from the sample edge,  $F_2$  and  $F_3$  are approximately equal to one (1.0), and the expression of the semiconductor sheet resistance becomes:

$$R_s = \pi V / I \ln 2$$

The four-point probe method can eliminate the effect introduced by the probe resistance, probe contact resistance and spreading resistance. Therefore, it has more accuracy than the two-point probe method.

#### 2.5.2.4 The hot point probe method

The hot point probe method was used to determine whether the semiconductor is N- or P- type. The potential difference when measured between the hot and the cold contacts (thermal Seeback effect) and the center-zero meter deflection identify the carrier type. The cold probe polarity therefore indicates the conductivity type (see Figure 2.17 for n – type.). For current direction measurement standard digital multimeter were used.

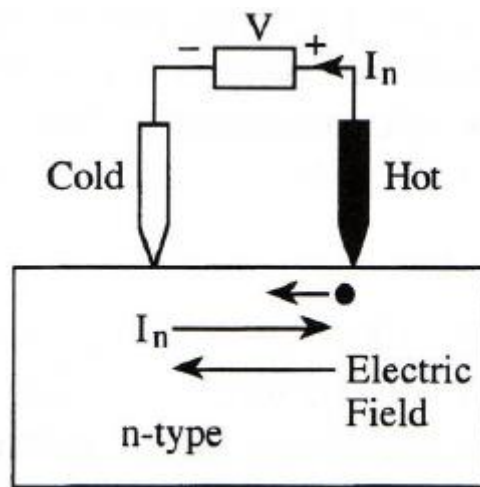


*Figure 2.17 Hot-point probe measurements for n- type semiconductor case*

Hot probes are effective in the resistivity range from  $10^{-3}$  to  $10^4$  Ohm·cm.

### **3. Experimental results**

#### **Introduction**



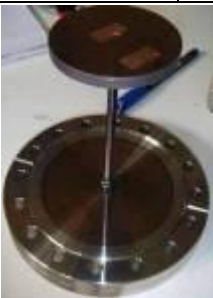

In view of the severe future ecological impacts of energy production by combustion of fossil fuels, solar energy is seriously considered as an alternative. However, the development of new solar energy converters with improved performance and lower cost requires new approaches focused on the use of cheap and non-toxic materials. Cuprous oxide ( $\text{Cu}_2\text{O}$ ) is an attractive semiconductor material for fabricating low-cost solar cells and other optoelectronic devices [134]. Cuprous oxide attracts the most interest because of its high optical absorption coefficient in the visible range and its reasonably good electrical properties [135]. Cuprous oxide is a semiconductor having a direct band gap of 2 eV which has been studied previously for application in solar energy converting devices [135]. Copper and copper oxide (metal-semiconductor) is one of the first photovoltaic cell invented [137].

It has been shown in [74] that to fabricate efficient  $\text{Cu}_2\text{O}$  solar cells, one must either utilize a MIS structure or a heterojunction.  $\text{TiO}_2$  has a band gap of p 3.2 eV, so interface with copper oxides must forms n- $\text{TiO}_2$ /p- $\text{Cu}_2\text{O}$  heterostructure junction [138], so heterojunction photovoltaic cell can be created. The objective of the present study is to develop solar cell based on  $\text{Cu}_2\text{O}$  thin film substrate using well know magnetron sputtering technique.

#### **3.1 $\text{Cu}_2\text{O}$ thin film deposition by reactive DC magnetron sputtering.**

In presented work, the thin films of copper oxide ( $\text{Cu}_x\text{O}$ ) were deposited by direct current (DC) magnetron reactive sputtering. Pure copper target were used. Oxygen plays role of reactive gas in order to obtain oxide films. The distance between target and substrate was 10 cm and after changed to 13 cm, because sample-holder heater was installed. The main conditions of the deposition are presented in Table 3.1.

Table 3.1:  $\text{Cu}_x\text{O}$  sputtering condition.

Sputtering type	Power-supply mode	Target	Reactive gas	Gas flux control mode	Substrate
DC Magnetron	Constant current	Cu	$\text{O}_2$	Constant total pressure	Quartz $10 \times 10 \text{ mm}^2$
					
<i>sputtering chamber</i>		<i>Sample heater</i>		<i>Room temperature sample holder</i>	<i><math>\text{Cu}_x\text{O}</math> sample</i>

In order to improve sputtering process and obtain necessary crystalline properties, electronic and adhesion of  $\text{Cu}_x\text{O}$  sputtered films, it was performed study of influence of oxygen and argon fluxes on mentioned parameters. The best temperature condition of deposition in range of  $100\text{-}600^\circ \text{C}$  was also determined.

### 3.1.1 Influence of oxygen/argon flux ratio on $\text{Cu}_x\text{O}$ sputtered films.

The sputtering depositions at various flux ratios of argon and oxygen in two experimental batches under room and  $200^\circ\text{C}$  temperature were done. It was experimentally shown that for good adhesion total working pressure (oxygen and argon) during sputtering process must be less than  $8 \cdot 10^{-3} \text{ mbar}$ . At higher total

sputtering pressure, all deposited films are peeled. So the optimal working pressure  $5 \cdot 10^{-3}$  mbar was chosen.

### 3.1.1.1 Sputtering at room temperature.

The runs 1A-5A were done at room temperature at constant current of sputtering and at various fluxes of oxygen and argon (see table 3.2).

*Table 3.2 Experimental data and sputtering condition of DC magnetron sputtering  $\text{Cu}_x\text{O}$  films depositions (Runs from 1A to 5A) at room temperature.*

Run	Flux Ar	Flux O <sub>2</sub>	O <sub>2</sub> /Ar Flux	V	I	Target - Sample distance	Lattice Parameter	Thickness	Sputtering rate
	<i>sccm</i>	<i>sccm</i>		<i>V</i>	<i>A</i>	<i>cm</i>	$\text{\AA}$	<i>nm</i>	$\text{\AA}/\text{s}$
1A	7	3	0,43	465	0,3	10	4,2378	1340	7,44
2A	6,5	4	0,62	473	0,3	10	4,2538	1480	7,71
3A	5,2	5,2	1	484	0,3	10	4,2632	1357	7,54
4A	6	4,5	0,75	468	0,3	10	4,2620	1113	6,18
5A	6,2	4,2	0,67	454	0,3	10	4,2594	413	3,44

On the Figure 3.1 is presented experimental data of lattice parameter as a function of ratio oxygen argon gases for the room temperature deposition. The crystallization level of the sputtered films is increases with this ratio increasing and comes to saturation after 0.7 value. Green line shows theoretic value of reticular parameter.

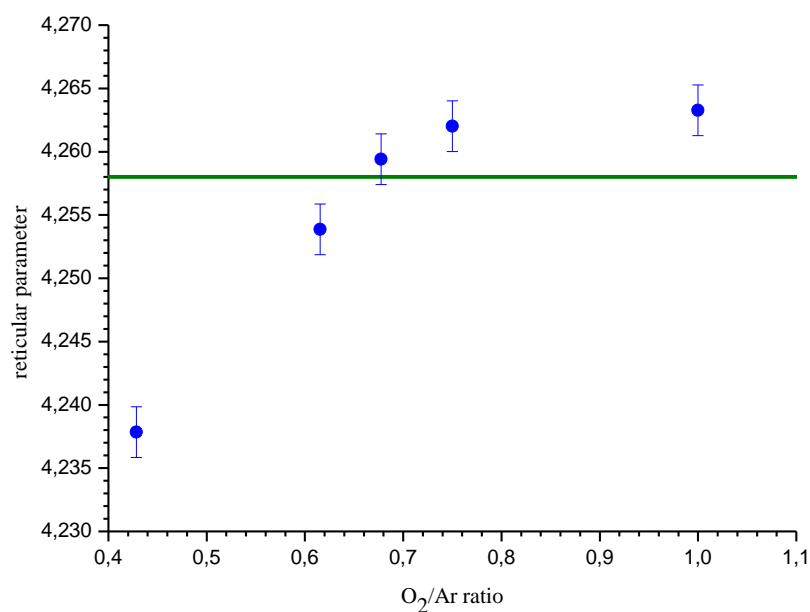


Figure 3.1 Reticular parameter versus  $O_2/Ar$  fluxes ratio for room temperature DC magnetron sputtering depositions of  $Cu_2O$  films (runs from

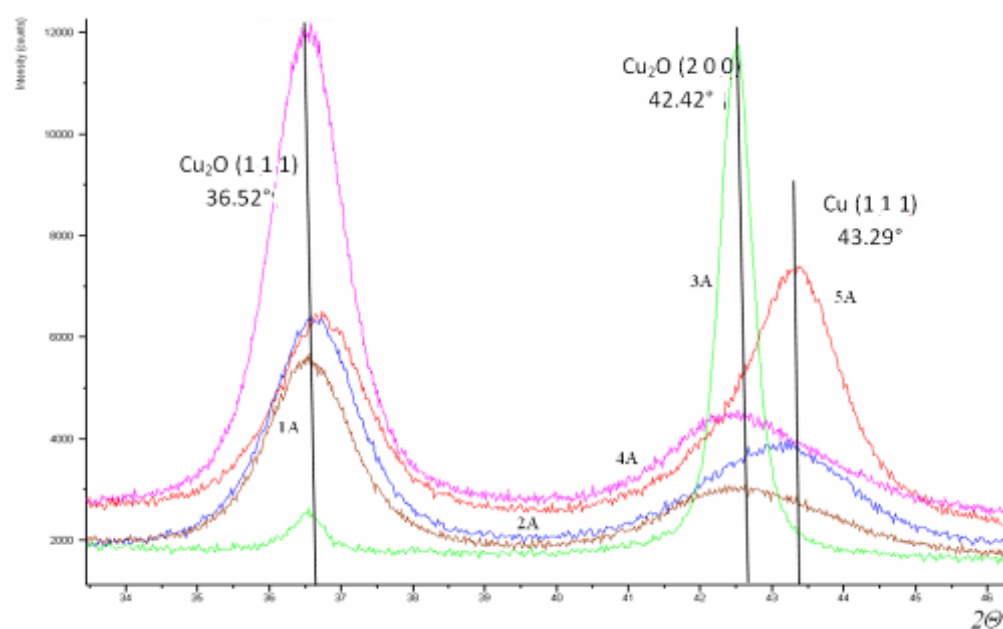
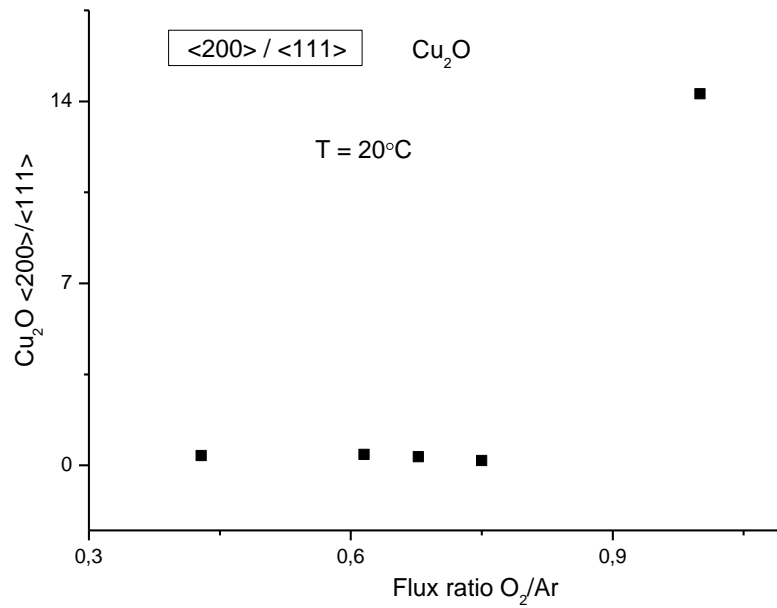


Figure 3.2 Room temperature depositions XRD  $2\theta$  spectra (Runs from 1A

The X-ray diffraction patterns of  $Cu_2O$  films deposited at room temperature are shown in Figure. 3.2. The ratio intensity of the diffraction peaks



corresponding to (200) and (111) lattice orientation as function of oxygen/argon fluxes ratio is increases rapidly after 0.8 value. Before this value (111) orientation is prevalent for  $\text{Cu}_2\text{O}$  sputtered films (see Figure 3.3).



*Figure 3.3  $\text{Cu}_2\text{O}$  diffraction peaks ratio for (200)/(111) orientation versus oxygen/argon flux ratio for room temperature depositions.*

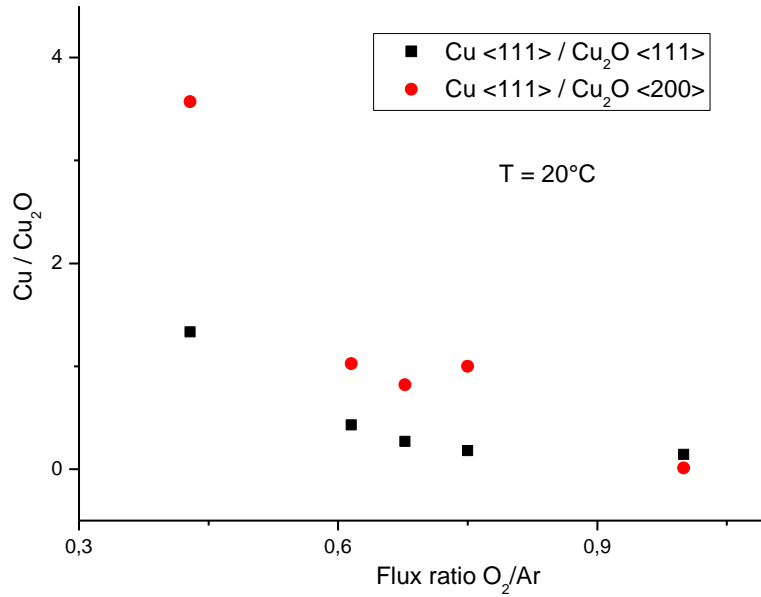


*Figure 3.4 Cu and Cu<sub>2</sub>O diffraction peaks ratio for Cu(111) /Cu<sub>2</sub>O (111) and Cu<sub>2</sub>O (200) orientation versus oxygen/argon flux ratio for room temperature*

In the Figure 3.4 is shown that with increasing oxygen flux and decreasing of argon the intensity of X-ray diffraction peak Cu<sub>2</sub>O (111) and Cu<sub>2</sub>O (111) are increasing, but decreasing Cu(111) is observed.

### **3.1.1.2 Sputtering depositions Cu<sub>2</sub>O at 200°C (runs from 1B to 7B).**

In order to study of influence of O<sub>2</sub> and Ar gas fluxes at 200°C on the properties of deposited Cu<sub>2</sub>O thin film and optimize sputtering process the series of experimental sputtering was performed (runs 1B-7B). The sputtering current was constant. In table 3.3 experimental data and parameters of the Cu<sub>2</sub>O film sputtering are presented. In the Figure 3.5 is presented analysis of experimental results of dependence of the Cu<sub>2</sub>O sputtered thin film lattice parameter versus oxygen/argon gases fluxes ratio. The green line is theoretical parameter. One can see that lattice parameter is close to theoretical at oxygen/argon gases fluxes ration value higher than 1.5. In the Figure 3.6 are presented measured 2 $\theta$  XRD spectra of films deposited at 200°C.

Table 3.3 Experimental data and condition DC magnetron sputtering depositions of  $\text{Cu}_x\text{O}$  films (Runs from 1B to 7B).

Run	Flux Ar	Flux $\text{O}_2$	$\text{O}_2/\text{Ar}$ Flux	V	I	Target - Sample distance	Lattice Parameter	Thickness	Sputtering rate
	sccm	sccm		V	A	cm	Å	nm	Å/s
1B	6	4,5	0,75	673	0,40	13	4,2540	5021	16,74
2B	5,5	5	0,91	678	0,40	13	4,2590	5317	17,72
3B	4,5	6	1,33	706	0,40	13	4,2649	6115	16,99
4B	3,5	7	2,00	713	0,40	13	4,2582	3702	15,43
5B	2,5	8	3,20	696	0,41	13	4,2654	3895	12,98
6B	4,1	6,2	1,51	653	0,40	13	4,2575	5096	16,99
7B	2,9	7,6	2,62	658	0,40	13	4,2576	3101	11,49

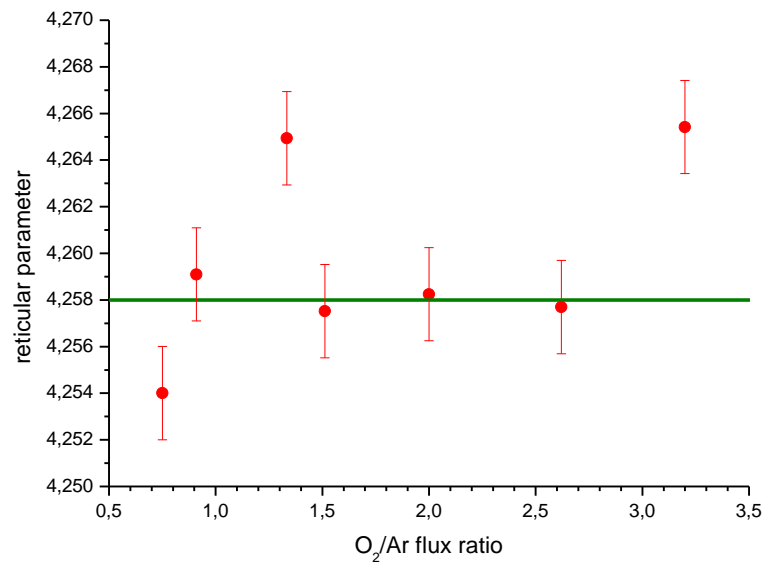


Figure 3.5 Reticular parameter as a function of  $\text{O}_2/\text{Ar}$  fluxes ratio for DC magnetron sputtering depositions of  $\text{Cu}_2\text{O}$  films (Runs from 18 to 26) at  $200^\circ\text{C}$ .

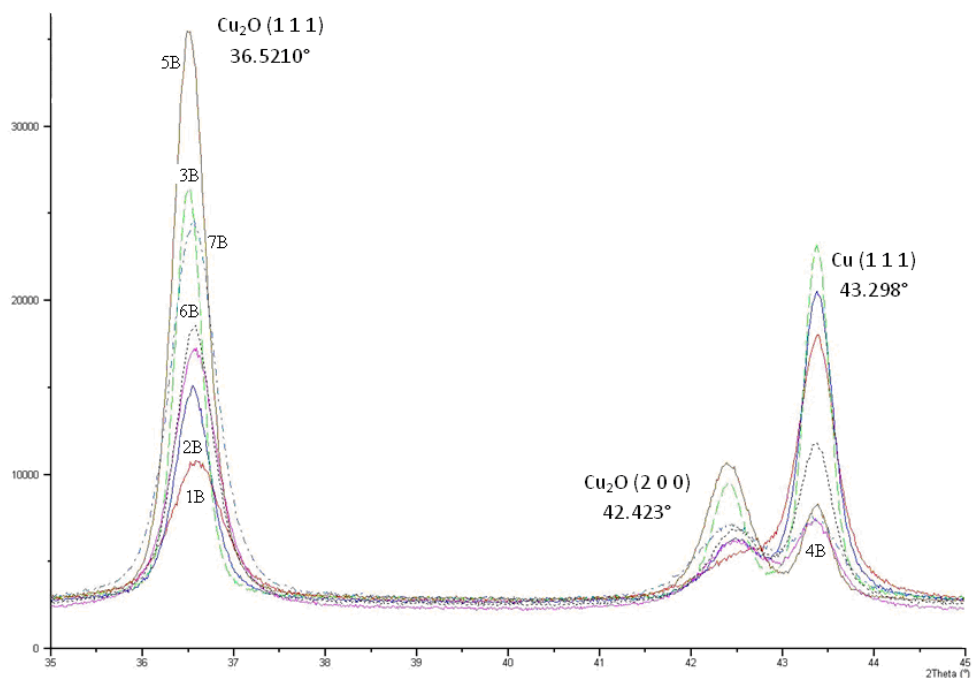


Figure 3.6  $200^\circ\text{C}$  depositions XRD  $2\theta$  spectra (Runs 1B-7B).

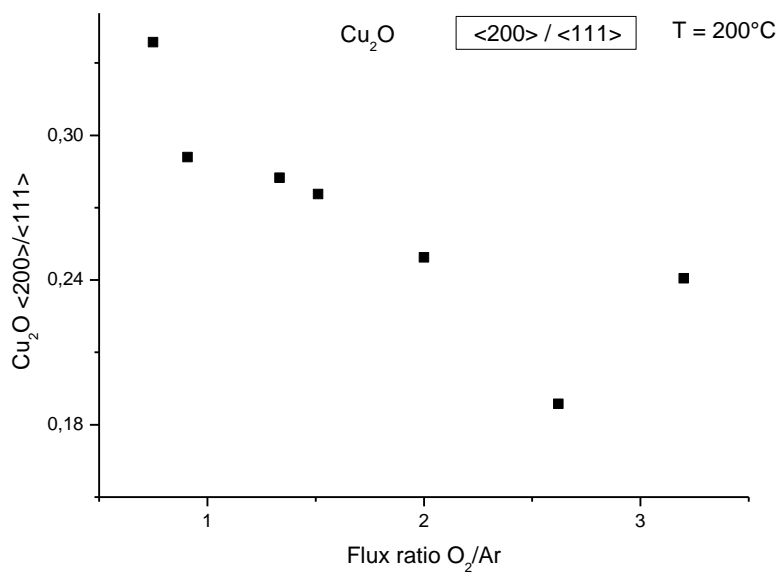
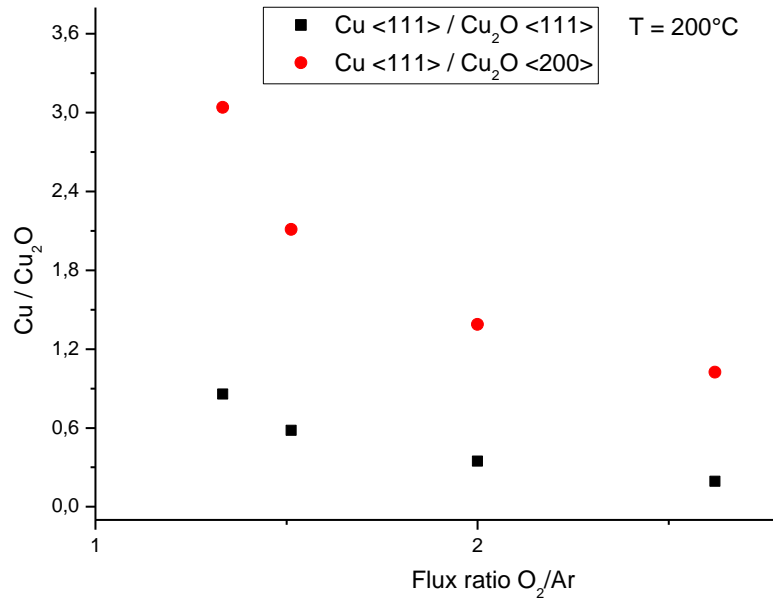


Figure 3.7  $\text{Cu}_2\text{O}$  diffraction peaks intensity ratio for (200)/(111) orientation versus oxygen/argon flux ratio for  $200^\circ\text{C}$  depositions.



*Figure 3.8 Cu and Cu<sub>2</sub>O diffraction peaks intensity ratio for Cu(111) /Cu<sub>2</sub>O (111) and Cu<sub>2</sub>O (200) orientation versus oxygen/argon flux ratio for 200°C depositions.*

In the films deposited by sputtering technique at 200°C at various ratio oxygen/argon fluxes increase of Cu<sub>2</sub>O (111) XRD peak intensity with increasing of fluxes ratio value is observed(see Figure 3.7). The diffraction peaks intensity of Cu<sub>2</sub>O (200) is decreases with oxygen/argon fluxes ratio. The peak of Cu (111) is decreased, but Cu<sub>2</sub>O (200) and (111) orientation increased respect the Cu(111) peak with fluxes ratio increasing(see Figure 3.8).

Summarizing data obtained for room and 200°C deposition, X-ray diffraction spectra of films at sputtered room and 200°C temperature were analyzed. Scherrer equation used that allows to evaluate grain size. The results are presented in Figure 3.9.

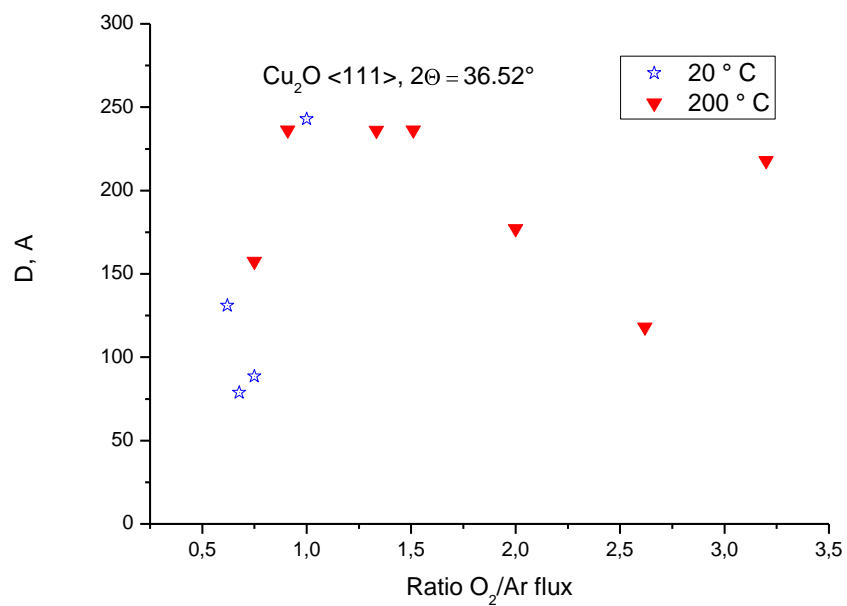


*Figure 3.9 Debye-Scherrer calculation of grain size for  $\text{Cu}_2\text{O}$  (111) orientation diffraction peak versus oxygen/argon flux ratio for room and 200°C temperature sputtering depositions.*

### 3.1.2 Influence of temperature on cuprous oxide thin film properties

Influence substrate temperature on properties of deposited copper oxide film was studied. The reactive direct current magnetron sputtering depositions were done at constant sputtering current 0.4 A, voltage 640 V, distance between target and substrate 13 cm and constant oxygen/argon fluxes ratio was 3.2. The sputtering process has been performed in temperature range from 100 to 600°C. In Table 3.4 is presented measured characteristic of obtained copper oxide thin films.

*Table 3.4 Experimental data DC magnetron sputtering deposited  $Cu_xO$  films in temperature range of 100-600°C (Runs from 1C to 5C).*

Run	Temperature, °C	Lattice Parameter, Å	Thickness, nm	Sputtering rate, Å/s
1C	100	4,2808	2486	4,97
2C	200	4,2654	3895	12,98
3C	300	4,2654	3349	11,16
4C	400	4,2644	3475	7.30
5C	600	4,2626	3145	6,29

Reticular parameter as a function of reactive sputtering is presented in Figure 3.10. The black line on the graph is theoretical value for cuprite  $Cu_2O$ . One can see that with temperature increasing experimental value is approximating to theoretical.

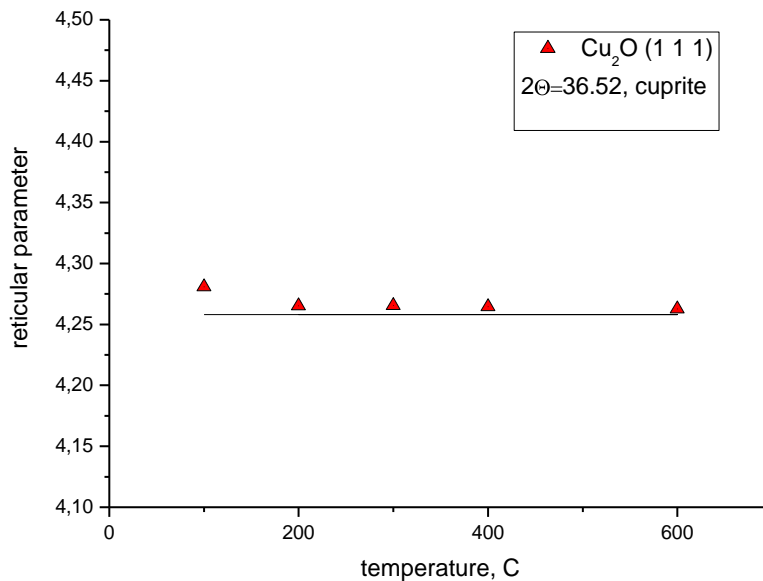


*Figure 3.10 Reticular parameter of  $\text{Cu}_2\text{O}$  as a function of reactive sputtering temperature in range of  $100^\circ\text{C}$ -  $600^\circ\text{C}$ .*

In this work, it is experimentally proved that copper oxide semiconductor film sputtered at room temperature has n-type (electronic) conductivity. On the other hand all thin film deposited at temperature higher  $200^\circ\text{C}$  has p-type (holes) conductivity. Measurements were performed by “Hot point” method described before.

The specific resistance of sputtered copper oxide films sputtered at temperature lower  $100^\circ\text{C}$  is very low, close to 0. On the contrary, samples obtained at the temperature higher  $200^\circ\text{C}$  specific resistance have very high value of resistivity and after decreases with the temperature of sputtering (see Figure 3.11).

Specific resistance was measured by standard “four – probe” method. In “thin film” condition, so sample area can be neglected.



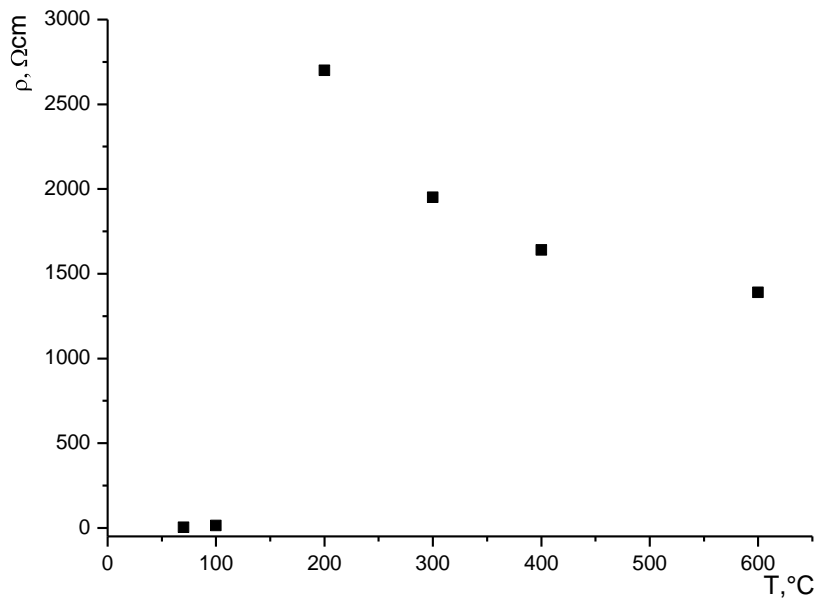


*Figure 3.11 Specific resistance  $\text{Cu}_x\text{O}$  thin films versus sputtering temperature.*

#### **Results:**

At the room temperature, we have obtained  $\text{Cu}_2\text{O}$  phase, but copper or copper oxide  $\text{CuO}$  is also present. These films have electrons (n-type) conduction.

Film deposition on heated at  $200^\circ\text{C}$  substrate have higher crystal structure and P-type conductivity as have to be in  $\text{Cu}_2\text{O}$  semiconductor.

Increasing temperature  $\text{Cu}_2\text{O}$   $\langle 111 \rangle$  and  $\text{Cu}_2\text{O}$   $\langle 200 \rangle$  peaks increase while Cu peak  $\langle 100 \rangle$  decrease significantly.

The thin films of copper oxide deposited at room temperature have very low resistivity.

Films prepared at high temperature deposition have high resistivity.

### **3.2 Reactive DC sputtering of $\text{TiO}_x$ thin film**

Titanium oxide ( $\text{TiO}_x$ ) thin film was deposited on quartz substrate by DC magnetron sputtering using Ti target in reactive oxygen gas ambient. The main sputtering condition is presented in Table 3.5:

*Table 3.5 Reactive sputtering condition of Titanium oxide (TiO<sub>x</sub>) thin film*

<b>Sputtering:</b>	<b>Regime:</b>	<b>P-Supply mode:</b>	<b>Target:</b>	<b>Reactive Gas :</b>	<b>Target - Sample distance</b>	<b>Gas Flux Control Mode:</b>	<b>Substrate:</b>
Magnetron	DC	Constant Current and Pulse mode	Ti	O <sub>2</sub>	13 cm	Constant total pressure 5.2 10 <sup>-3</sup> mbar	Quartz 10 x 10 mm <sup>2</sup>

After film deposition, thickness of the film has been measured in order to determine deposition rate. X-ray diffraction spectra were measured to identify thin film properties. The main experimental results and sputtering parameters are presented in Table 3.6. Where  $T_0$  is temperature of sample-holder, measured by thermocouple at the beginning of sputtering process and  $T_{max}$ - maximal temperature measured during deposition process, total working pressure of Ar and O<sub>2</sub> gases was constant 5.2 10<sup>-3</sup> mbar and measured by capacitance type vacuum detector during deposition process.

*Table 3.6 Experimental data and results on TiO<sub>x</sub> reactive sputtering:*

<b>Run</b>	<b>O<sub>2</sub>/Ar Flux</b>	<b>T<sub>0</sub>, C°</b>	<b>T<sub>max</sub>, C°</b>	<b>Current supply mode</b>	<b>Voltage V</b>	<b>Current A</b>	<b>Deposition rate nm/min</b>	<b>Film Structure</b>
t1	1,33	32	70	DC	440	0,4		Amf
t2	1,33	27	120	DC	500	1		Amf
t3	0,11	33	91	DC	463	1	26,4	Ti
t4	0,40	33	78	DC	459	1	25,6	Ti
t5	0,91	33	86	DC	435	1	19,8	Ti
t7	3,35	30	215	DC	447	1	2,0	R
t8	2,67	35	155	DC	460	1	1,5	R+A
t9	2,50	200	245	DC	464	1	1,7	A
t10	2,53	400	408	DC	460	1	1,5	A
t11	2,50	300	339	DC	460	1	1,5	A
t12	2,50	30	156	Pulsed	800	1	0,7	Amf
t13	2,50	33	224	Pulsed	1000	1	#	Amf

XRD spectra (see Figure 3.12) analysis results that amorphous (Amf) structure (no peaks on XRD spectra) was obtained for the Runs 1t-2t for oxygen/argon fluxes ratio 1.33 and Runs t7-8 in case of pulse mode of power source.

Titanium Ti thin film was obtained for Runs t3-t5 when oxygen/argon fluxes ratio is below 1.

TiO<sub>2</sub> rutile(R) phase(Run t7) is observed for oxygen/argon fluxes ratio 3.35 and with its decreasing to 2.5 value titanium oxide passed to mixed rutile and anatase (A) phase(Run t8).

Pure anatase phase of titanium oxide was observed for Runs t9-t11 when sputtering deposition was performed in temperature range from 200°C to 400°C.

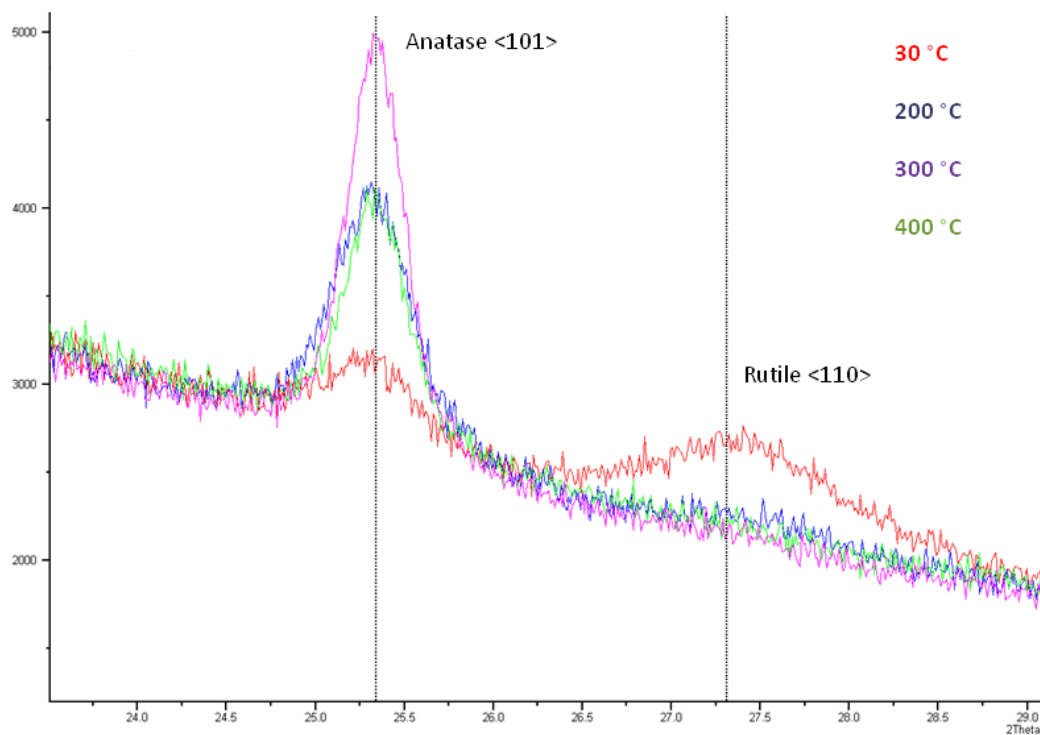


*Figure 3.12 XRD spectra of thin film of titanium oxide, deposited by reactive magnetron sputtering in temperature range 30-400°C. The most significant peak for Anatase phase (101)  $2\theta = 25.28^\circ$  and for Rutile phase (110)  $2\theta = 27.25^\circ$ .*

Analyzing X-ray diffraction spectra we obtain reticular parameter of titanium oxide phases presented on Figure 3.13. The colour lines are representing theoretical values. The value of reticular parameter shows very close experimental value to theoretical ones.

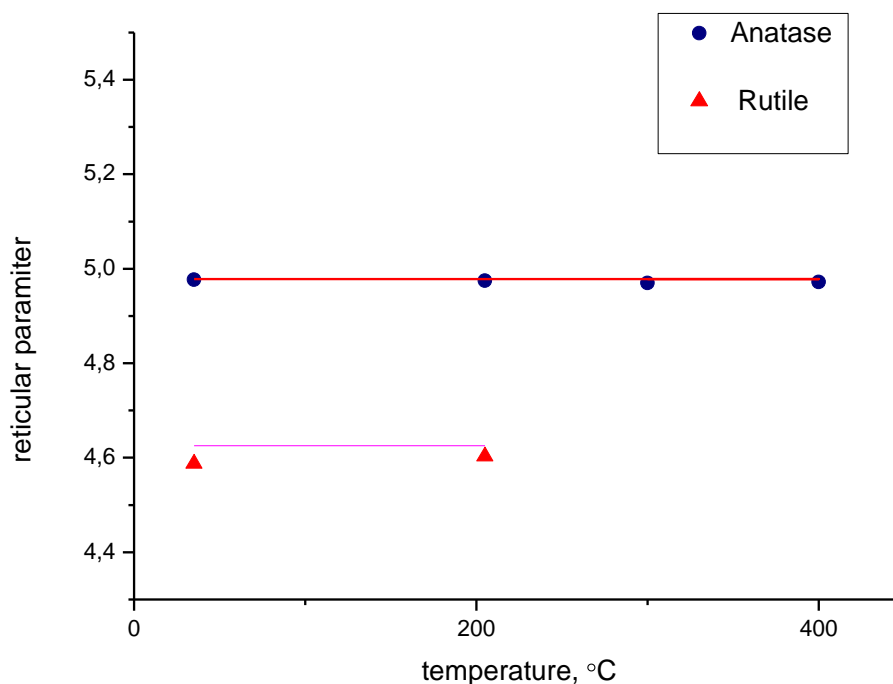


*Figure 3.13 Reticular parameter for Anatase phase (101)  $2\theta = 25.28^\circ$  and Rutile phase (110)  $2\theta = 27.25^\circ$  as function of temperature. Thin film of titanium oxide, deposited by reactive magnetron sputtering in temperature range 30-400°C. Colored lines are theoretic value.XRD spectra.*

## Results

It has been obtained two crystalline phase of  $\text{TiO}_2$ : Anatase and Rutile.

The peak intensity of Anatase is increasing with the temperature of sputtering while Rutile's peak is decreasing.

The sputtering condition such partial pressure of gases and temperature of sputtering are strongly influence on properties of obtained titanium oxide films.

### 3.3 Copper oxide photovoltaic cell development.

The “wet” (copper/copper oxide/electrolyte), metal-semiconductor (copper/copper oxide) and hetero-junction (copper oxide/titanium oxide) were constructed and studied.

#### 3.3.1 Cu<sub>2</sub>O photovoltaic “wet” solar cell.

The “wet” copper oxide photovoltaic elements were produced. 3 copper discs (run 1) have diameter 12.5, and area of electrode of 117.2 cm<sup>2</sup>. Disk number 1 was oxidized by “methane torch” and slightly mechanically grinded in order to remove CuO residuals. Disk number 2 oxidized by “methane torch” and not grinded (see Figure 3.14). The black oxide coating was peeled under water. Disk 3 Not oxidized and used as electrode.



*Figure 3.14 Photo of disk 1 e disk 2 respectively after oxidation:*

The electrodes were completely introduced in NaCl electrolyte solution of 4 liters volume (see Figure 3.15). Distance between electrodes was 15 cm.

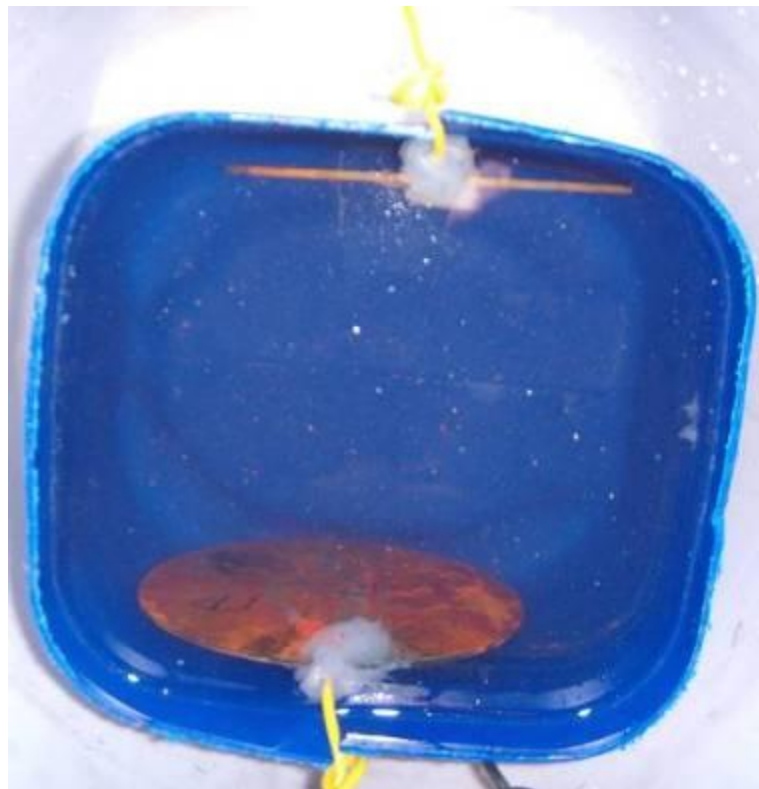


*Figure 3.15 Photo of disk 1 and electrode in NaCl electrolyte solution.*

The current and voltage were measured by Kiethley 195A multimeter (see table 3.6). To illumination has been used usual bulb lamp (100W) in order to obtain photovoltaic effect. The distance between lamp and solution was about 2 cm.

Cu disk	U dark, m V	U photo, m V	I dark, $\mu$ A	I photo, $\mu$ A	delta U, m V	delta I, $\mu$ A	electrolyte NaCl, gr/l	P, nW
1	129	149	115	136	20	21	20	420
2	49	96	40	92	47	52	20	2444
1	143	156	129	142	13	13	30	169
2	90	106	80	102	16	22	30	352
1	163	179	156	163	16	7	40	112
2	112	146	97	130	34	33	40	1122
1	165	190	149	166	25	17	50	425
2	113	153	97	133	40	36	50	1440
1	161	173	153	177	12	24	60	288

2	112	144	94	130	32	36	60	1152
1	163	188	148	174	25	26	70	650
2	105	154	93	138	49	45	70	2205

Other kind of experiment has been done with the same Cu discs from Run 1 (Run 2) after polishing. The mechanical and electrical setup was the same as at Run 1. Only 50 gr/l NaCl electrolyte concentration was used. Disk 1 (see Figure 3.16) oxidized in electrical oven during 12 hours up to 850 °C, and after was leaved for the night in order the temperature was going down slowly. Disk 2 (Figure 3.17) oxidized in same condition and together with Disk 1. After it was annealed during 2 hours at 500°C and slowly cooled. Disk 3 was not oxidized and used as electrode.



*Figure 3.16 Photo of disk 1 after oxidation in electric oven:*



*Figure 3.17 Photo of disk 2 after oxidation in electric oven and annealed at 500°C*

*Table 3.7 Run 2 experimental data*

<b>Name of Cu disk</b>	<b>U<sub>dark</sub>, m V</b>	<b>U photo, m V</b>	<b>I dark, μA</b>	<b>I photo, μ A</b>	<b>delta U, m V</b>	<b>delta I, μA</b>	<b>electrolyte NaCl, gr/l</b>	<b>P, nW</b>
<b>1 (not annealed)</b>	97	175	70	160	78	90	50	7020
<b>2 (annealed)</b>	148	160	124	144	12	20	50	240



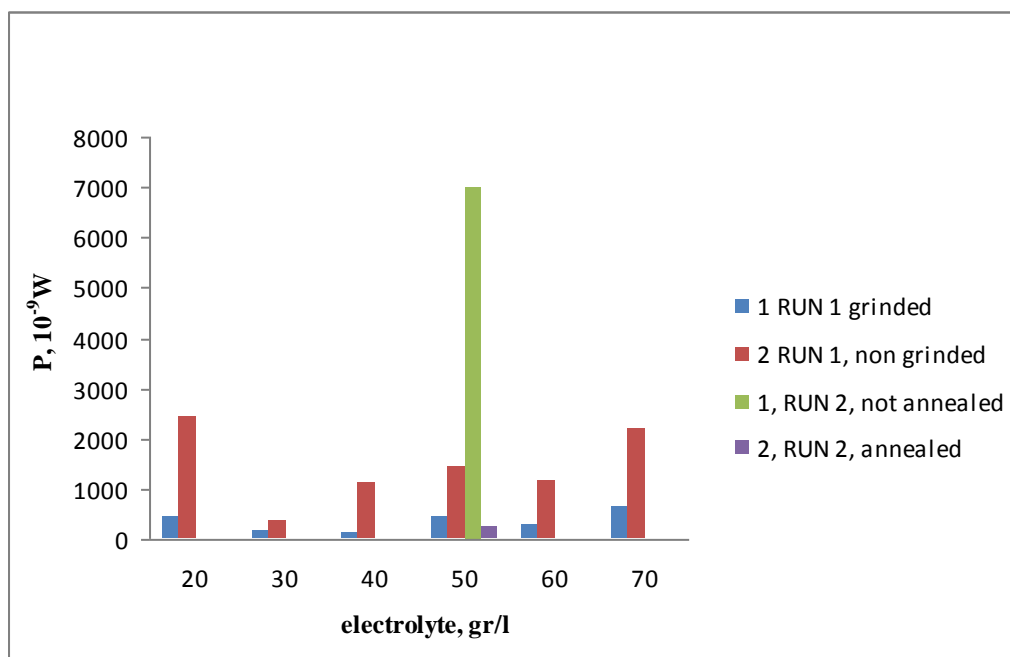


*Figure 3.18 Electric power measured in short circuit connection for bulb lamp illumination for setup Run 1 and Run 2 versions versus electrolyte concentration.*

From the experimental data presented in Table 3.7 and the figure 3.18 one can come to conclusion that “wet” photovoltaic the performance cannot be improved by annealing and cleneaning of CuO layer. The proper chose of electrolite concentration can significantly improve cell performace (see Figure 3.19, 3.20).

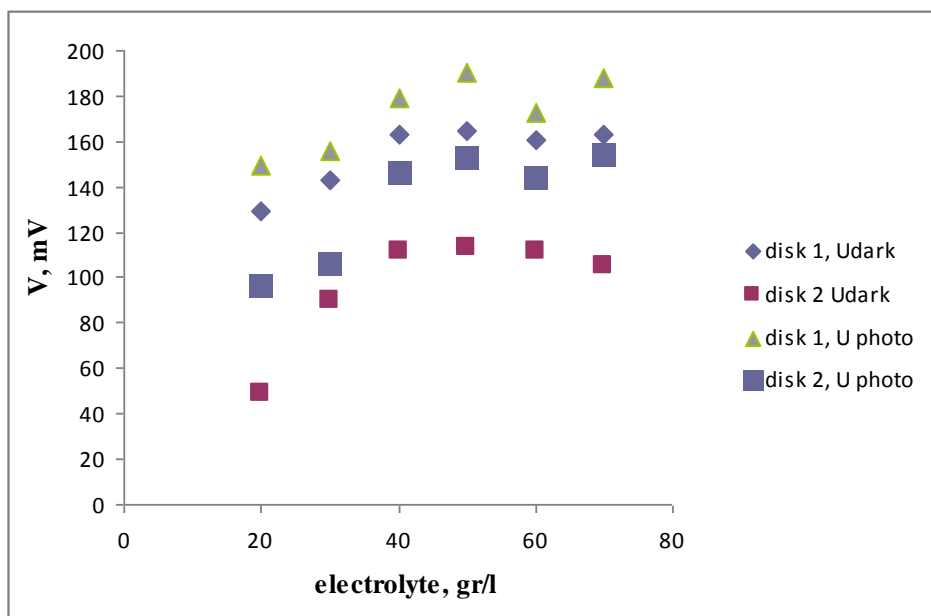


Figure 3.19 Dark and photo voltage versus electrolyte concentration.

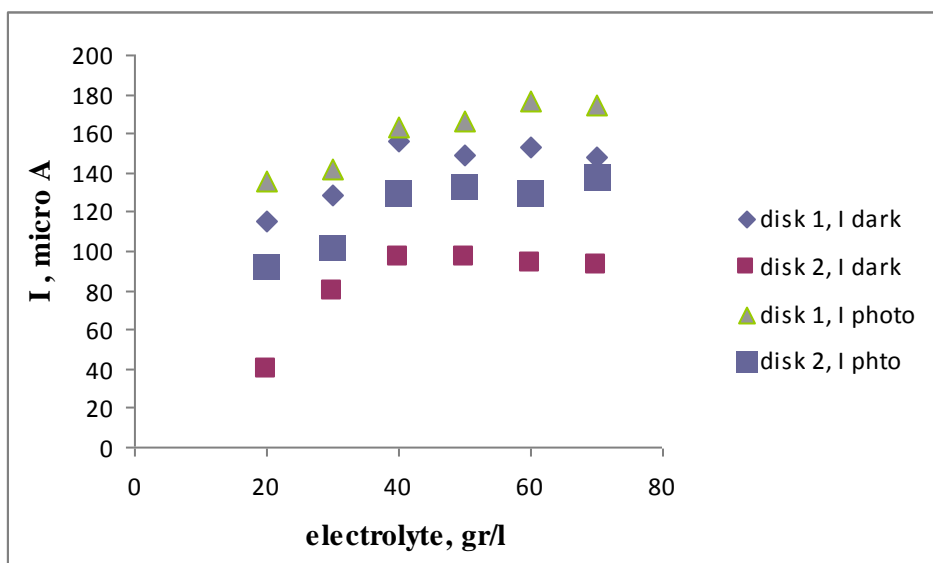


Figure 3.20 Dark and photo current versus electrolyte concentration.

### 3.3.2 Cu/Cu<sub>2</sub>O/Cu (metal/semiconductor) thin film structure created by reactive DC sputtering at various temperatures

The main parameters of experimental setup used for creation the metal-semiconductor Schottky photovoltaic cell are presented in Table 3.8:

*Table 3.8 Sputtering condition and parameters.*

Sputtering	Regime	Power Supply mode	Target	Reactive Gas	Target - Sample distance	Gas Flux Control Mode	Substrate
Magnetron	DC	Constant Current	Cu	O <sub>2</sub>	13 cm	Constant Total Pressure	Quartz 10 x 10 mm <sup>2</sup>

Cu target were cleaned before every deposition by pre-sputtering. Schematic presentation of prepared by magnetron sputtering depositions presented in Table 3.9. Cu/Cu<sub>2</sub>O/Cu structures is presented in Figure 3.21. Thin layer of Cu were sputtered at quartz on the top of it were sputtered Cu<sub>2</sub>O thin film and after other Cu thin layer. For electrical characterization obtained metal/semiconductors structure connected by tungsten needle for electrical characterization to standard multimeter.

*Table 3.9 Sputtering operation steps, sputtering parameters and deposited film characteristic.*

Step	Film deposited	Target	Ar Flux (sccm)	O <sub>2</sub> Flux (sccm)	P 10 <sup>-3</sup> mbar	T (C°)	V (V)	I (A)	Thickness (nm)	Size (mm)
1	Cu	Cu	7	0	6	30	468	0.4	500	10x10
2	Cu <sub>2</sub> O	Cu	2.5	8	7.6	300 <sup>1</sup> 400 <sup>2</sup> 600 <sup>3</sup>	557	0.4	2200	Ø 9
3	Cu	Cu	7	7.5	5.7	30	447	1	150	Ø 6

---

<sup>1</sup> Run 1D;

<sup>2</sup> Run 2D)

<sup>3</sup> Run 3D

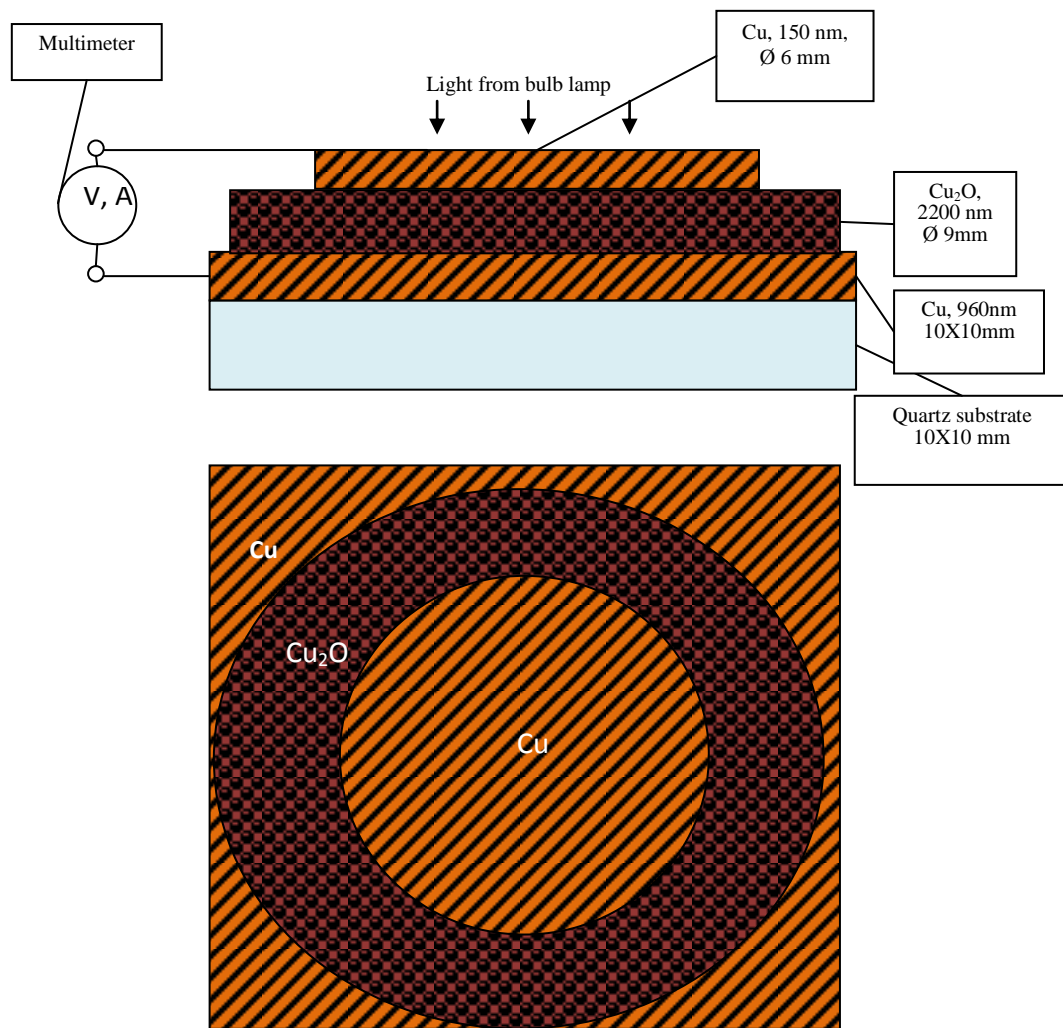


*Figure 3.21 Schematic view of Cu/Cu<sub>2</sub>O/Cu structures.*

## Results

We have obtained Cu/Cu<sub>2</sub>O/Cu. This structure does not show sensitivity to visible light.

The structure does not show diode behavior.

The possible reason is that wrong combination of metal semiconductor was used.

### 3.3.3 Photovoltaic effect in Cu/Cu<sub>2</sub>O/TiO<sub>2</sub>/Au (heterojunction) thin film structure created by reactive DC sputtering.

Heterojunction photovoltaic thin film cell based on Cu<sub>2</sub>O/TiO<sub>2</sub> junction have been created (see Figure 3.22) The Cu and gold layers play role of ohmic contacts. The main production steps are shown in Table 3.11. TiO<sub>2</sub> film was sputtered in condition to obtain anatase phase.

*Table 3.10: Main sputtering conditions:*

Sputtering	Regime	P-Supply mode	Target	Reactive Gas	Target - Sample distance	Gas Flux Control Mode	Substrate
Magnetron	DC	Constant Current	Cu, Ti, Au	O <sub>2</sub>	13 cm	Constant Total Pressure	Quartz 10 x 10 mm <sup>2</sup>

*Table 3.11 Experimental data and results of Cu/Cu<sub>2</sub>O/TiO<sub>2</sub>/Au structure production.*

Run	Target	Ar Flux	O <sub>2</sub> Flux	P <sub>w</sub> , 10 <sup>-3</sup> mbar	T, C°	Voltage V	Current A	thickness nm	Size mm	Film deposited
D-1	Cu	7	0	6	30	468	0.4	960	10x10	Cu
D-2	Cu	2.5	8	7.55	600	557	0.4	2250	Ø 9	Cu <sub>2</sub> O
D-3	Ti	3	7.5	5.66	300	447	1	8	Ø 9	TiO <sub>2</sub> , Anatase
D-4	Au	7	0	6.54	29	684	0.4	219	Ø 3	Au

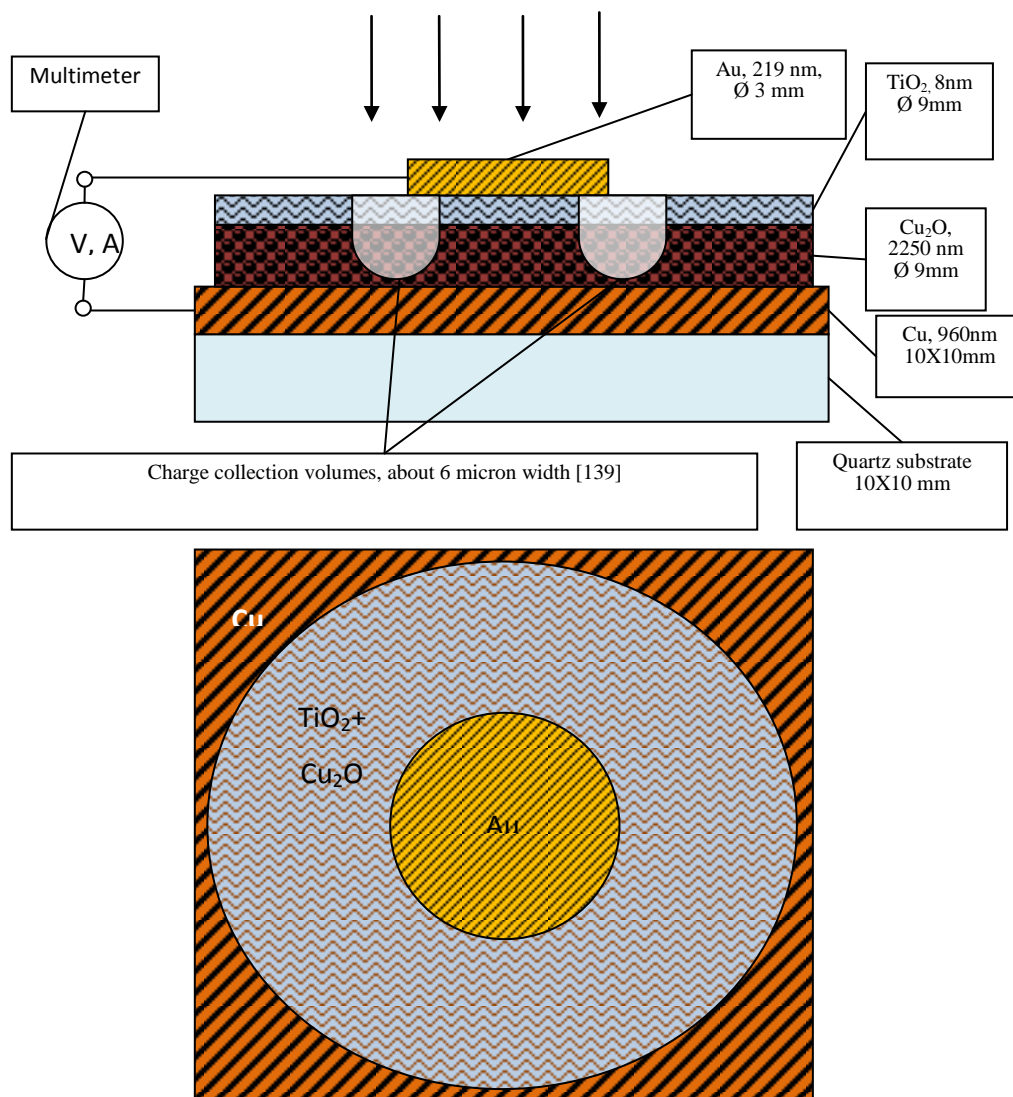
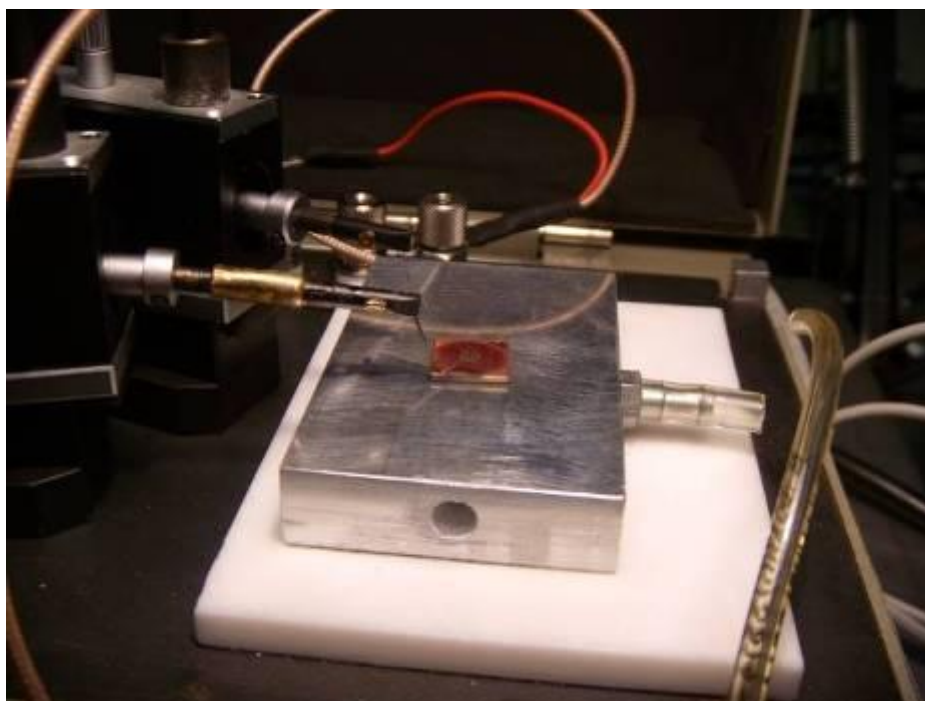
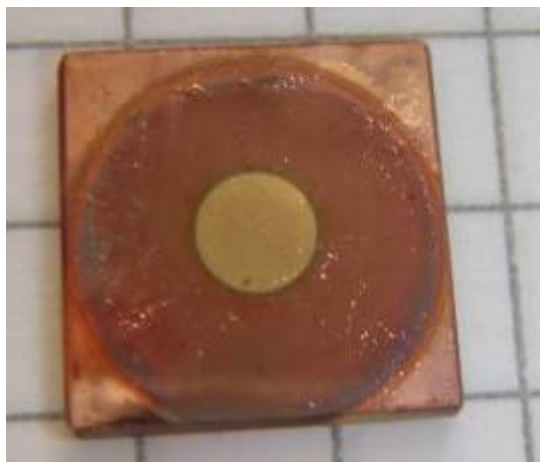


Figure 3.22 Schematic presentations of Cu/Cu<sub>2</sub>O/TiO<sub>2</sub>/Au structures.



*Figure 3.21 Photo of tested sample. Structure connected by tungsten needle for electrical characterization*

The  $\text{Cu/Cu}_2\text{O/TiO}_2/\text{Au}$  heterojunction structures have been electrically characterized (see Figure 3.21). The photovoltaic characteristic and comparison of “wet” photovoltaic cell versus “sputtering” photovoltaic elements are presented in Table 3.12. From this table one can see that heterojunction photovoltaic cell is one order higher light conversion performance respect to wet” photovoltaic.

Other Runs 1H and  $\text{Cu/Cu}_2\text{O/TiO}_2/\text{Au}$  heterojunction photovoltaic cell were prepared. As substrat have been used 2 inch in diameter Cu sheet of 0.08 mm

thickness. The structures were created by the same technique used for the quartz substrate, mentioned before. One structure is created by sputtering at 600°C Run 1H (see Figure 3.13), but other at 300°C Run 2H (see Figure 3.14).

In order to optimize front Au contact, structure 1H was divided in two parts. On the one part contact have shape of grid. Other part was totally covered by semitransparent 100 nm thick gold (see Figure 3.14).

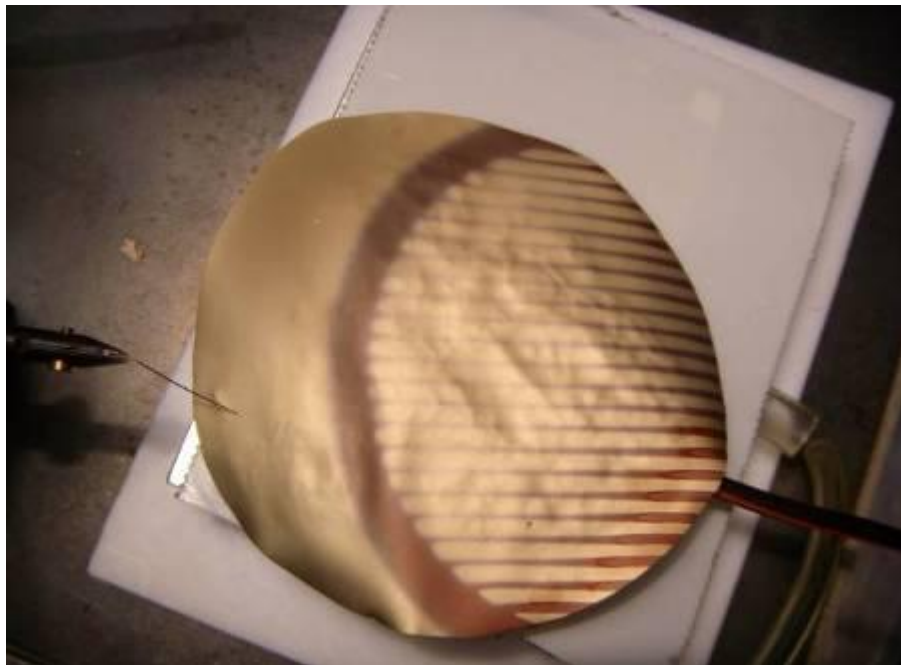


*Figure 3.13 Run 1H. Thin film 2-inch heterojunction photovoltaic solar cell fabricated by sputtering technology at 600°C. As the substrate and back contact Cu sheet 0.08 mm thickness is used.*





*Figure 3.14 Run 2H. Thin film 2-inch heterojunction photovoltaic solar cell fabricated by sputtering technology at 300°C. As the substrate and back contact Cu sheet 0.08 mm thickness is used.*

### **3.3.4 Performance comparison of different photovoltaic cell build**

The power of photovoltaic devices normalized to area measured under bulb lamp light illumination is presented in Table 3.12. It was calculated by the formula:

$$P = V_{os} \cdot I_{sc} / A$$

Where:

$V_{os}$  -open circuit voltage (measurement done with good voltmeter satisfy this condition)

$I_{sc}$  -short circuit current (measurement done with good amperemeter satisfies this condition)

A - active area:

For “sputtered” samples was taken in consideration the ring around ohmic Au contact and for “thermal” samples was taken in consideration only one side of Cu oxidized plate.

*Table 3.12 Performance comparisons of different photovoltaic cells build*

Type	Active Area ( cm <sup>2</sup> )	Power, 10 <sup>-8</sup> (W/cm <sup>2</sup> )	Note
Cu/Cu <sub>2</sub> O/electrolyte (Thermal oxidation)	122,7	5,7	maximum value
Cu/Cu <sub>2</sub> O/electrolyte (Thermal oxidation)	122,7	0,89	average value
Cu/Cu <sub>2</sub> O/TiO <sub>2</sub> +Au (Sputtering)	0,57·10 <sup>-3</sup>	42,8	device 7.1
Cu+Cu <sub>2</sub> O+TiO <sub>2</sub> +Au (Sputtering)	0,57·10 <sup>-3</sup>	72,4	device 7.2
Cu+Cu <sub>2</sub> O+TiO <sub>2</sub> +Au (Sputtering)	8	95,7	Run1H, 600°C, Grid shape contact
Cu+Cu <sub>2</sub> O+TiO <sub>2</sub> +Au (Sputtering)	6	0,85	Run1H, 600°C, plane shape contact
Cu+Cu <sub>2</sub> O+TiO <sub>2</sub> +Au (Sputtering)	19.6	1,5	Run2H, 300°C, Grid shape contact

From Table 3.12 one can see that performance of heterojunction thin film photovoltaic is in one order higher than for “wet” solar cell. The higher performance of heterojunction photovoltaic was predicted in [74]. It is experimentally shown that shape of the front contact strongly influence on performance of solar cell. Run 1H with semitransparent Au front contact has very low performance, on the other hand the same sample with a grid contact have highest efficiency. The sample with  $\text{Cu}_2\text{O}$  layer sputtered at  $300^\circ\text{C}$  has low conversion efficiency.

Short circuit current  $I_{sc}$  measured in heterojunction photovoltaic has positive direction. This fact is proving that p-n junction is obtained. From  $\text{Cu}_2\text{O}$  part holes collection is observed, for  $\text{TiO}_2$  side electron are collected.

## CONCLUSIONS

If one is interested to invest in this research see summarizing table presented below. Photovoltaic Cu/Cu<sub>2</sub>O/TiO<sub>2</sub>/Au cells structures were created by DC magnetron reactive sputtering in O<sub>2</sub> reactive gas ambient. O<sub>2</sub> and Ar and have constant partial gas pressure and fluxes.

Device	Front contact	Cu <sub>2</sub> O, deposition	Target	Active Area (cm <sup>2</sup> )	Power, 10 <sup>-8</sup> (W/cm <sup>2</sup> )
7.1	Plane	600°C	Cu, Ti, Au	0,57·10 <sup>-3</sup>	42,8
7.2	plane	600°C	Cu, Ti, Au	0,57·10 <sup>-3</sup>	72,4
1.1H	Grid	600°C	Cu, Ti, Au	8	95,7
1.2H	plane	600°C	Cu, Ti, Au	6	0,85
2H	Grid	300°C	Cu, Ti, Au	19.6	1,5

At the room temperature, we have obtained Cu<sub>2</sub>O phase, but copper or copper oxide CuO is also present. These films have electrons (n-type) conduction.

Film deposition on heated at 200°C substrate have higher crystal structure and P-type conductivity as have to be in Cu<sub>2</sub>O semiconductor.

Increasing temperature Cu<sub>2</sub>O <111> and Cu<sub>2</sub>O <200> peaks increase while Cu peak <100> decrease significantly.

The thin films of copper oxide deposited at room temperature have very low resistivity.

Films prepared at high temperature deposition have high resistivity.

We have obtained two crystalline phase of TiO<sub>2</sub>: Anatase and Rutile.

The peak intensity of Anatase is increasing with the temperature of sputtering while Rutile's peak is decreasing.

The sputtering condition such partial pressure of gases and temperature of sputtering are strongly influence on properties of obtained titanium oxide films.

It has been obtained Cu/Cu<sub>2</sub>O/Cu. This structure do not show sensitivity to visible light. The structure does not show diode behavior. The possible reason is that wrong combination of metal semiconductor was used.

It has been obtained Cu/Cu<sub>2</sub>O/TiO<sub>2</sub>/Au solid thin film photovoltaic elements by DC magnetron reactive sputtering. This thin film structures are sensitive to light. The specific power of these samples is in two orders higher than in “thermal” oxidized electrolyte solar elements. Photovoltaic performance of these structure is strongly depends on sputtering temperature and front electrode shape.

Photovoltaics constitutes a new form of producing electric energy that is environmentally clean and very modular. In stand-alone installations, it must use storage or another type of generator to provide electricity when the sun is not shining.

Photovoltaics is very suitable as the power supply for remote communication equipment. Its use is increasing rapidly to produce electricity in grid-connected houses and buildings in industrialized countries, despite a 5 to 10 times higher cost than conventional electricity.

Crystalline Si technology, both monocrystalline and multicrystalline is today clearly dominant, with about 90% of the market.

Thin-film technology is one of the candidates to take over from Si technology. There are many technological options regarding thin-film materials and methods of deposition but their primary claim to the throne currently occupied by Si is that they can be ultimately produced at much lower cost.

Copper oxide is a good candidate for low cost photovoltaic element. It is non toxic and has high absorption in visible spectra of light. In order to improve its performance doping methods and “partner” component for hetero- or homo – junction have to be studied.

In summary, it is very likely that photovoltaics will become in the next half century an important source of world electricity. Public support and global environmental concerns will keep photovoltaics viable, visible, and vigorous both

in new technical developments and user applications. Nations which encourage photovoltaics will be leaders in this shining new technology, leading the way to a cleaner, more equitable twenty-first century, while those that ignore or suppress photovoltaics will be left behind in the green, economic energy revolution.

## **Reference:**

1. V. S. Arunachalam (*Center for Study of Science, India*) and E. L. Fleischer (MRS) *MRS Bulletin* (2008).
2. Maycock P, *Renewable Energy World* 3, 59–74 (2000).
3. Maycock P (Ed), *PV Energy Systems*, *PV NEWS* 20(3), 2 (2001).
4. *Physics Today* (2007) G. W. Crabtree and N. S. Lewis.
5. Fritts C, *Proc. Am. Assoc. Adv. Sci.* 33, 97 (1883).
6. Chapin D, Fuller C, Pearson G, *J. Appl. Phys.* 25, 676, 677 (1954).
7. Reynolds D, Leies G, Antes L, Marburger R, *Phys. Rev.* 96, 533, 534 (1954).
8. Jenny D, Loferski J, Rappaport P, *Phys. Rev.* 101, 1208, 1209 (1956).
9. Prince M, *J. Appl. Phys.* 26, 534–540 (1955).
10. Loferski J, *J. Appl. Phys.* 27, 777–784 (1956).
11. Wysocki J, Rappaport P, *J. Appl. Phys.* 31, 571–578 (1960).
12. Shockley W, Queisser H, *J. Appl. Phys.* 32, 510–519 (1961).
13. Cusano D, *Solid State Electron.* 6, 217–232 (1963).
14. Wysocki J et al., *Appl. Phys. Lett.* 9, 44–46 (1966).
15. Alferov Z, *Fiz. Tekh. Poluprovodn.* 4, 2378 (1970).
16. Lindmayer J, Allsion J, *COMSAT Tech. Rev.* 3, 1–22 (1973).
17. Hovel H, Woodall J, *Proc. 10th IEEE Photovoltaic Specialist Conf.*, 25–30 (1973).
18. Sumner D, Whitaker C, Schlueter L, *Proc. 20th IEEE Photovoltaic Specialist Conf.*, 1289–1292(1988).
19. Green M et al., *Proc. 18th IEEE Photovoltaic Specialist Conf.*, 39–42 (1985).
20. Sinton R, Kwark Y, Gruenbaum P, Swanson R, *Proc. 18th IEEE Photovoltaic Specialist Conf.*, 61–65 (1985).
21. Friedman D et al., *Prog. Photovolt.* 3, 47 (1995).
22. Gratzel M, *Prog. Photovolt.* 8, 171–186 (2000).
23. Contreras M et al., *Prog. Photovolt.* 7, 311–316 (1999).
24. Bower W, *Prog. Photovolt.* 8, 113–126 (2000).

25. Fitzgerald M, Mrohs M, *Proc. 26th IEEE Photovoltaic Specialist Conf.*, 1225–1229 (1997).
26. Nieuwenhout F et al., *Prog. Photovolt.* 9, 455–474 (2001).
27. Cabraal A, Cosgrove-Davies M, Schaeffer L, *Proc. 25th IEEE Photovoltaic Specialist Conf.*, 1357–1362 (1996).
28. Hoff T, Jennings C, *Proc. 18th IEEE Photovoltaic Specialist Conf.*, 235–240 (1985).
29. Shugar D, Hoff T, *Prog. Photovolt.* 1, 233–250 (1993).
30. Byrne J, Hegedus S, Wang Y, *Prog. Photovolt.* 2, 235–248 (1994).
31. Yordi B, Gillett W, *Prog. Photovolt.* 5, 175–185 (1997).
32. Iuchi M, *2nd World Conference and Exhibition on Photovoltaic Solar Energy Conversion*, 3304–3307 (1998).
33. Strong S, *Proc. 25th IEEE Photovoltaic Specialist Conf.*, 1197–1202 (1996).
34. Bardeen, J. 1947. Surface states and rectification at a metal semiconductor contact. *Phys. Rev.* 71:717-727.
35. Copeland, A. W., O. D. Black, and A. B. Garrett. 1942. The photovoltaic effect. *Chem. Rev.* 31:177-226.
36. Henisch, H. K. 1949. *Metal rectifiers*. Oxford University Press, London.
37. Houstoun, R. A. 1948. The efficiency of the barrier layer photocell. *Phil. Mag.* 39: 902-910.
38. Kosenko, V. and G. Miselyuk. 1948. Physical characteristics of silver sulfide photocells.
39. W.Siripalaetal./SolarEnergyMaterials&SolarCells77(2003).
40. K. L. Chopra, P. D. Paulson and V. Dutta, *Thin-film solar cells: an overview*, *Progress in Photovoltaics: Research and Applications*, 12, 69–92 (2004).
41. Z. Q. Ma, B. X. Liu, *Boron-doped diamond-like amorphous carbon as photovoltaic films in solar cells*, *Solar Energy Materials and Solar Cells*, 69(4), 339–344 (2001).
42. E. A. Katz, D. Faiman, V. Lyubin, *Persistent internal photopolarization in C60 thin-films: proposal for a novel fullerene-based solar cells*, *Conference Digest of the 29th IEEE Photovoltaic Specialist Conference*, New Orleans, May 19–24, 2002, 1298–1301.



43. Noguét, C., Tapiero, M., Zielinger, J. P.: *Phys. Status Solidi* 24 (1974) 565.
44. Pollack, O. P., Trivich, D.: *J. Appl. Phys.* 46 (1975) 163.
45. Parreta, A., Jayaraj, M. K., Di Nocera, A., Loreti, S., Quercia, L., Agati, A.: *Phys. Status Solidi (a)* 155 (1996) 399.
46. Tapiero, M., Noguét, C., Zielinger, J. P., Schwab, C., Pierrat, D.: *Rev. Phys. Appl.* 14 (1979) 231.
47. Wang, G. J., Weichman, F. L.: *Can. J. Phys.* 60 (1982) 1648.
48. Maluenda, J., Farhi, R., Petot-Ervas, G.: *J. Phys. Chem. Solids* 42No10 (1981) 911.
49. Prévot, B., Carabatos, C., Sieskind, M.: *Phys. Status Solidi (a)* 19 (1972) 455.
50. Goltzené, A., Schwab, C.: *Phys. Status Solidi (b)* 92 (1979) 483.
51. Duvvury, C., Kenway, D. J., Weichman, F. L.: *J. Lumin.* 10 (1975) 415.
52. Kenway, D. J., Duvvury, C., Weichman, F. L.: *J. Lumin.* 16 (1978) 171
53. Chee, K. T., Kedwsim, T., Weichman, F. L.: *Can. J. Phys.* 57 (1979) 988.
54. Kreingol'd, F. I., Kulinkin, B. S., Krivolapchuk, V. V.: *Fiz. Tekh. Poluprovodn.* 11 (1977) 836.
55. Fortin, E., Rochon, P., Zielinger, J. P.: *J. Phys. Chem. Solids* 36 (1975) 1299.
56. Assimos, J. A., Trivich, D.: *Phys. Status Solidi (a)* 26 (1974) 477.
57. Tapiero, M., Zielinger, J. P., Noguét, C.: *Phys. Status Solidi (a)* 33 (1976) 155.
58. Zielinger, J. P., Noguét, C., Tapiero, M.: *Phys. Status Solidi (a)* 42 (1977) 91.
59. Swanson, Fuyat., *Natl. Bur. Stand. (U.S.), Circ.* 539, II, 23, (1953)
60. *Structure: Restori, R., Schwarzenbach, D., Acta Crystallogr., Sec.B:Struc. Science*, 42,201(1986)
61. T.J. Richardson, J.L. Slack, M.D. Rubin, *Electrochim. Acta* 46 (2001) 2281.
62. A. Mittiga, E. Salza, F. Sarto, M. Tucci, R. Vasanthi, *Appl. Phys. Lett.* 88 (2006)
63. H. Tanaka, T. Shimakawa, T.Miyata, H. Sato, T.Minamia, *Appl. Surf. Sci.* 244 (2005) 568.

64. M. Izaki, T. Shinagawa, K.T. Mizuno, Y. Ida, M. Inaba, A. Tasaka, *J. Phys. D: Appl. Phys.* 40 (2007) 3326.
65. T. Minami, T. Miyata, K. Ihara, Y. Minamino, S. Tsukada, *Thin Solid Films* 494 (2006) 47.
66. H. Tanaka, T. Shimakawa, T. Miyata, *Thin Solid Films* 469–470 (2004) 80.
67. B. Balamurugan, B.R. Mehta, *Thin Solid Films* 396 (2001) 90.
68. A.O. Musa, T. Akomolafe, M.J. Carter, *Sol. Energy Mater. Sol. Cells* 51 (1998) 305.
69. M.F. Al-Kuhaili, *Vacuum* 82 (2008) 623.
70. H.H. Lee, C. Lee, Y.L. Kuo, Y.W. Yen, *Thin Solid Films* 498 (2006) 43.
71. C.A.N. Fernando, S.K. Wetthasinghe, *Sol. Energy Mater. Sol. Cells* 63 (2000) 299.
72. S.C. Ray, *Sol. Energy Mater. Sol. Cells* 68 (2001) 307.
73. L. Wang, M. Tao, *Electrochem. Solid-State Lett.* 10 (2007) H248.
74. A.S. Reddy, S. Uthanna, P.S. Reddy, *Appl. Surf. Sci.* 253 (2007) 5287.
75. A.S. Reddy, H.H. Park, V.S. Reddy, K.V.S. Reddy, N.S. Sarma, S. Kaleemulla, S. Uthanna, P.S. Reddy, *Mater. Chem. Phys.* 110 (2008) 397.
76. A.S. Reddy, P.S. Reddy, S. Uthanna, G.V. Rao, A. Klein, *Phys. Status Solidi A* 203 (2006) 844.
77. A.S. Reddy, G.V. Rao, S. Uthanna, P.S. Reddy, *Phys. B* 370 (2005) 29.
78. J.H. Hsieh, P.W. Kuo, K.C. Peng, S.J. Liu, J.D. Hsueh, S.C. Chang, *Thin Solid Films* 516 (2008) 5449.
79. A. Parretta, M.K. Jayaraj, A.D. Nocera, S. Loreti, L. Quercia, A. Agati, *Phys. Status Solidi A* 155 (1996) 399.
80. Hsin-Chun Lu, Chun-Lung Chu, Chi-You Lai, Yu-Hsiang Wang *Thin Solid Films* 517 (2009) 4408–4412
81. A.Sivasankar Reddy, G. Venkata Rao, S. Uthanna, P. Sreedhara Reddy *Physica B* 370 (2005) 29–34
82. J.F. Pierson, A. Thobor-Keck, A. Billard *Applied Surface Science* 210 (2003) 359–367.
83. A.Sivasankar Reddy, S. Uthanna, P. Sreedhara Reddy *Applied Surface Science* 253 (2007) 5287–5292
84. Calos, N.J., Forrester, J.S., Schaffer, G.B., *J. Solid State Chem.*, 122, 273, (1996)

85. Hailing Zhu, Junying Zhang, Chunzhi Li, FengPan, TianminWang, BaibiaoHuang *Thin Solid Films* 517 (2009) 5700–5704.
86. Sugiyama, K., Takeuchi, Y., *Z. Kristallogr.*, 194, 305, (1991)
87. Sanchez, E., Lopez, T., Gomez, R., Bokhimi, Morales, A., Novaro, O., *J. Solid State Chem.*, 122, 309, (1996)
88. Crystallographic Laboratory, Cambridge, England, UK., Private Communication
89. Dana's System of Mineralogy, 7th Ed.
90. I. Sopyan, S. Murasawa, K. Hashimoto, A. Fujishima, in: D.E. Ollis *Photocatalytic Purification and Treatment of Water and Air*, Elsevier, Amsterdam, 1993, p. 747.
91. D.E. Olli et al., *Proc. 1st Int. Conf. TiO<sub>2</sub> Photocatalytic Purification and Treatment of Water and Air*, Elsevier, Amsterdam, 1993, p. 747.
92. A. Fujishima, K. Honda, *Nature* 238 1972.37.
93. M. Graetzel, *Comments Inorg. Chem.* 12 1991.93.
94. O. Carp, C.L. Huisman, A. Reller, *Prog. Solid State Chem.* 32 (2004) 33.
95. A. Mills, S. Le Hunt, *J. Photochem. Photobiol., A Chem.* 108 (1997) 1.
96. T. Ohno, K. Tokieda, S. Higashida, M. Matsumara, *Appl. Catal., A Gen.* 244 (2003) 383.
97. M. Anpo, M. Takeuchi, *J. Catal.* 216 (2003) 505.
98. S. Sato, *Chem. Phys. Lett.* 123 (1986) 126.
99. R. Asahi, T. Morkawa, T. Ohwaki, K. Aoki, Y. Taga, *Science* 293 (2001) 269.
100. Z.G. Li, S. Miyake *Applied Surface Science* 255 (2009) 9149–9153
101. Z. Ding, X.J. Hu, P.L. Yue, *Catal. Today* 68 (2001) 173.
102. J.S. Kim, H.K. Joo, T.K. Lee, *J. Catal.* 194 (2000) 484.
103. J.G. Yu, X.J. Zhao, *Mater. Res. Bull.* 35 (2000) 1293.
104. K. Baba, R. Hatada, *Surf. Coat. Technol.* 136 (2001) 241.
105. M. Terashima, N. Inoue, S. Kashiwabara, *Appl. Surf.* 169-170 (2001).
106. S.K. Zheng, T.M. Wang, G. Xiang, C. Wang, *Vacuum* 62 (2001) 361.
107. T.M. Wang, H.Y. Wang, P. Xu, *Thin Solid Films* 334 (1998) 103.
108. S. Takeda, S. Suzuki, H. Odaka, *Thin Solid Films* 392 (2001) 338.

109. P. Lobl, M. Huppertz, D. Mergel, *Thin Solid Films* 251 (1994) 72.
110. W.J. Zhang, Y. Li, F.H. Wang, *J. Mater. Sci. Technol.* 18 (2002) 101.
111. K. Eufinger, E.N. Janssen, H. Poelman *Thin Solid Films* 515 (2006) 425 – 429
112. Satoshi Takeda,\_, Susumu Suzukia, *Thin Solid Films* 392Ž2001.338\_344
113. K.A. Vorotilov, E.V. Drlova, V.I. Petrovsky, *Thin Solid Films* 207 (1992) 180.
114. J.P. Lu, J. Wang, R. Raj, *Thin Solid Films* 204 (1991) 113.
115. N. Martin, C. Rousselot, C. Savall, F. Palmينو, *Thin Solid Films* 287 (1996) 154.
116. L. C. Olsen and R. C. Bohara *Appl. Phys. Lett.*, Vol. 34, No. 1,1 January 1979.
117. Alberto Mittiga, Enrico Salza, Francesca Sarto, Mario Tucci, and Rajaraman Vasanthi *Appl. Phys. Lett.*, 88, 163502 (2006).
118. J.L. Li, L. Liu, Y. Yu, Y.W. Tang, H.L. Li, F.P. Du, *Electrochem. Commun.* 6 (2004) 940.
119. M.K.I. Senevirathna, P.K.D.D.P. Pitigala, K. Tennakone, *J. Photochem. Photobiol A: Chem.* 171. (2005) 257.
120. J.P. Yasomanee, J. Bandara, *Solar Energy Mater. Solar Cells* 92 (2008) 348.
121. M. Nolan, S.D. Elliott, *Phys. Chem. Chem. Phys.* 8 (2006) 5350.
122. M. Mensson, T. Claesson, T. Muro, T. Matsushita, T. Nakamura, T. Kinoshita, U.O. Karlsson, O. Tjernberg, *Phys. Rev. B* 76 (2007) 115127.
123. B. Balamurugan, I. Aruna, B.R. Mehta, S.M. Shivaprasad, *Phys. Rev. B* 69 (2004)165419.
124. U. Diebold, *Surf. Sci. Rep.* 48 (2003) 53.
125. W. Siripala, A. Ivanovskaya, T.F. Jaramillo, S.-H. Baeck, E.W. McFarland, *Solar Energy Mater. Solar Cells* 77 (2003) 229.
126. Y. Bessekhoud, D. Robert, J.-V. Weber, *Catal. Today* 101 (2005) 315.
127. Y.G. Zhang, L.L. Ma, J.L. Li, Y. Yu, *Environ. Sci. Technol.* 41 (2007) 6264.
128. A.D. Katnani, G. Margaritondo, *Phys. Rev. B* 28 (1983) 1944.

129. T. Ohta, A. Klust, J.A. Adams, Q. Yu, M.A. Olmstead, F.S. Ohuchi, *Phys. Rev. B* 69 (2004).
130. Y. Bessekhoud, D. Robert, J.-V. Weber *Catalysis Today* 101 (2005) 315–321
131. Cristian Pira, *Master thesis*, 2007.
132. Bonisconi, Ricci-Bitti, *La Diffrattometria dei Raggi X per Materiali Policristallini, aspetti pratici*, ed. Tecniche Nuove, Milano 1988.
133. Schroder Dieter K., *Semiconductor Material and Device Characterization*, 2nd Edition, (John Wiley & Sons, New York, 1998)
134. B. Balamurugan, B.R. Mehta, *Thin Solid Films* 396 (2001) 90.
135. Musa, A.O., Akomolafe, T., Cartner, M.J., 1998. *Production of cuprous oxide, a solar cell material, by thermal oxidation and a study of its physical and electrical properties*. *Sol. Energy Mater. Sol. Cells* 51, 305–316.
136. B.P. Rai, *Sol. Cells* 25 (1988) 265.
137. Pollack, G.P., Trivich, D., *Photoelectric properties of cuprous oxide*. *J. Appl. Phys.* 46, 163–172. 1975.
138. Withana Siripala, Anna Ivanovskaya, Thomas F. Jaramillo et al, *Solar Energy Materials & Solar Cells* 77 (2003) 229–237.
139. Jef Poortmans and Vladimir Arkhipov, *Thin Film Solar Cells Fabrication, Characterization and Applications* 2006 John Wiley & Sons Ltd.